Study on The Effect of Physical Properties of Microtubules on their Collective Motion by Kinesins

微小管の集団運動における物理特性の影響に関する研究

Tamanna Ishrat Farhana

Graduate School of Chemical Sciences and Engineering,
Hokkaido University, Japan
2017

Contents

Chapter 1

General Introduction

1.1 Overview

Self-propelled particles are referred to as the autonomous agents, which can convert energy from the environment into directed or persistent motion. They can move along as well in large groups giving rise to some fascinating group behavior. The collective motion is an entrancing display of the coordinated behavior of the self-propelled particles, which is often associated with formation of fascinating large-scale patterns[1-3]. Examples of this complex self-organization process is common in nature, exhibited by a wide range of self-propelled objects ranging from human crowds, animals, birds, cells, bacteria, to subcellular cytoskeletal filaments[4-10]. The detailed study on collective motion may provide us insights into the emergent structures, and function, which consequently will allow us obtaining information about how to assemble a large number of collectively moving self-propelled objects to more ordered structure with a view to application in technology and molecular robotics.

The composition of a system where particles or agents are collectively moving is generically simple-composed of a sufficiently dense ensemble of moving objects. However, the dynamical properties of such autonomous moving objects are quite complex. Numerous approaches have been put forward by the researchers to explore the underlying principal of collective motion. These approaches were set up mostly by considering the agent-based simulation[11-22]. However, these theoretical results are lacking proper experimental verifications. Some macroscopic and microscopic systems including micro-organisms, bacterial colonies, artificial machines, self-propelled colloids etc., have offered some experimental systems to study collective motion but they had their own limitations e.g; expensive, difficult to control, space restirction etc.[23-31]. Recently, the biomolecular motor systems have emerged as an ideal candidate for experimentally demonstrating the collective motion through *in vitro* gliding assay. This is a simple system where the cytoskeletal filamentous proteins (actin; microtubules) are propelled by associated motor-proteins (myosin; dynein/kinesin) on a substrate and is advantageous over other self-propelled system in terms of simplicity, universality, controlled environment, and adjustable parameters.

In this study, I will present detailed investigations on the collective motion of self-propelled particles by *in vitro* gliding assay of microtubules propelled by kinesins. I have demonstrated the first-ever collective motion of kinesin driven microtubules via regulating mutual interactions among the gliding microtubules, by employing depletion force among them. How different parameters, like depletion force and microtubules concentration influence the kinetics of collective motion will be discussed here. I will also describe how the mechanical property of microtubule govern the pattern formation in collective motion. The response of collectively moving microtubules to external stimuli such as mechanical stress will be discussed here.

1.2 Theoretical and experimental approaches to study the collective motion of self-propelled particles

The eye-catching displays of collectively moving objects has fascinated most of us and drawn attention to explore the underlying mechanism of emerging group behavior of self-propelled objects.

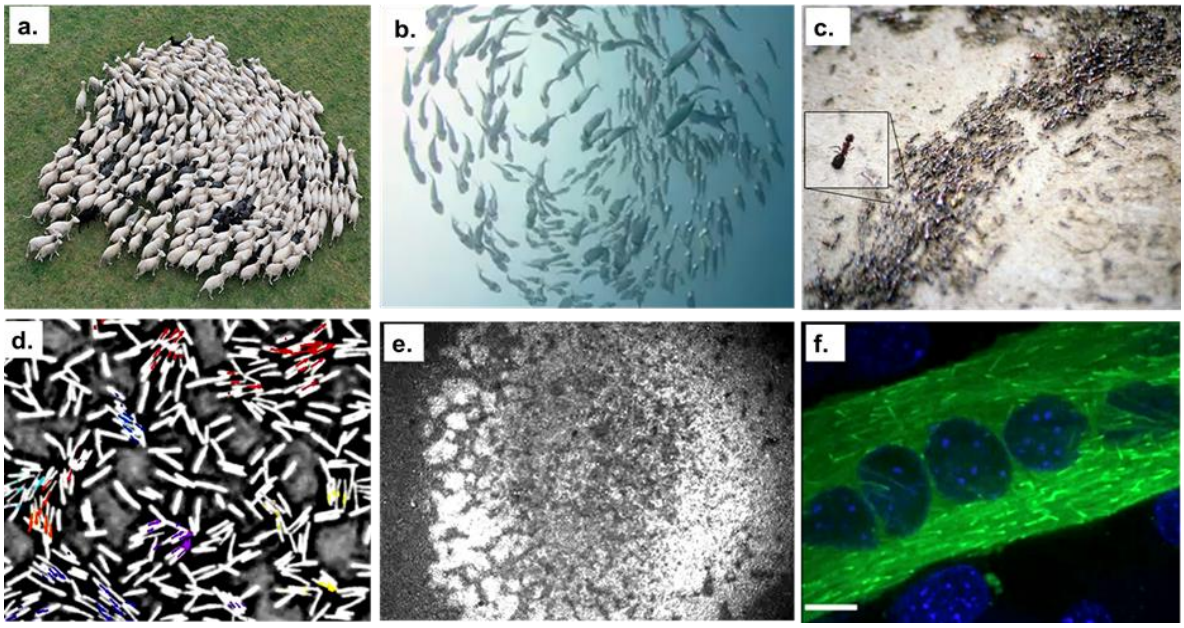

Figure 1.1: A gallery of images related to collective behavior[32]: (a) herd of sheep, (b) vortex by schools of fish, (c) swarming of ants, (d) assembly of bacteria, (e) cell migration, and (f) collective motion of cytoskeletal filaments *in vivo*.

The collective motion can be regarded as an emerging field on the borderline of several scientific disciplines. Thus, it is a multidisciplinary area with many applications, involving

statistical physics, technology, and branches of life sciences. A quantitative frame for describing the collective behavior of self-propelled particles enables important, highly desirable features of treating actual situations. For example, prediction of the global displacement of huge schools of fish may have direct economic advantages. Understanding the collective reaction of people to situations including panic may lead to saving lives. Using computer models to simulate migration of birds or mammals can assist in preserving biodiversity. In the field of technology, an excellent application of collective motion is in construction of programmable robots e.g; kilobots[33-35].

There are a huge number of examples of self-propelled objects both from the living (for instance; flock of birds, schools of fish, bacterial colony etc.) [Figure 1.1][32] and the non-living (e.g.; Janus particles, self-propelled colloids) worlds are known to exhibit collective motion. At first glance, these examples may look very diverse but a closer observation suggested all these systems share some common features. Such aforementioned non-equilibrium systems are consisted of many similar units. The interactions between the units can be simple (attraction/repulsion) or more complex (combinations of simple interactions) and can occur between neighbors in space or in an underlying network. These all suggest a universal organizing principle underlying the pattern formation in collective motion. Over the course of the last twenty-five years, several self-propelled particle models have been introduced to describe the collective motion. The first theoretical model to describe collective motion was introduced by Vicsek *et al.* in 1995[16]. In this *in silico* analysis, he suggested the density of moving agents and noise in movement of those agents are important parameters that govern the phase transition from disorder to ordered state in their collective motion[16]. The simplest version of Vicsek model was presented by Czirok *et. al* (1999) that have been used to model the collective motion in animals[17]. In 2002, Couzin *et al.* introduced the concept of multi-interactions between agents that was absent in Vicsek model[18]. Recently Konagaya group has developed a real-time 3D simulation method using graphics processor unit programming to study the dynamics of self-propelled objects[19-22]. However, all these models characteristically have a broad, partially empirically chosen parameter space and present generation of different mode of patterns, unfortunately most of which are not experimentally verified so far[36-50]. In order to explore the details of collective motion some large-scale data collection is now technologically possible by studying collective movements of animals in nature but they arise from observations rather than controlled experiments[51]. Therefore, it is indeed justified to

elucidate that the theory currently is ahead of the experiments to describe collective motion[52-53].

To overcome these limitations, well-controlled and quantifiable experimental systems is an urgent requirement. Multicellular biological systems such as, bacteria colonies or tissues allowed more control system but may have many hidden variables and interactions hindering proper examination of the theoretical models. Alongside, the ensembles of non-living motile particles such as shaken grains, and active colloids were also employed to study collective motion but still there are lack of sufficient controllable parameters. Recently, the bimolecular motor systems have attained considerable attention to study the behavior of self-propelled systems *in vitro*. The molecular nature of this system provides truly large system size in a well-controlled environment with system parameters that can be adjusted to a high precision.

1.3 Biomolecular motor system

Biomolecular motors are referred to as the smallest molecular machines that can convert chemical energy of adenosine tri-phosphate (ATP) into mechanical work[54-55]. Bimolecular motor systems consisted of cytoskeletal filaments and associated biomolecular motors. The availability and functionality of such autonomous actuators are experienced widely in cytoskeleton of the living cell.

1.3.1 Cytoskeleton: an ensemble of filamentous proteins

Cytoskeleton is the mechanical scaffold of the cells that maintain mechanical stiffness of the cells and assist numerous cellular function including cellular transport, cytokinesis, signaling, migration etc. In all eukaryotic cells, the cytoskeletal network consists of three different protein filaments namely intermediate filaments, actin, and microtubules associated with different regulatory proteins and cross-linkers[56]. Each type of filaments are assembled from different protein subunits and take parts in cellular activities. The intermediate filaments provide the cells mechanical strength[57-58]. The actin filaments determine the shape of the cells and whole-cell locomotion[57, 59].

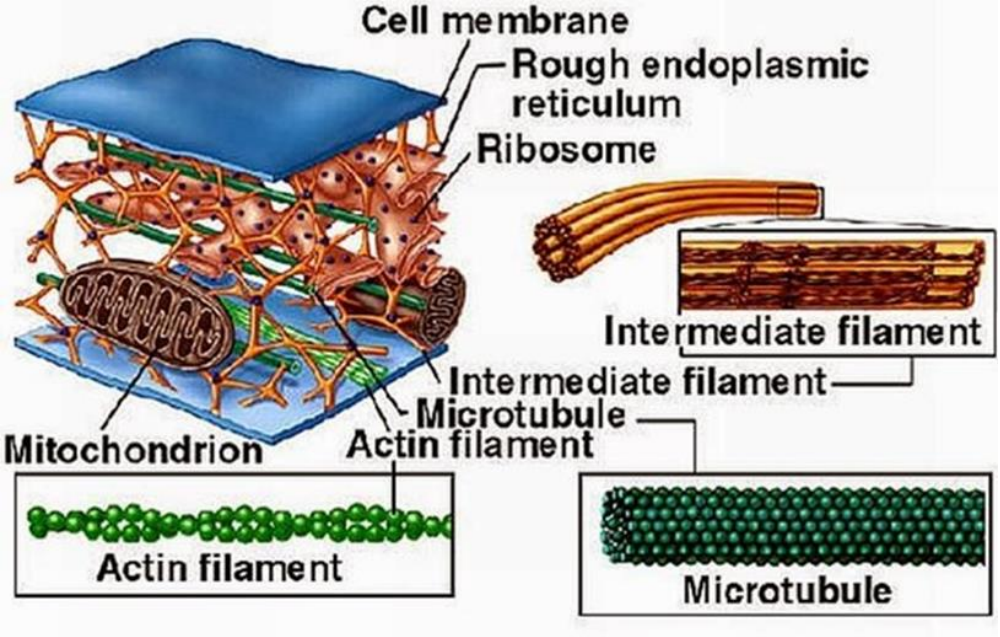

Figure 1.2: Illustration of cytoskeleton and protein filaments.

The microtubules determine the positions of membrane-enclosed organelles, shapes of the cells and direct intracellular transport[56, 60]. The eukaryotic cells.2, specifically the cytoskeleton has the ability to sense and respond to external mechanical stress[62, 64]. As a major component of the cytoskeleton, microtubules help transmitting the mechanical stresses and modulating mechanotransduction[65, 66].

1.3.2 Microtubules

Microtubules are filamentous protein polymers with an outer diameter of 25 nm[61]. It is polymerized from heterodimer α, β-tubulin. Each tubulin heterodimer has the molecular mass of ~110 kDa and is 8 nm long. The α and β tubulin consist of 450 and 445 amino acid residues respectively with ~40% amino acid sequence identical[63-65]. The α and β tubulin heterodimers are arranged head to tail into linear protofilaments (PFs),[61, 70] which in turn associate laterally and form pseudo helical structure of microtubules. The microtubule most commonly comprises of thirteen PFs *in vivo*, but this number can vary from nine to sixteen *in vitro*. In the course of microtubule assembly, the end exposed with β-tubulin monomer, called the plus end generally grows significantly faster than the other end with the exposed α-tubulin monomer, called minus end. The tubulins in adjacent protofilaments are laterally connected through homologous monomer contacts α-α, β-β expect for a seam where it is α-β[71-72]. Structural analysis revealed that the inter-PF tubulin bonds are weaker than the longitudinal ones along individual PFs[73].

The PF structure plays an important role in controlling microtubule mechanics. The different number of PFs in microtubule indicates the ability of larger deformations of the inter-PF bonds by PF twisting and which ultimately control the structural rigidity of microtubules[74].

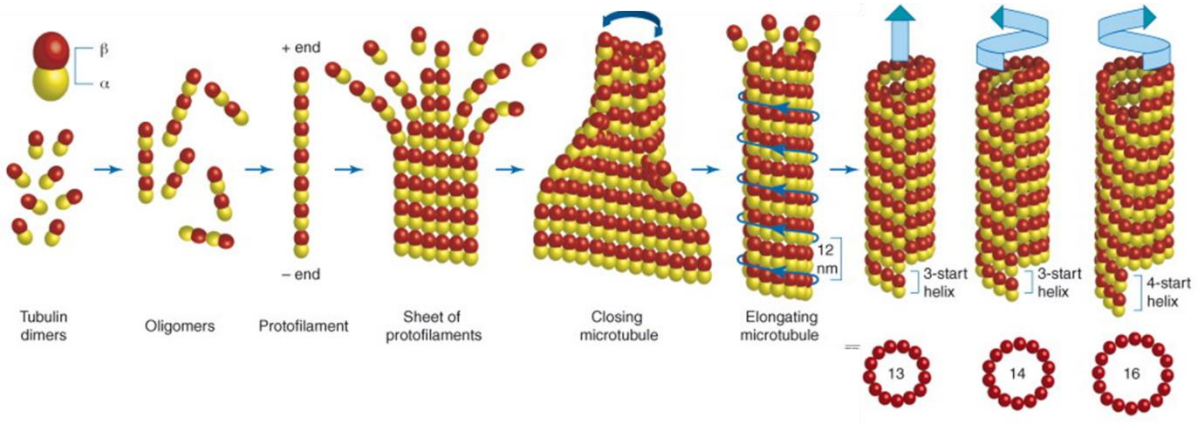

Figure 1.3: Polymerization and polymorphism of microtubules[74].

1.3.3 Biomolecular motors

Biomolecular motors such as kinesin, dynein and myosin are kinds of cytoskeletal filaments associated proteins, and they move along respective filaments by using the energy of ATP (adenosine triphosphate) hydrolysis. For example, kinesin and dynein move along microtubules and myosin does along F-actin. In this dissertation, I will use kinesin motor protein. kinesin motors are composed of dimer chains, where each amino acid chain folds into an ATPase domain, i.e. motor domain which bind with their associated filament and a tail domain which forms a coiled coil and bind with cargo molecules as shown schematically in **Figure 1.4**. Kinesin walks along microtubules uni-directionally (towards plus ends) by conformational change of motor domain induced by ATP binding and hydrolysis (**Figure 1.4**) [71-73]. The bimolecular motor systems play important roles in cell motility, cytokinesis, intracellular transport, cytoplasmic streaming, ciliary movement, muscle contraction, and so on[78].

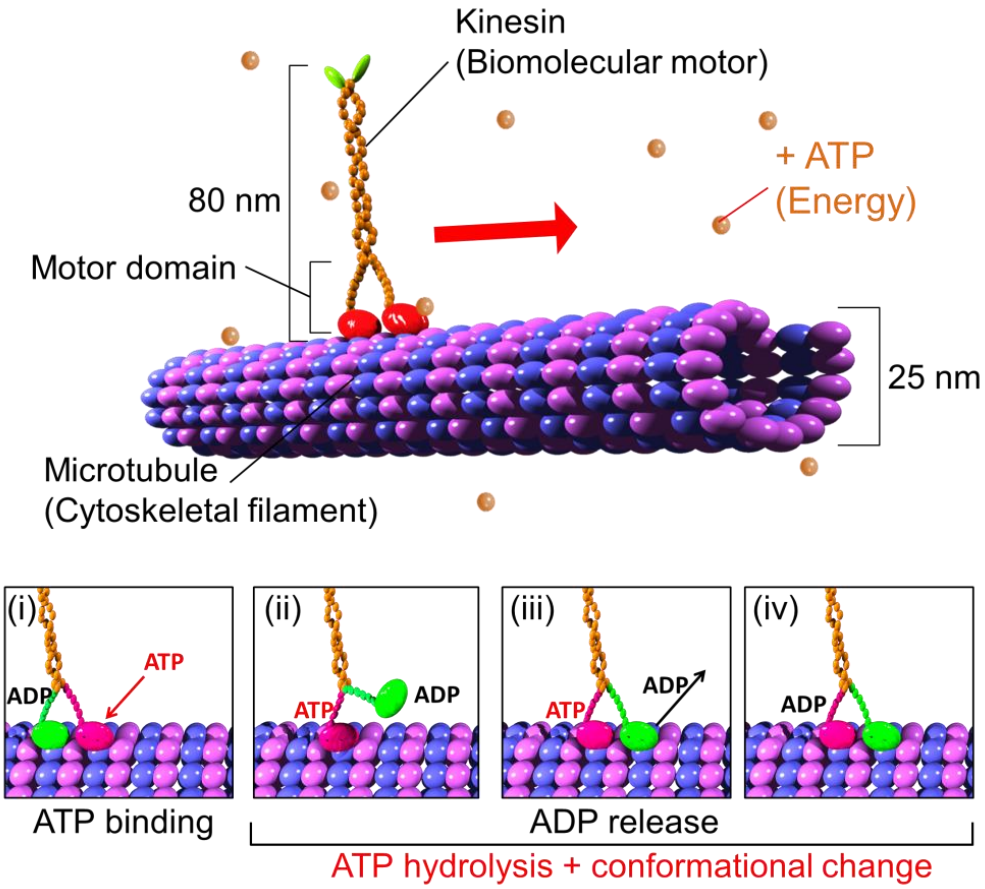

Figure 1.4: Schematic images of biomolecular motor system. This figure shows microtubule and kinesin system. (i)-(iv) Walking mechanism of kinesin along microtubule.

1.4 *In vitro* motility assay: tool to investigate dynamic behavior of self-propelled particles

In cells, the motor-proteins convert chemical energy, obtained from ATP hydrolysis, into mechanical work by moving along the associated cytoskeletal filaments. The system can be reversed *in vitro* where the motor-proteins adsorbed on a substrate, can use their ATPase sites to cause translation motion of the associated filaments. For instance, in the microtubule/kinesin system kinesin adsorbing on a surface of a substrtae i.e. the experimental flow cell, and propel microtubules in a persistent random walk over the substrate and in total, might be considered as self-propelled system. The self-propelled property by converting energy rendered them as biomolecular actuator, which can be designed for developing molecular shuttle by guiding over their direction of motion and transport properties.

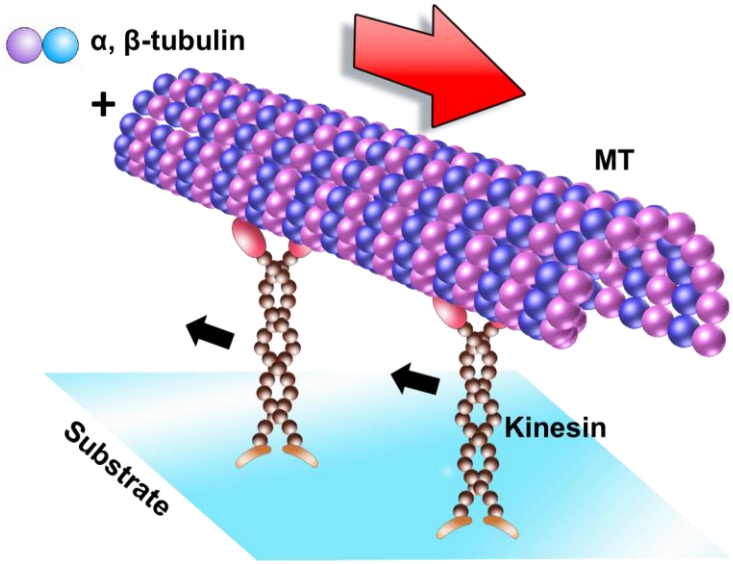

Figure 1.5: *In vitro* gliding assay of microtubule on kinesins.

The history of gliding assay is old enough and started from the discovery of Vale and his colleagues. In 1985 they discovered uni-directional gliding motion of microtubules in the cell extract from squid axon on a substrate[79]. They revealed gliding motion of microtubules was driven by biomolecular motors (kinesin and dynein) absorbed on the substrate and named this method as "*in vitro* motility assay" (Figure 1.5). Later, Spudich also developed a similar *in vitro* motility assay in which F-actin moved on a glass surface coated with myosin[80].

To further explore the collective motion using *in vitro* motility assay, considerable efforts have been made to achieve directed motility, control of moving direction, by employing different methods like chemical patterning of biomolecular motors[82-86] or fabricating topographical patterns by using photolithography technique[87-99]. With a view of application as nano-machine in nanotechnology and other fields, the effect of external mechanical stimuli on the motility of the individuals has been also studied and found that direction of the moving filaments can be controlled by applying various external stimuli like electric field (**Figure 1.6A**)[100-104] and magnetic field (**Figure 1.6B**)[105]. Recently, Inoue *et al*. has investigated the response of microtubules to external mechanical stress and found that microtubules can change their moving direction according to mode of stress [Figure 1.6C][106].

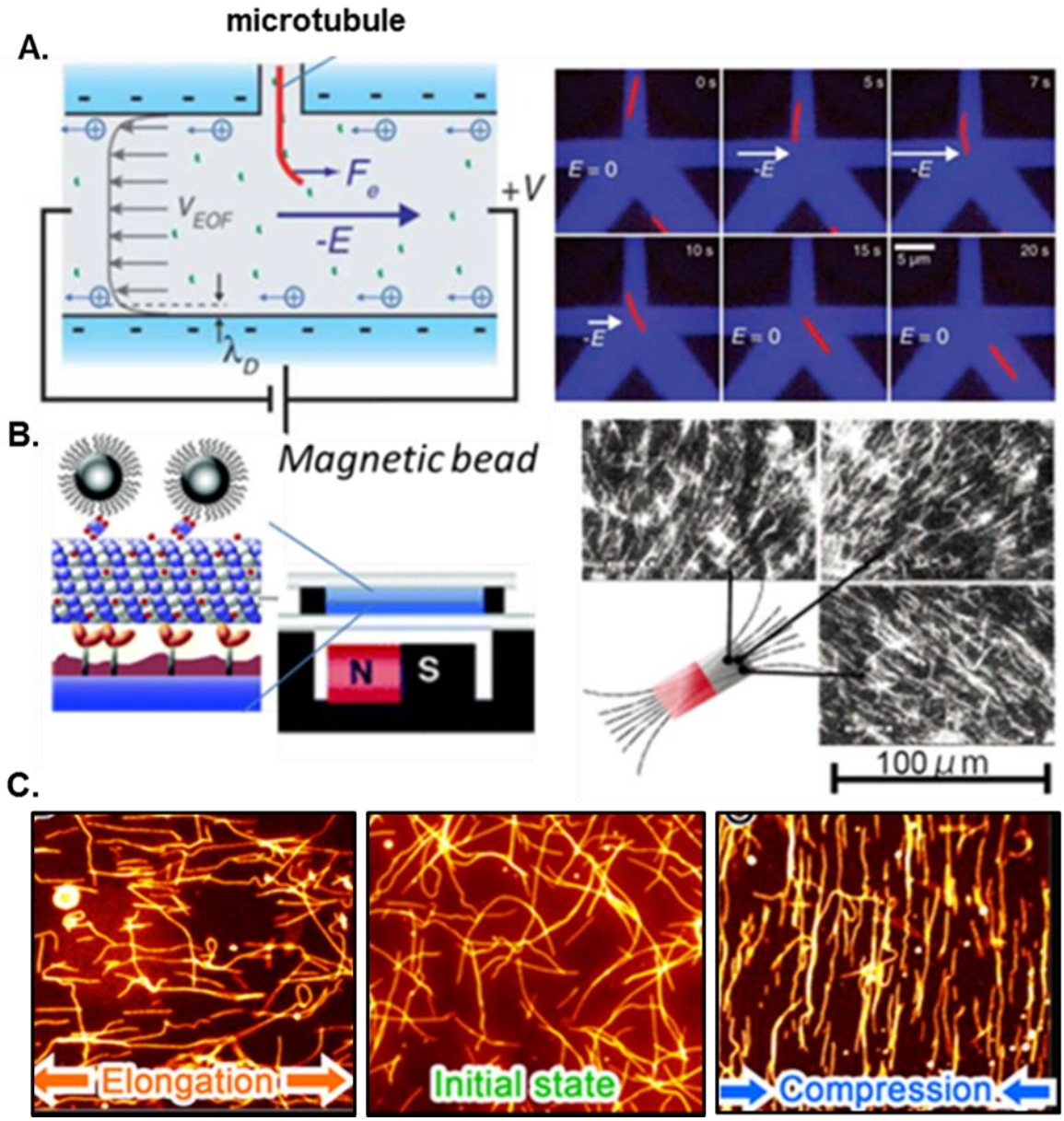

Figure 1.6: Controlling the direction of microtubule movements by electrical steering (A), alignment of magnetic nanoparticle functionalized microtubules (B) and response of microtubule to external mechanical stress (C).

Thus, the *in vitro* motility assay that has been developed to demonstrate gliding motion of filamentous proteins actin or microtubule on the surface coated with biomolecular motor such as myosin or kinesin and dynein respectively might be a suitable method to study the behavior of self-propelled objects and opened the door to develop artificial micro-devises.

1.5 Collective motion of bio-molecular motor systems

One of the most fundamental feature of collective motion is the evolution of fascinating large-scale patterns through active self-organization of biomolecular motor systems. Such self-organization of biomolecular motor systems will foster the development of motor protein based artificial robot and at the same time will help to understand various *in vivo* phenomena observed in the living world.

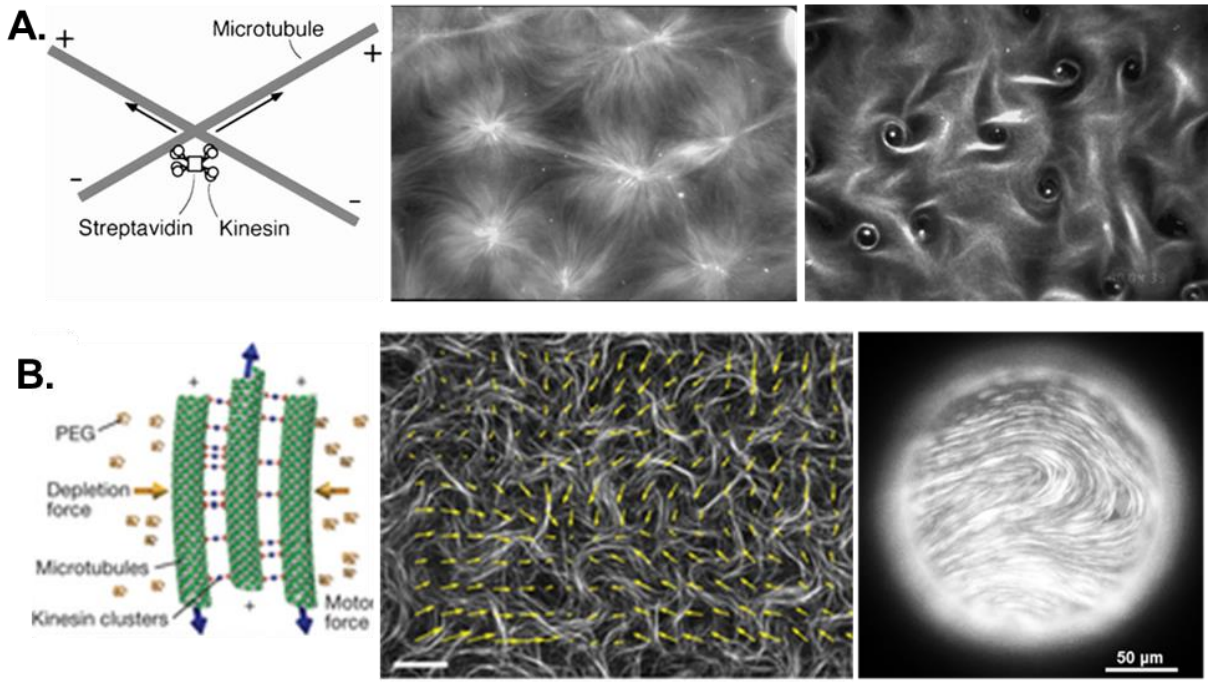

Figure 1.7: Active self-organization of microtubules cross-linked by kinesin multi cluster (**A**) Schematic diagram of microtubules with kinesin multi cluster and formation of aster and vortex pattern emerging from microtubules[107]. (**B**) Active nematic network of microtubules assembled through kinesin clusters[109].

Hence, many research groups tried to establish a well-defined system to study the collective motion of biomolecular motor system and demonstrate pattern formation using it. Nedelec, Surrey and Karsenti have reconstructed aster and vortex pattern from microtubules conjugating with kinesin multi cluster (Figure 1.7A) [107]. This could be implicated in the self-assembly processes observed *in vivo* e.g; the formation of the mitotic spindle. Recently, this method also contributes to reproduce active nematic network of microtubules like cytoplasmic streaming observed in *in vivo* (Figure 1.7B) [107-109].

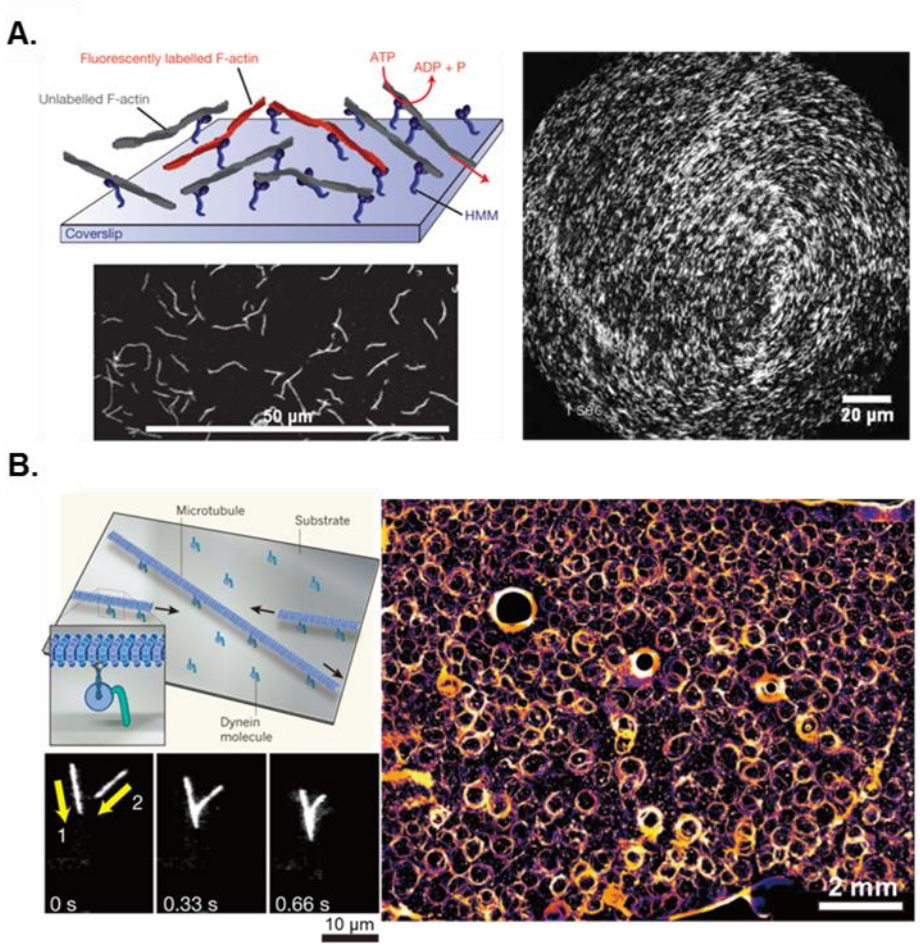

Figure 1.8: Spontaneous generation of patterns in collective motion of biomolecular motor systems. (A) Polar patterns generated in acto-HMM system[110] and (B) large-scale vortex lattices emerged in microtubule-dynein system[111].

Later on, Bausch *et al.* used the *in vitro* motility assay of highly concentrated F-actins propelled by immobilized myosin on a glass surface to perform collective motion[110]. They reported F-actins can exhibit synchronized motion (collective motion) due to excluded volume effect and fascinating wave-like or a vortex patterns emerge from collective motion of large population of F-actin (**Figure 1.8A**). A new dimension in field of collective motion opened when Oiwa group reported the emergence of streaming like pattern and lattice of vortices pattern from highly concentrated microtubules moving on a dynein-coated surface **(Figure 1.8B)**[111]. Thus, these all experimental verifications suggest that individual cytoskeletal filaments propelled by biomolecular motors move independently and randomly in low density that they exhibit collective behavior and assemble into hierarchical structures by self-organization obtained through collective motion at high density. However, failure in demonstrating the collective motion of microtubules driven by kinesins, the most widely used

biomolecular motor *in vitro*, raised a question about the universality of the biomolecular motor systems for demonstrating the collective motion.

1.6 Purpose of this dissertation

In this dissertation, the *in vitro* study on the emergence of collective motion of microtubules driven by kinesin and effects of physical properties of microtubules on the collective motion have been summarized in 5 chapters including general introduction and concluding remarks.

In **chapter 1**, the purpose of this dissertation and background of this research have been described.

In **chapter 2**, I have demonstrated the collective motion of microtubules on kinesin-coated substrate through employing depletion force in the gliding assay. The role of concentration of microtubules and extent of depletion force in the kinetics of collective motion of microtubules has been also studied and described here.

In **chapter 3**, I have explored how the mechanical properties of microtubules can govern the pattern formation in collective motion. I found that the rigidity of microtubules can regulate the mode of collective motion of microtubules and reported that structurally flexible microtubules generate local streams and rigid microtubules form large spiral pattern in collective motion.

In **chapter 4**, I have investigated the response of collectively moving microtubule to external stimuli such as mechanical stress. First, development of an indentation chamber for applying external stimuli to substrate of motility assay was established. The effect of indentation stress on the collective behavior of microtubules was studied and discussed here.

In **chapter 5**, all the important outcomes and future prospects of this research work have been discussed.

1.7 References

1. T. Vicsek, *Nature,* 2001, **411,** 421.

2. T. Vicsek, and A. Zafeiris, *Phys. Rep*., 2012, **517**, 71.

3. J. K. Parrish, S. V Viscido, and D. Grunbaum, *Biol. Bull*., 2002, **202**, 296.

4. K. Kruse, J. F. Joanny, F. Julicher, J. Prost, and K. Sekimoto, *Phys. Rev. Lett.,* 2004, **92**, 078101.

5. M. Loose, E. Fischer-Friedrich, J. Ries, K. Kruse, and P. Schwille, *Science,* 2008, **320**, 789.

6. I. D. Couzin, J. Krause, N. R. Franks, and S. A. Levin, *Nature,* 2005, **433**, 513.

7. I. H. Riedel, K. Kruse, and J. A. Howard, *Science,* 2005, **309**, 300.

8. C. Dombrowski, L. Cisneros, S. Chatkaew, R. E. Goldstein, and J. O. Kessler, *Phys. Rev. Lett.,* 2004, **93**, 098103 (1-4).

9. A. Czirok, E. Ben-Jacob, I. Cohen, and T. Vicsek, *Phys. Rev. E,* 1996, **54**, 1791.

10. F. J. Nedelec, T. Surrey, A. C. Maggs, and S. Leibler, *Nature,* 1997, **389**, 305.

11. J. Buhl, D. J. T. Sumpter, I. D. Couzin, J. Hale, E. Despland, E. Miller, and S. J. Simpson, *Science,* 2006, **312**, 1402.

12. I. D. Couzin, and J. Kraus, *Adv. Stud. Behav.,* 2003, **32**, 1.

13. I. D. Couzin, J. Krause, N. R. Franks, and S. A. Levin, *Nature,* 2005, **433**, 513.

14. F. Cucker, and E. Mordecki, *J. Math. Pure. Appl.,* 2008, **89**, 278.

15. F. Cucker, and S. Smale, *IEEE. T. Automat. Contr*., 2007, **52**, 852.

16. T. Vicsek, A. Czirok, E. Ben-Jacob, I. Cohen, and O. Shochet, *Phys. Rev. Lett*., 1995, **75**, 1226.

17. A. Czirók, and T. Vicsek, *Statistical Mechanics of Biocomplexity*, 1999, Springer Berlin / Heidelberg, 152.

18. I. D. Couzin, J. Krause, R. James, G. D. Ruxton, and N. R. Franks, *J. Theor. Biol.*, 2002, **218**, 1.

19. G. Gutmann, D. Inoue, A. Kakugo, and A. Konagaya, "Parallel Interaction Detection Algorithms for a Particle-based Live Controlled Real-time Microtubule Gliding Simulation System Accelerated by GPGPU" New Generation Computing , DOI 10.1007 / s 00354-017-0011- Five

20. G. Gutmann, D. Inoue, A. Kakugo, and A. Konagaya, *New Generation Computing*, 2016, **13**, 108.

21. G. Gutmann, D. Inoue, A. Kakugo, and A. Konagaya, *Int. J. Autom. Comput*., 2016, 2, 1

22. G. Gutmann, D. Inoue, A. Kakugo, and A. Konagaya, Communications in Compuer and Information Science, 2014, **461**, 13.

23. A. Tero, S.Takagi, T. Saigusa, K. Ito, D. P. Bebber, M. D. Fricker, K. Yumiki, R. Kobayashi, T. Nakagaki, and T. Nakagaki, *Science*, 2010, **327**, 439.

24. S. R. McCandlish, A. Baskarana and M. F. Hagan, *Soft Matter*, 2012, **8**, 2527.

25. M. Rubenstein, A.Cornejo, and R. Nagpal, *Science* 2014, **345**, 795.

26. A. Kudrolli, G. Lumay, D. Volfson, and L. S. Tsimring, *Phys. Rev. Lett*., 2008, **100**, 058001.

27. J. S. Olafsen, and J. S. Urbach, *Phys. Rev. Lett*., 1998, **81**, 4369.

28. J. C. Tsai, F. Ye, J. Rodriguez, J. P. Gollub, and T. C Lubensky, *Phys. Rev. Lett*., 2005, **94**, 214301.

29. P. B. Umbanhowar, F. Melo, and H. L Swinney, *Nature*, 1996, **382**, 793.

30. J. Deseigne, S. Leonard, O. Dauchot, and H. Chaté, *Soft Matter*, 2012, **8**, 5629.

31. H. P. Zhang, A. Beer, E.-L. Florin, and H. L. Swinney, *Proc. Natl Acad. Sci. USA*, 2010, **107**, 13626.

32. T. Vicsek, and A. Zafeiris, *Physics Reports*, 2012, **517**, 71.

33. W.-M. Shen, and M. Rubenstein, *Intelligent Robots and Systems (IROS), 2010 IEEE/RSJ International Conference*, 2014, 508.

34. M. Rubenstein, C. Ahler, and R. Nagpal, *IEEE International Conference on Robotics and Automation*, 2014, 3293.

35. N. Hurst, "These $10 Robots Will Change Robotics Education". Wired, 2014.

36. D. L. Blair, T. Neicu, and A. Kudrolli, *Phys. Rev. E*, 2003, **67**, 031303.

37. A. Kudrolli, G. Lumay, D. Volfson, and L. S. Tsimring, *Phys. Rev. Lett.*, 2008, **100**, 058001.

38. J. Deseigne, O. Dauchot, and H. Chate, *Phys. Rev. E*, 2010, 105.

39. V. Narayan, N. Menon, and S. Ramaswamy, *Journal of Statistical Mechanics: Theory and Experiment*, 2006, 01005.

40. D. Yamada, T. Hondou, and M. Sano, *Phys. Rev. E*, 2003, **67**, 040301.

41. M. Ibele, T. E. Mallouk, and A. Sen, *Angewandte Chemie International Edition*, 2009, **48**, 3308.

42. A. Baskaran, and M. C. Marchetti, *Phys. Rev. E*, 2008, **77**, 011920.

43. A. Baskaran, and M. C. Marchetti, *Proc. Natl. Acad. Sci. U. S. A.*, 2009, **106**, 15567.

44. E. Bertin, M. Droz, and G. Gregoire, *Phys. Rev. E*, 2006, **74**, 022101.

45. A. Besser, and U. S. Schwarz, *N. J. Phys*. 2007, **9**, 425.

46. K. Kruse, and F. Jülicher, *Phys. Rev. Lett*., 2000, **85**, 1778.

47. K. Kruse, S. Camalet, and F. Jülicher, *Phys. Rev. Lett*., 2001, **87**, 138101

48. K. Kruse, and F. Jülicher, *Phys. Rev. E*, 2003, **67**, 051913.

49. T. B. Liverpool, and M. C. Marchetti, *Phys. Rev. Lett*., 2003, **90**, 138102.

50. R. Peter, V. Schaller, F. Ziebert, and W. Zimmermann, *New J. Phys*., 2008, **10**, 035002

51. N. R. Franks, A.Worley, K. A. J. Grant, A. R. Gorman, V. Vizard, H. Plackett, C.Doran, M. L. Gamble, M. C. Stumpe, and A. B. Sendova-Franks, *Proc. R. Soc. B*, 2016, **283**, 20152946;

52. J. Deseigne, O. H. Dauchot, and Chaté, *Phys. Rev*. *Lett.*, 2010, **105**, 098001.

53. J. Toner, Y. H. Tu, and S. Ramaswamy, *Ann. Physc*., 2005, **318**, 170.

54. J. A. Cooper, *Annu. Rev. Physiol.*, 1991, **53**, 585.

55. M. Umeda, and K. Emoto, *Chem. Phys. Lipids*, 1999, **101**, 81.

56. B. Alberts, A Johnson, J. Lewis, M. Raff, K. Roberts, P. Walter, *Molecular biology of the cell*, Gaeland Science, 2008, 5th edition, 965.

57. B. T. Helfand, L. Chang, and R. D. Goldman, *J. Cell Sci.*, 2004, **117**, 133.

58. H. Hermann, and H. Aebi, *Annu. Rev. Biochem*, 2004, **73**, 749

59. J. Howard, Mechanics of motor proteins and the cytoskeleton, Sinauer, Sunderland 2001

60. J. Lippincott-schwartz, J. G. Donaldson, A. Schwizer, E. G. Berger, H. Hauri, L. C. Yuan, and R. D. Klausner, 1990, **60**, 821.

61. E. Nogales, *Annu, Rev. Biophysc. Struct*. 2001, **30**, 397

62. M. A. Wozniak, and C. S. Chen, *Nature Rev Mol. Cell Biol*, 2009, **10**, 34.

63. C. M. Nelson, R. P. Jean, J. L. Tan, W. F. Liu, N. J. Sniadecki, A. A. Spector, and C. S. Chen, *Proc. Natl. acad. Sci. USA*, 2005, **102**, 11594.

64. G. W. Brodland, and R. J. Gordon, *Biomech. Eng*, 1990, **112**, 319.

65. S. Na, O. Collin, F. Chowdhury, B. Tay, M. Ouyang, and Y. Wang, *N. Proc. Natl. Acad. Sci. USA*, 2008, **105**, 6626.

66. J. P. Kerr, P. Robison, G. Shi, A.y I. Bogush, A. M. Kempema, J. K. Hexum, N. Becerra, D. A. Harki, S. S. Martin, R. Raiteri, B. L. Prosser, and C. W. Ward, *Nat. Commun*., 2015, **6**, 8526.

67. *E. Nogales, S. G. Wolf, K. H. Downing, Nature, 1998, **391**, 199*

68. H. Ponstingl, E. Kraush, M. Little, and T. Kempf, *PNAS*, 1981, **78**, 2757

69. E. Kraushs, M. Little, T. Kempf, R. H. warbinek, W. Ade, and H Ponstingl, *PNAS*, 1981, **78**, 4156.

70. A. Desai, and T. J. Mitchison, *Annu. Rev. Cell Dev, Biol*, 1997, **13**, 83.

71. H. W. Wang, and E. Nogales, *Nature*, 2005, **435**, 911

72. E. Nogales, M. Whittaker, R. A. Milligan, and K.H. Downing, *Cell*, 1999, **96**, 79

73. O. Kononova, Y. Kholodov, K. E. Theisen, K. A. Marx, R. I. Dima, F. I. Ataulllakhanov, E. L. Grishchuk, and V. J. Barseov, *J. Am. Chem. Soc.*, 2014, **136**, 17036

74. R. D. Vale, C. M. Capoin, F. Malik, F. J. kull, and R. A. Millgai, *J. Biol. Chem*.,1994, **269**, 23769.

75. F. Pampaloni, and E. Florin, *Trends. Biotechnol.* 2008, **26**, 302.

76. R. D. Vale, *Cell*, 2003, **112**, 467.

77. R. B. Valee, J. C. Willaimas, D. Varma, and L. E. J. Barnhart, *Neurobiol*, 2004, **58**, 189

78. A. Gennerich, and R. D. Vale, *Curr. Opin. Cell Biol*. 2009, **21**, 59.

79. B. Alberts, J. Lewis, M. Raff, P. Walter, K. Roberts, A. Johnson, and K. Nakamura, *Molecular Biology of the Cell 5th edition, Garland Science*, 2010, 965.

80. B. J. Schnapp, R. D. Vale, M. P. Sheetz, and T. S. Reese, *Cell*, 1985, **40**, 455.

81. S. J. Kron, and A. Hudspeth, *J. Proc, Natl. Acad. Sci. USA*, 1986, **83**, 6272.

82. J. A. Jaber, P. B. Chase, and J. B. Schlenoff, *Nano Lett*., 2003, **3**, 1505.

83. L. Ionov, M. Stamm, and S. Diez, *Nano Lett*., 2005, **5**, 1910.

84. C. Reuther, L. Hajdo, R. Tucker, A. A. Kasprzak, and S. Diez, *Nano Lett*., 2006, **6**, 2177.

85. V. Schroeder, T. Korten, H. Linke, S. Diez, and I. Maximov, *Nano Lett*., 2013, **13**, 3434.

86. A. Biswas, A. Saha, D. Ghosh, B. Jana, and S. Ghosh, *Soft Matter*, 2014, **10**, 2341.

87. C. Reuther, R. Tucker, L. Ionov, and S. Diez, *Nano Lett*., 2014, **14**, 4050

88. H. Suzuki, A. Yamada, K. Oiwa, H. Nakayama, and S. Mashiko, *Biophys. J.* 1997, **72**, 1997.

89. Y. Hiratsuka, T. Tada, K. Oiwa, T. Kanayama, and T. Q. P. Uyeda, *Biophys. J.*, 2001, **81**, 1555.

90. H. Hess, J. Clemmens, D. Qin, J. Howard, and V. Vogel, *Nano Lett*., 2001, **1**, 235.

91. J. Clemmens, H. Hess, R. Doot, C. M. Matzke, G. D. Bachand, and V. Vogel, *Lab Chip*, 2004, **4**, 88.

92. C. T. Lin, M. T. Kao, K. Kurabayashi, and E. Meyhofer, *Nano Lett.*, 2008, **8**, 1041.

93. M. G. L. Van den Heuvel, C. T. Butcher, R. M. M. Smeets, S. Diez, and C. Dekker, *Nano Lett*., 2005, **5**, 1117.

94. S. G. Moorjani, L. Jia, T. N. Jackson, and W. O. Hancock, *Nano Lett,*. 2003, **3**, 633.

95. H. Hess, C. M. Matzke, R. K. Doot, J. Clemmens, G. D. Bachand, B. C. Bunker, and V. Vogel, *Nano Lett*., 2003, **3**, 1651.

96. M. Lard, L. ten Siethoff, J. Generosi, A. Mansson, and H. Link, *Nano Lett.*, 2014, **14**, 3041.

97. Ji. Li, Y. Jia, W. Dong, X. Feng, J. Fei, and J. Li, *Nano Lett.,* 2014, **14**, 6160.

98. D. Steuerwald, S. M. Früh, R. Griss, R. D. Lovchik, and V. Vogel, *Lab Chip* 2014, **14**, 3729.

99. S. B. Asokan, L. Jawerth, R. L Carroll, R. E. Cheney, S. Washburn, and R. Superfine, *Nano Lett.*, 2003, **3**, 431.

100. M. G. L Van den Heuvel, M. P. De Graaff, and C. Dekker, *Science,* 2006, **312**, 910.

101. T. Kim, M.-T. Kao, E. F. Hasselbrink, and E. Meyhofer, *Nano Lett.*, 2007, **7**, 211.

102. T. Kim, M. T. Kao, E. F. Hasselbrink, and E. Meyhofer, *Biophys. J.*, 2008, **94**, 3880.

103. Y. Lee, and P. Famouri, *J. Colloid Interface Sci*, 2013, **394**, 318.

104. A. Sikora, J. Ramón-Azcón, K. Kim, K. Reaves, H. Nakazawa, M. Umetsu, I. Kumagai, T. Adschiri, H. Shiku, T. Matsue, W. Hwang, and W. Teizer, *Nano Lett,*. 2014, **14**, 876.

105. M. Platt, W. O. Hancock, G. Muthukrishnan, and M. E. Williams, *J. Am. Chem. Soc*., 2005, **127**, 15686.

106. D. Inoue, T. Nitta, A. M. R. Kabir, K. Sada, J. P. Gong, A. Konagaya, and A. Kakugo, Nat. Commun., 2016, 7, 12557:1-10.

107. F. J. Nédélec, T. Surrey, A. C. Maggs, and S. Leible, *Nature,* 1997, **389**, 305.

108. T. Sanchez, D. Welch, D. Nicastro, Z. Dogic, *Science* 2011, **333**, 456

109. T. Sanchez, D. T. N. Chen, S. J. DeCamp, M. Heymann, and Z. Dogic, *Nature,* 2012, **431**, 491.

110. V. Schaller, C. A. Weber, C. Semmrich, , E. Frey, and A. R. Bausch, *Nature*, 2010, **467**, 73.

111. Y. Sumino, H. K. Nagai, Y. Shitaka, D. Tanaka, K. Yoshikawa, H. Chate, and K. Oiwa, *Nature*, 2012, **483**, 448.

Chapter 2

Emergence of collective motion of microtubules driven by kinesins: role of depletion force and microtubule concentrations

Abstract

Collective motion is a fascinating exhibition of coordinated behavior of self-propelled objects, which is often associated with the formation of large-scale patterns. Nowadays, *in vitro* gliding assay is being considered a model system to experimentally investigate various aspects of group behavior and pattern formation by self-propelled objects. In the *in vitro* gliding assay, cytoskeletal filaments F-actin or microtubules are driven by surface immobilized associated biomolecular motors myosin or dynein respectively. Although F-actin/myosin or microtubule/dynein system was found promising in understanding the collective motion and pattern formation by self-propelled objects, the most widely used biomolecular motor system microtubule/kinesin could not be successfully employed so far in this regard. Failure in exhibiting collective motion by kinesin driven microtubules is attributed to the intrinsic property of kinesin, which was speculated to affect the behavior of individual gliding microtubules and mutual interaction among them. In this work, for the first time, I have demonstrated the collective motion of kinesin driven microtubules by regulating mutual interaction among the gliding microtubules, by employing depletion force among them. Proper regulation of the mutual interaction among the gliding microtubules through employment of the depletion force was found to allow the exhibition of collective motion and stream pattern formation by microtubules. I also investigated the role of concentration of microtubules and depletion force in the emergence of collective motion of microtubules. Critical concentrations are found for both the microtubules and depletant for demonstrating the collective motion of microtubules. More importantly, kinetics of the collective motion is found significantly dependent on both of the concentration of microtubules and depletant. Substantial variations in time course of emergence of the collective motion of microtubules were observed in response to the changes in concentration of the microtubules and depletant.

2.1 Introduction

Collective motion is an entrancing display of coordinated behavior of moving or self-propelled objects[1-3]. A wide range of self-propelled objects such as animals, birds, cells, bacteria, etc. exhibit collective motion in nature, most often which is associated with formation of fascinating large scale patterns[4-10]. *In silico* works significantly contributed to much of our understandings of the coordinated behavior and pattern formation by the self-propelled objects[11-18]. A suitable experimental system has long been awaited for demonstrating the collective motion *in vitro* in order to verify the mechanisms of collective motion and pattern formation. In recent years, biomolecular motor systems F-actin/myosin and microtubule/dynein have emerged as ideal candidates for experimentally demonstrating the collective motion through *in vitro* gliding assay[19-20]. These experimental evidences have emphasized the importance of local interaction between gliding cytoskeletal filaments in the collective motion and pattern formation. Thus, the *in vitro* gliding assay offers simple technique to investigate experimentally roles of parameters that govern collective motion and pattern formation. However, the investigation using biomolecular motor system was not always successful due to failure of biomolecular motor systems in exhibiting collective motion. For instance, it was reported that microtubule/kinesin, the most widely used biomolecular motor system [20], failed to exhibit collective motion and consequently formed no pattern which has been attributed to the intrinsic property of kinesin that is speculated to affect the behavior of individual microtubules and local interaction among them[19]. Although formation of an active gel of microtubules cross-linked via kinesin clusters has been reported[21], it was not sufficient to understand the coordinated behavior of kinesin driven microtubules, demonstrated for other biomolecular motors systems using the *in vitro* gliding assay.

In this work, the first ever collective motion of microtubules on kinesin based motility assay has demonstrated. It is found that regulation of local interaction among gliding microtubules allows them exhibiting collective motion even on a kinesin coated surface. The interaction of gliding microtubules has been regulated by employing depletion force among them. In a suspension of large and small colloidal particles, the pressure of the latter produces an attractive force between the former. This is referred to as the depletion force. For instance, the colloidal particles or macromolecules suspended in polymer solution such as methyl cellulose or poly(ethylene glycol)[22-29] experience depletion force. Methyl cellulose induced depletion force is found to increase the probability of attractive collision between gliding microtubules, which

consequently allowed emergence of collective motion and finally resulted in pattern formation by microtubules.

Moreover, how different parameters influence the emergence of collective motion of the kinesin driven microtubules has not been well understood since role of different parameters in the collective motion of microtubules have not been investigated yet. Next, by examining the effects of concentration of microtubules and a depletant (methyl cellulose), the time course of emergence of collective motion i.e., kinetics of transition of microtubule's orientation from an isotropic (random) to a nematic phase has been explore in detail. The concentration of both the microtubules and methyl cellulose has profound influence on the kinetics of emergence of collective motion of the kinesin driven microtubules. High concentration of microtubules or methyl cellulose can substantially accelerate the phase transition of microtubules, i.e. emergence of the collective motion of microtubules. Moreover, I have determined minimal concentration of both of the microtubules and methyl cellulose is required for demonstrating the collective motion. The minimal concentration of microtubules is altered when the concentration of methyl cellulose employed in the gliding assay is varied and vice versa.

These results on depletion force mediated collective motion and subsequent pattern formation by microtubules on a kinesin coated substrate indicate that emergence of collective motion is independent of the type of biomolecular motor used in the *in vitro* gliding assay, if the interaction among the cytoskeletal filaments is properly regulated. The work in this chapter offers a universal method for demonstrating the collective motion of biomolecular motor driven cytoskeletal protein filaments using the *in vitro* gliding assay. This work also provides a comprehensive scenario of the role of microtubule concentration and depletion force on the kinetics of collective motion of microtubules driven by kinesins, which consequently would help obtain a better understanding of the coordinated behavior of other self-propelled objects[30-32].

2.2 Results and discussion

2.2.1 Design of an experimental system to investigate the collective motion of microtubules

To study the collective motion of microtubules in kinesin based i*n vitro* motility assay, first I constructed a simple experimental system [Figure 2.1] consisting rhodamine-labeled microtubules attached to kinesin motor proteins adsorbed on a glass substrate (see experimental section 2.4.2). The microtubules were prepared by polymerizing fluorescence labeled tubulins (molecular weight ~55 KDa) in presence of guanosine-5′-triphosphate (GTP). Due to the stochastic assembly process the length of the microtubules varied over a wide range. I calculated the number average length (<Ln>) and weight-average length (<Lw>) of microtubules as 15.23 μm and 16.69 μm respectively (number of microtubules considered: 100), from which the polydispersity index (Lw / Ln) was found to be ~1.1[33].

The motility of microtubules was initiated by adding 10 mM adenosine tri-phosphate (ATP). Depletion force was introduced to the system by employing methyelcellulose as a depletant. Methyl cellulose was employed in the system by mixing methyl cellulose solution with ATP buffer and applying in flow cell after fixing microtubules on kinesin motor proteins.

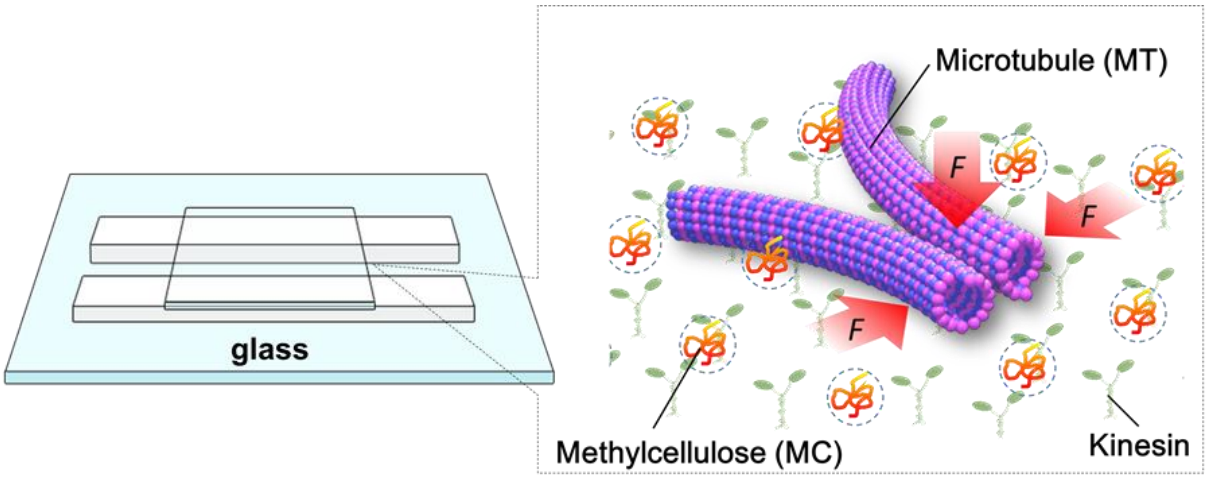

Figure 2.1: Schematic diagram of the experimental set up and illustration of the *in vitro* motility assay used to investigate collective motion of microtubules driven by kinesins.

2.2.2 The effect of depletion force on the assembly of microtubules

Colloids and proteins immersed in a suspension of small, non-adsorbing particles, collectively called the depletant experience effective attractive interactions known as the depletion interaction[34]. The mechanism of such effective attractive interaction was first predicted theoretically by Asakura and Oosawa (A-O)[34]. They has suggested that if the inter distance between colloids or proteins in the suspension is less than the size of suspending depletant species, the latter are expelled (depleted) from the gap between the colloids or proteins leading to an anisotropy of the local pressure. Therefore, the accessible volume for the depletant increases and which consequently upraises the total entropy of the system. As, the mixture of colloids and depletant is an athermal system, their free energy $\Delta G = -T\Delta S$ decreases, resulting in an attractive interaction. This is a purely entropic force, which means that its' properties are not determined by the underlying microscopic interaction such as the van der Waals interaction between like objects. The properties of this force is determined by the tendency of the whole system to increase its entropy as stated by the second law of thermodynamics. This leads to the force favoring clustering of objects immersed in such a suspension[35]. This ubiquitous effect plays a vital role to induce robust *in vitro* bundling of biological filaments, even in the absence of any specific crosslinking proteins. For instance, both actin filaments and microtubules are found to spontaneously assemble into bundles in the presence of non-adsorbing polymers[36-40].

So firstly, I want to investigate how depletion force induced by methyl cellulose will affect the assembly of microtubules in bulk solution. To do so, the fluorescence labeled microtubules were suspended in methyl cellulose of different concentration and their organization was monitored using fluorescence microscope. At 0.1 wt% of methyl cellulose solution, microtubules were found to form asters like aggregation [Figure 2.2]. On further increasing the methyl cellulose concentration to 0.3 wt%, thick and long bundles of microtubule were formed owing to increased attractive interaction among microtubules [Figure 2.2]. In contrast, aggregation and bundle formation of microtubules were not observed in the absence of methyl cellulose (0.0 wt%) as shown in Figure 2.2. This result indicates that depletion force induced by methyl cellulose can effectively enhance the attractive interaction among microtubules and allow their assembly formation, which coincides well with the previous reports[36-40].

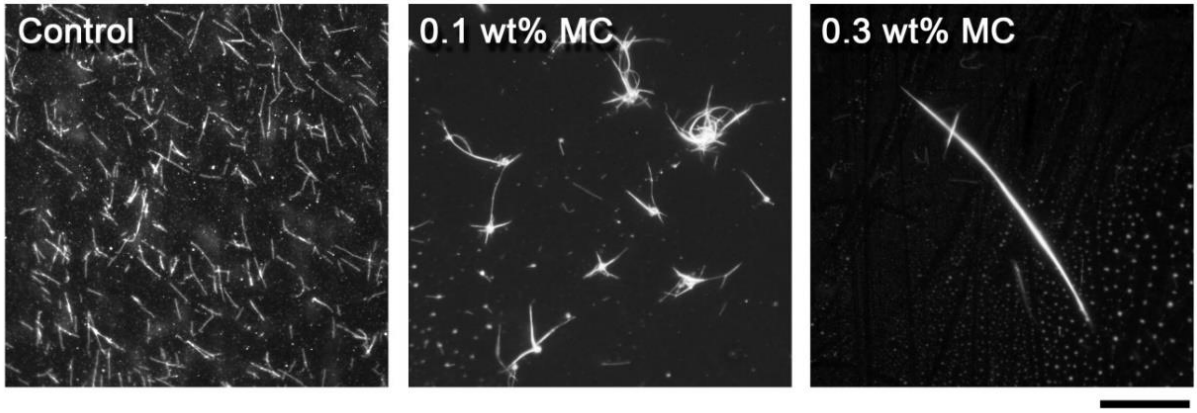

Figure 2.2: Depletion force induced bundle formation of microtubules. Fluorescence microscopic images of microtubules, which were suspended in solution (left) without methyl cellulose and (middle, right) with methyl cellulose. Scale bar: 10 μm.

The induction of depletion force by methyl cellulose to the microtubules can be explained using the A-O model. According to the A-O model, the entropic force between the microtubules approaching to one another depends on their lateral inter-filament distance, which in turn depends on the excluded volume or radius of gyration of depletant. Firstly, I considered each microtubules as a cylinder with radius R_{MT} =12.5 nm surrounded by depletion layer[26]. The depletion force between two microtubules induced by 0.3 wt% methyl cellulose was calculated using A-O model. The radius of gyration (Rg) of 140 kDa methyl cellulose is ~30 nm. To apply the A-O model, flexible polymers like methyl cellulose are typically treated as freely interpenetrating hard spheres of radius R_{AO}, which are excluded from the colloid surface by a thin layer of thickness R_{AO}[37]. R_{AO} was determined as $2Rg/\sqrt{9}$ = 33.85 nm. Then the extent of the depletion force was calculated as ~0.11 pN or ~26 K_BT/μm [detailed in section **2.4.5**]**.** The amount of entropic forces generating here lies in the range of entropic force (0.02 to 0.2 pN) required for the bundle formation of microtubules[40].

2.2.3 Role of depletion force on gliding behaviour of microtubules

To investigate the effect of depletion force on the behaviour of gliding microtubules, I performed an *in vitro* gliding assay of microtubules (concentration ~250 nM) in the presence of methyl cellulose (0.3 wt%). In the *in vitro* motility assay, microtubule filaments experience two types of events during collisions of two microtubules. One is the strong interactions due to volume exclusion occurs overwhelmingly, leading either to parallel or anti-parallel alignment of one filament respected to another and named as snuggling event [Figure 2.3A]. The rest of

the event is the crossing over, where the microtubules crossed each other with little effect on their trajectories [Figure 2.3A II]. Snuggling is considered the most important behaviour of gliding microtubules for producing collective motion that often leads to form stream or vortex patterns of microtubules[20]. Experimental results revealed that in presence of methyl cellulose most of the microtubule filaments (76%) exhibit snuggling event during their movement [Figure 2.3B]. In contrary, in absence of methyl cellulose only 18% events of the total collisions are snuggling, remaining 82% events are crossing over [Figure 2.3B].

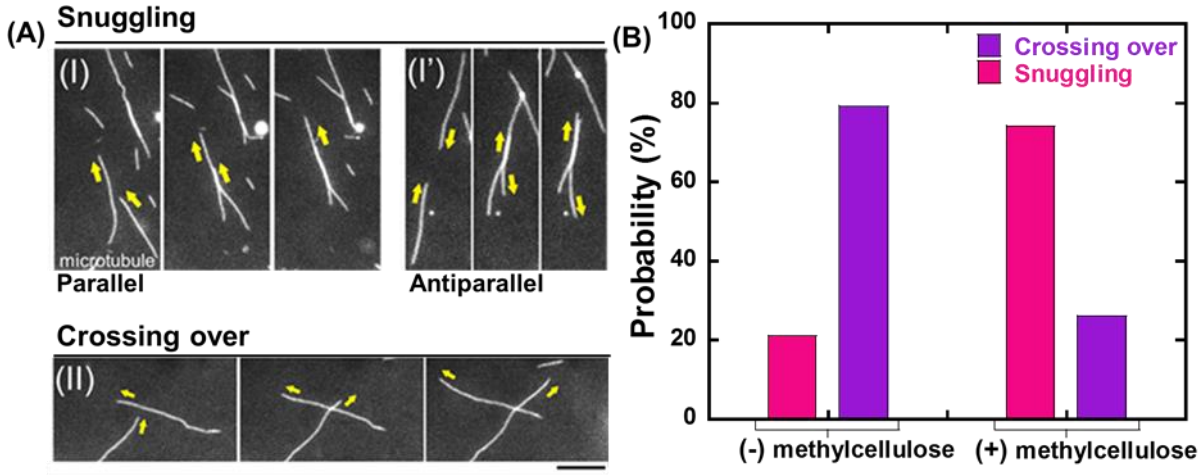

Figure 2.3: Effect of depletion force on the behaviour of gliding microtubules. (A) Different types of collisions among microtubules with different orientations. Snuggling of two microtubules moving toward (I) same and (I′) opposite directions. (II) Crossing over of moving microtubules. Scale bars: 10 μm. (B) Probability of snuggling and crossing over of microtubules in the absence and presence of 0.3 wt% methyl cellulose. Here (+) and (-) signs refer to the presence and absence of methyl cellulose respectively.

Thus, the depletion force generated by methyl cellulose (depletant) can regulate the behavior of microtubule filaments in the motility assay and enhance the probability of effective collision (snuggling event) among them, which is a pre-requisite of generation of collective motion.

2.2.4 Depletion force induced collective motion of kinesin driven microtubules

To obtain collective motion, I performed some preliminary experiments and discovered methyl cellulose can play an important role in regulating interactions between microtubule filaments. It is considered that methyl cellulose can suppress detachment of microtubules from the

substrate and fluctuation of leading head of microtubules, which are resulting in increase in collision of microtubules on planer surface and lead synchronization of moving direction of individual microtubule. In addition, methyl cellulose also enhance the depletion interaction between microtubules, which tend to assemble individually dispersed microtubules into bundles.

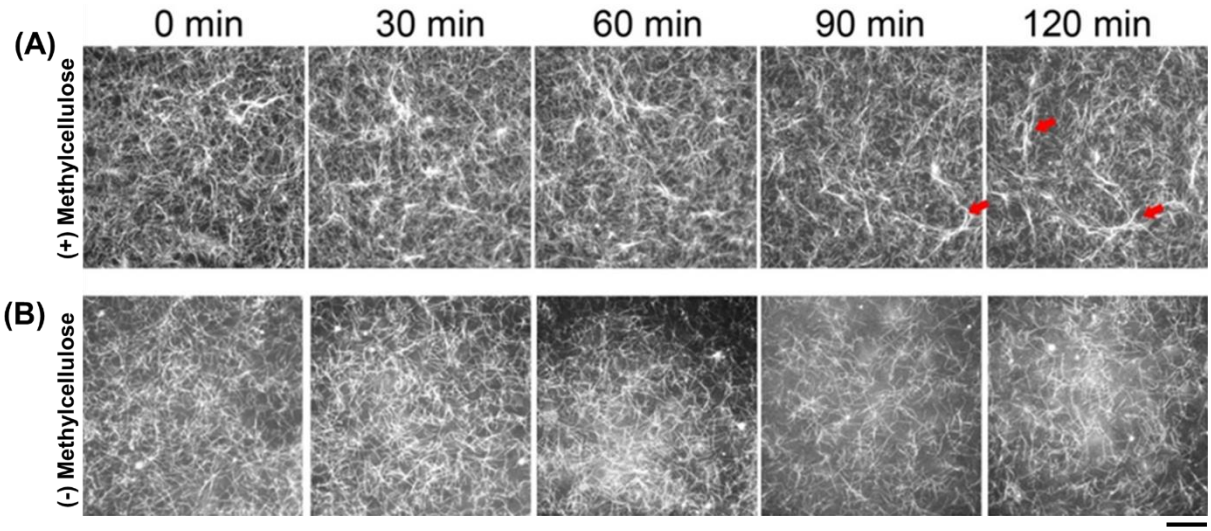

Figure 2.4: Fluorescence images of microtubules in the (A) presence and (B) absence of methyl cellulose (0.15 wt%). Here (+) and (-) signs refer to in presence and absence of methyl cellulose. The red arrows show the stable bundle formation of microtubules. Scale bar: 10 μm.

Therefore, to commence collective motion of microtubules, 0.15 wt% methyl cellulose has been employed in high density (5 μM) *in vitro* motility assay of microtubules. Initially, on addition of ATP (at 0 min), the microtubules moved randomly at a constant velocity (mean velocity of 180 ± 20 μm s^{-1} at 25 °C) without showing any specific directional preference. However, in the presence of methyl cellulose within 90 min after the addition of ATP, microtubules gradually formed small local streams [Figure 2.4A] (indicated by red arrows) which was completely absent in absence of methyl cellulose. [Figure 2.4B]

The aforementioned experimental results indicate that depletion force is playing a major role in the emergence of collective motion of kinesin driven microtubules. In addition, the previous experimental results and theoretical analysis emphasize that collective motion of self-propelled objects highly depends on the presence of sufficient number of moving agents in the considered system. Therefore, the change of concentration of microtubules should have important influence in the emergence of collective motion. Next, I attempt to understand the mechanism

and kinetics of emergence of collective motion of microtubules by investigating the influence of some relevant parameters, such as concentration of microtubules and depletant (methyl cellulose).

2.2.5 Role of depletion force and concentration of microtubules0 on the emergence of collective motion of microtubules

In the previous section, I have described about how methyl cellulose can regulate the gliding behavior of microtubules. However, in general the collective motion also depends on the density of moving particles in the system[19, 20]. Hence, to explore the kinetics of collective motion of microtubules driven by kinesins, I investigated in detail the role of concentration of microtubules and a depletant (methyl cellulose), in the collective motion.

Orientation of microtubules in the absence of methyl cellulose:

As the first step, I performed the gliding assay of microtubules on the kinesin coated substrate in the absence of the depletant, i.e., methyl cellulose, varying the concentration of the microtubules over a wide range (1-15 μM). The gliding assay of microtubules was performed on a flow cell made from cover glass (for details see in section 2.2.1 and experimental section). By adding ATP buffer, motility of the microtubules was initiated on the kinesin carpet at room temperature (25 ^{o}C). The microtubules were monitored under a fluorescence microscopy. On addition of ATP the microtubules started moving with an average velocity of ~480±21 nm/s and no directional preference of the gliding microtubules was observed just after the ATP addition. Such random movement of microtubules observed just after the addition of ATP was confirmed by measuring the angle of orientation of the microtubules[43] (Figure 2.5B i.).

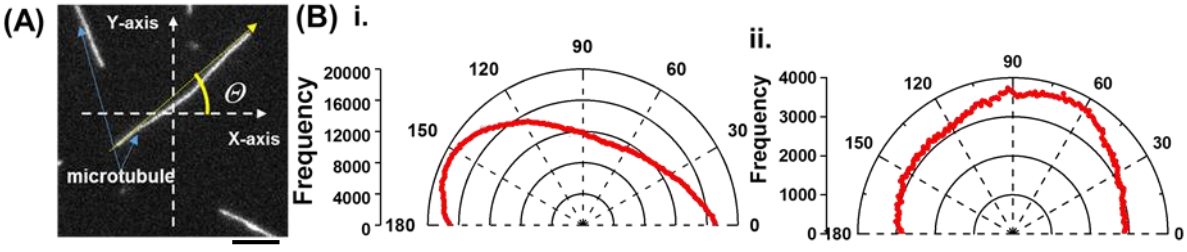

Figure 2.5: (A) Schematic representation of analysis of microtubule orientation angle *Θ*. Yellow arrow represents moving direction of microtubules. As shown here, the orientation angle was measured with respect to the X-axis. Scale bar: 5 μm. (B) Circular histogram of orientation angle of of microtubules in absence of methyl cellulose at (i) 0 min and (ii) 120 min

after ATP addition. The dispersion of orientation angle in circular histogram indicates randomness in moving direction of microtubules. Here the concentration of microtubules was 15.0 μM

However, over time, no collective motion was observed and the microtubules kept moving randomly which is obvious from the fluorescence microscopy images [Figure 2.6A] and the analysis of orientation angle [Figure 2.5B]. In the Figure 2.6A, I presented the time lapse fluorescence images of microtubules at very low (1.0 μM) and high (10 μM) concentrations. The random orientation of microtubules at both low and high density can be easily observed from the images.

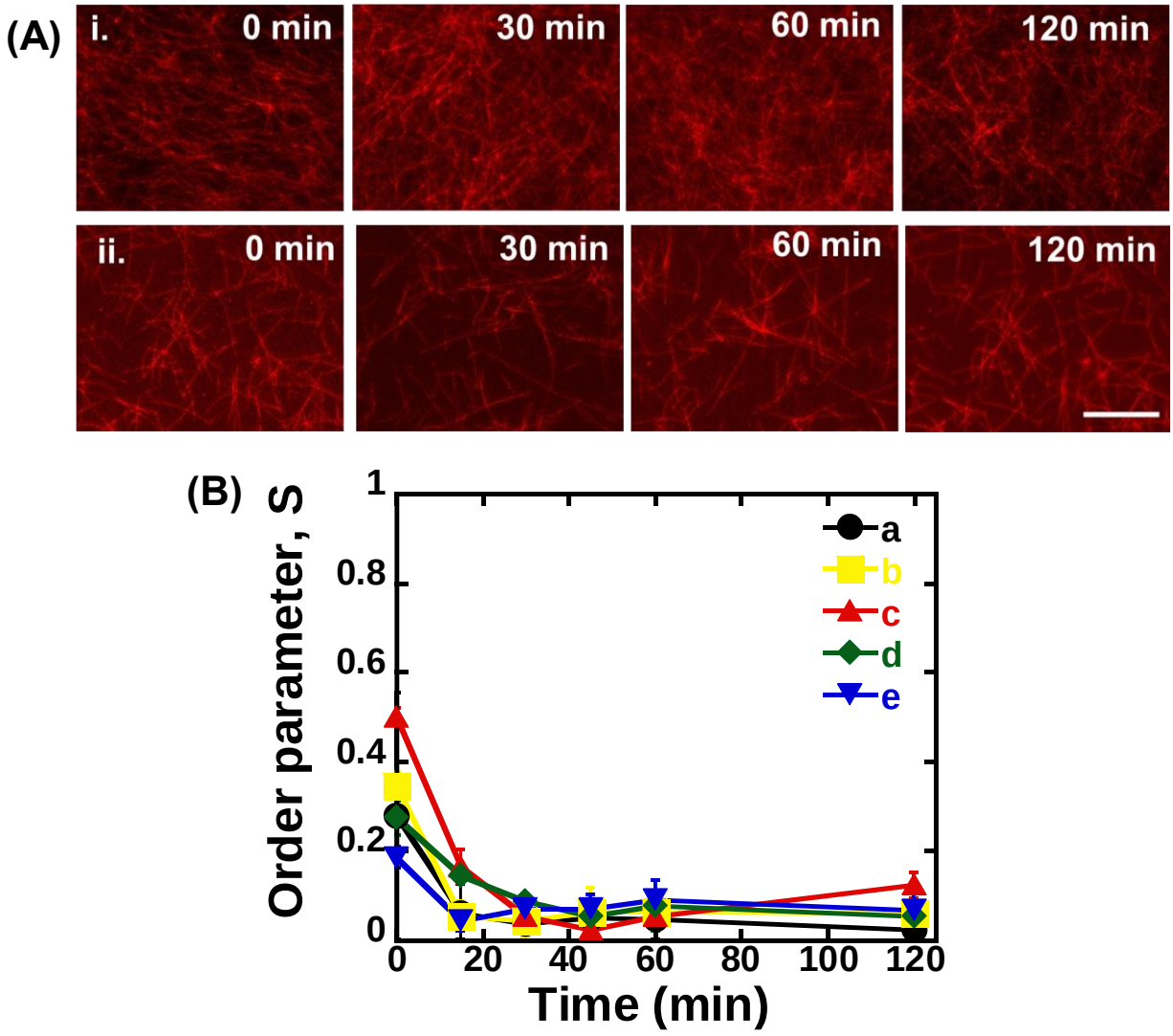

Figure 2.6: The orientation of microtubules in absence of methyl cellulose. (A) The time lapse fluorescence images of microtubules at (i) 10 μM and (ii) 1 μM concentrations. Scale bar: 20 μm. (B) Change of the orientation of microtubules with time at microtubule concentration. In the figures the lines a, b, c, d, and e represent order parameter for 1.0, 3.0, 5.0, 10.0, and 15.0 μM microtubules respectively.

To quantify the orientation of microtubules, I calculated nematic order parameter of the microtubules, *S* that is a measure of the orientation of the microtubules[44, 45] [see details in section 2.4.4]. The value of *S* ranges between 0 and 1, where S=0 or 1 represents random or ordered/aligned orientation of the microtubules respectively. The analysis reveals that the nematic order parameter decreased until ~30 min after ATP addition and then remained almost constant with time within the investigation period [Figure 2.6 B]. This decrease in the nematic order parameter confirms that no phase transition of microtubules took place from the isotropic to the nematic state. This observation is in an agreement to a previous result [section 2.2.4] where no collective motion of microtubules was observed in the absence of depletion force induced by methyl cellulose. The change in the nematic order parameter with time was found independent of the concentration of microtubules employed in the gliding assay [Figure 2.6B]. On increasing the concentration of microtubules in the gliding assay system, the density of microtubules on the kinesin coated surface of the flow cell increased. However, the increased density of the microtubules had no effect on their orientation and failed to result in transition from the isotropic state. As reported in literature, snuggling of gliding microtubules is a prerequisite for demonstrating collective motion. Therefore, based on my results it can be said that, in the absence of methyl cellulose, even when the density of microtubules is much increased, behavior of the gliding microtubules is not changed appreciably, as a result of which no phase transition was observed. The random motion of microtubules at high concentrations on the kinesins observed in our work is in contrary to what was observed on dyenins, which suggests that type of motor protein employed in the gliding assay is an important factor in the emergence of collective motion of microtubules[20].

Effect of concentration of methyl cellulose on orientation of microtubules in collective motion:

To elucidate the effect of extent of depletion on kinetics of collective motion first I established the relationship between concentrations of methyl cellulose to induced depletion force. Previously, I calculated the amount of depletion force for 0.3 wt% methyl cellulose and it found

calculated as ~0.11 pN, which was almost comparable to that of PEG or methyl cellulose reported in previous literatures[24, 42]. As theoretically predicted, the depletion-force induced scaled linearly with polymer concentrations; similarly, I estimated the depletion force by changing concentration of methyl cellulose as shown in Figure 2.7. Here, if I consider the force of each kinesin as ~5 pN[43], the total force of kinesins interacting with each microtubule on the surface should be several tens of pN. The total force of kinesins is much larger than the depletion force. Despite the increase in snuggling by the depletion force, it was not enough to form stable bundle of microtubules moving on the kinesin-coated surface, although stable bundles were formed in bulk solution [Figure 2.2].

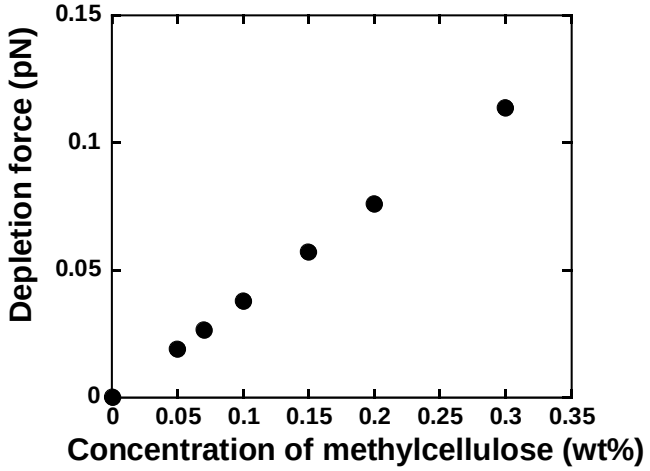

Figure 2.7: Relationship between depletion force and concentration of methyl cellulose.

I performed the gliding assay of microtubules of varying concentrations as described be. All the images were captured at 120 min after ATP addition. Scale bar: 10 μm.

In the Figure 2.8, it can be easily detected that when the concentration of methyl cellulose was 0.05 wt%, the microtubules of all the concentrations showed random orientation. Despite the fact that presence of methyl cellulose increases the probability of snuggling event among the gliding microtubules and favors the emergence of collective motion, I observed no collective motion of microtubules in the presence of the 0.05 wt% methyl cellulose for any of the concentrations of microtubules employed. In addition, the nematic order parameter was found to decrease over time for all the concentration of microtubules.

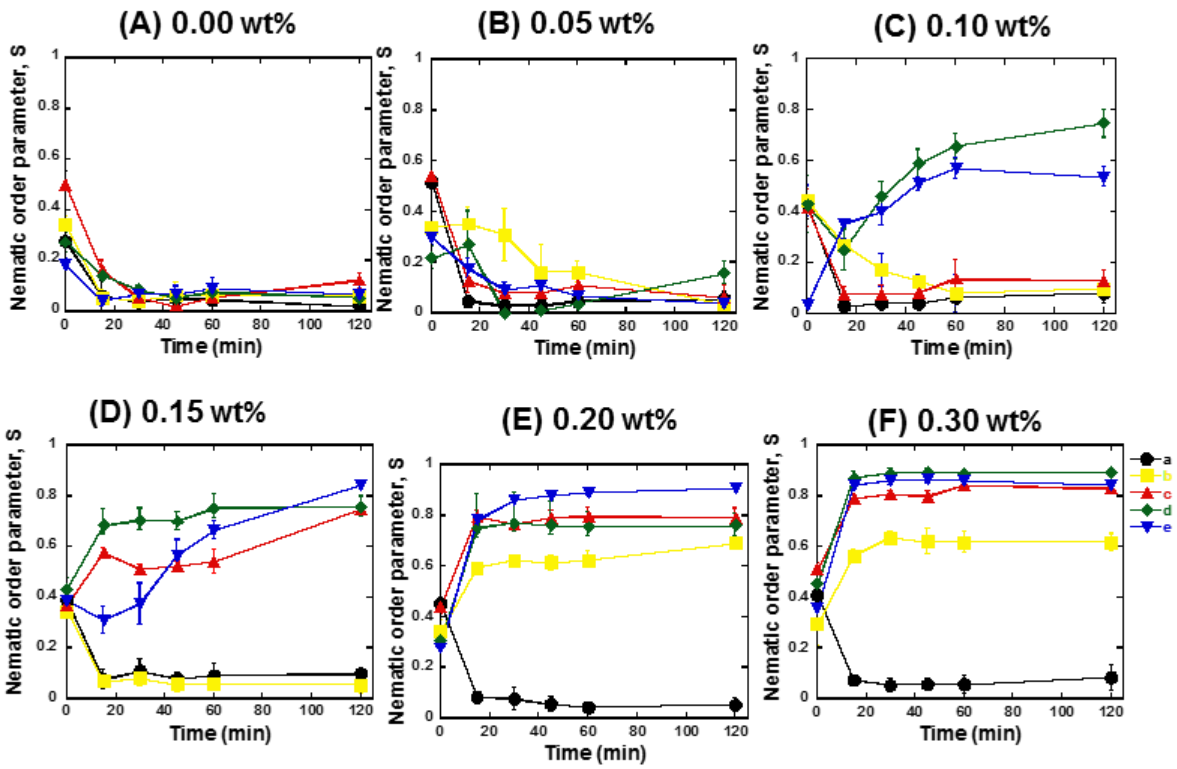

Figure 2.9: Change of the orientation of microtubules with time at different concentrations of methyl cellulose and microtubule. In each case the concentration of methyl cellulose is mentioned above the figure (from 0.0 to 0.3 wt%). In the figures the lines a, b, c, d, and e represent order parameter for 1.0, 3.0, 5.0, 10.0, and 15.0 μM microtubules respectively

In similar manner, on increasing the concentration of methyl cellulose to 0.1 wt%, I observed collective motion of microtubules for the concentrations of 10 and 15 μM, but I could not observe the collective motion for the concentrations of 1, 3, and 5 μM. For the 10 and 15 μM microtubules, the nematic order parameter of microtubules increased gradually with time and reached a plateau by ~60 min after ATP addition [Figure 2.9C]. At 0.15 wt% of methyl cellulose, collective motion was observed also for 5 μM microtubules, in addition to that for 10 and 15 μM microtubules. Interestingly I found that the time required to reach the plateau of nematic order parameter decreased at this condition. As shown in the Figure 2.9D, it took ~20 min to form stable nematic phase of microtubules when the concentration of methyl cellulose was 0.15 wt%. On further elevation of the methyl cellulose concentration, e.g. at 0.2 and 0.3 wt%, collective motion was observed for all the microtubule concentrations employed in this work, except for the concentration of 1 μM. At these methyl cellulose concentrations (0.2 and 0.3 wt%), no further decrease in the time required to form stable nematic phase was observed [Figure 2.9E and 2.9F]. This observation suggests that even for the high concentrations of

microtubules and methyl cellulose, a minimum time is required to cause the phase transition of the gliding microtubules from the isotropic to the nematic state.

2.2.6 Effect of depletion force and microtubule concentrations on the phase transition kinetics in collective motion of microtubules

The experimental results discussed earlier directly show the dependence of phase transition in collective motion of microtubules to the concentration of methyl cellulose and microtubules. Based on the investigations, I summarized my findings which are shown in Figure 2.10A and 2.10B. From the summarized results, it is evident that concentrations of both of the microtubules, and methyl cellulose have profound influence on the kinetics of the collective motion of microtubules on kinesins. For each of the two parameters a minimum or threshold value is found at or below which no phase transition of microtubules from an isotropic to a nematic state could be observed. Moreover, both the parameters are also found to be dependent on each other. The minimum concentration of methyl cellulose, which is required to induce collective motion of microtubules, decreased to lower values when the concentration of microtubules was much higher. On the other hand, a minimum concentration of microtubules is found at or below which no collective motion could be observed even if the concentration of methyl cellulose is very high. This minimum concentration of microtubules also depends on the concentration of methyl cellulose employed in the gliding assay. The effect of concentration of microtubules and methyl cellulose on the kinetics of phase transition of the microtubules is clearly evident from the heat maps of microtubule orientation at different observation time [Figure 2.10B]. Initially, just after ATP addition (0 min), no ordered orientation of microtubules was observed for any of the concentrations of microtubules or methyl cellulose. For this observation time, the heat map entirely represents random orientation of the microtubules. Although a little ordered orientation could be detected, this might has been due to transient ordering of the colliding microtubules. At 15 min, the nematic phase could be detected only for relatively higher concentrations of microtubules and methyl cellulose. In contrast, for the relatively lower concentrations of microtubules and methyl cellulose the emergence of collective motion was much slower (e.g., 30 or 45 min). From this stage (~45 min) a clear separation of the random isotropic and ordered nematic phase could be easily observed from the heat maps, with no further change in microtubule orientation with time.

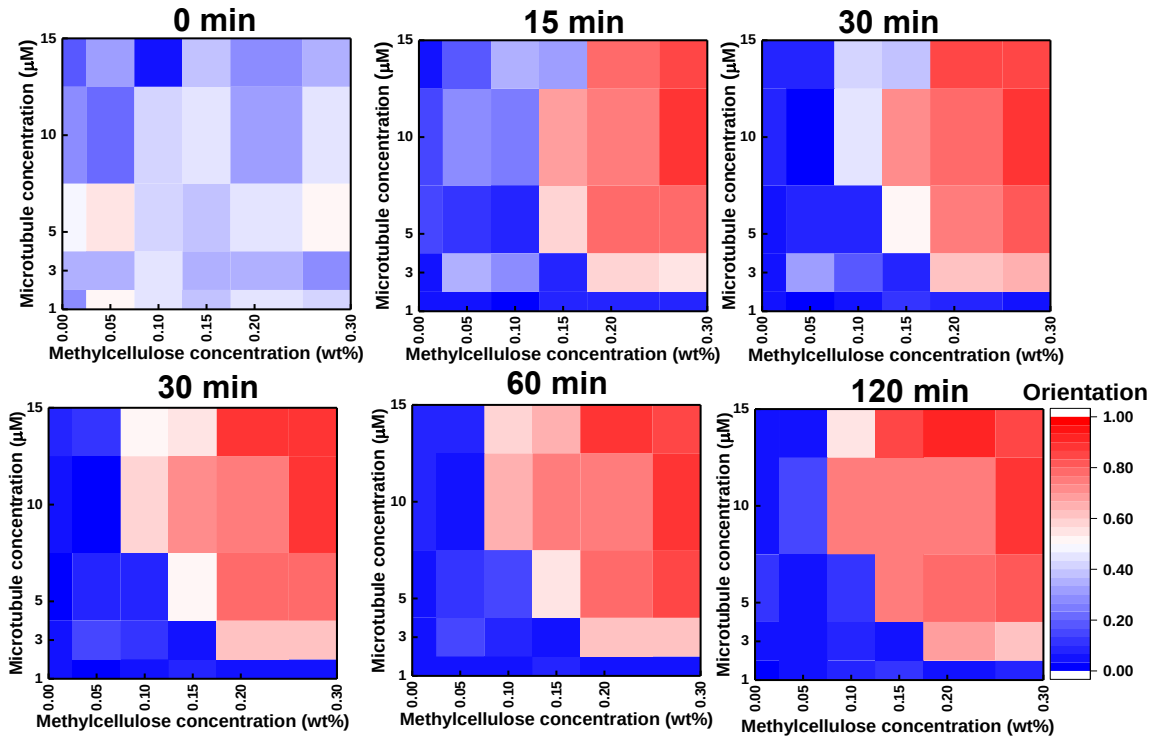

Figure 2.10 Heat maps showing the nematic order parameter of microtubules at different observation time as a function of microtubule and methyl cellulose concentration. From the heat maps organization of microtubules and transition of microtubule organization from an isotopic (indicated by blue color) to a nematic phase (indicated by red color) could be observed at different experimental conditions.

Therefore, we can conclude that, the concentration of microtubules and amount of depletion force play important role in the phase transition kinetics of microtubules in collective motion.

Based on the above discussion, the effect of concentration of microtubules and depletion force on the kinetics of collective motion of microtubules is clearly evident. To understand the mechanistic detail, I investigated the behavior of gliding microtubules at different experimental conditions. I quantified the probability of snuggling and crossing over event of gliding microtubules for different concentration of methyl cellulose. The results, shown in Figure 2.11, reveal that methyl cellulose has a significant effect on the behavior of gliding microtubules.

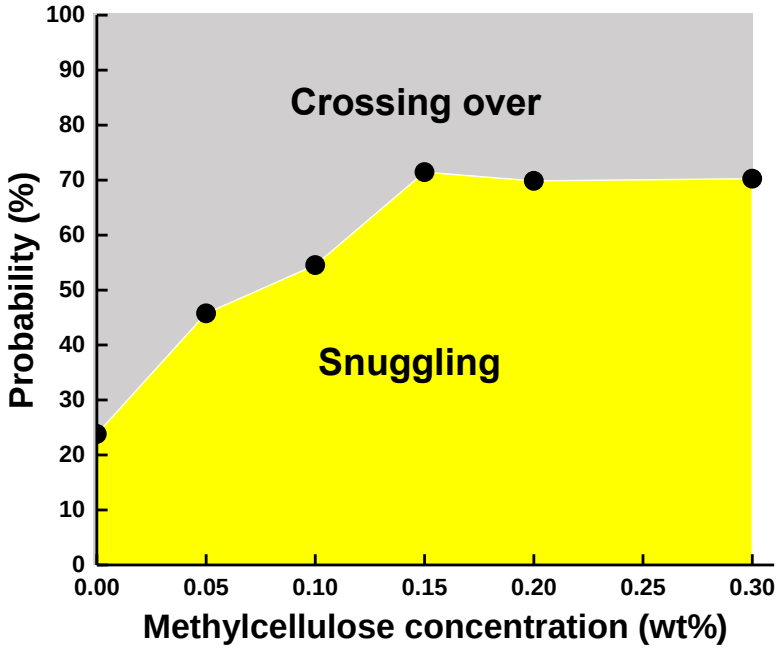

Figure 2.11: Effect of methyl cellulose concentration on the gliding behavior of microtubules. High concentration of methyl cellulose increased the probability of snuggling event.

In the absence of methyl cellulose, the probability of crossing over was much higher compared to that of the snuggling. Therefore, the higher probability of crossing over in the absence of methyl cellulose might has prevented the microtubules from exhibiting collective motion, even at very high concentrations of the microtubules. This result also implies that the gliding behavior of microtubules is not affected by the concentration of microtubules. Addition of the methyl cellulose in the gliding assay system (0.05 wt%) was found to increase the probability of snuggling of gliding microtubules over cross over. The probability of snuggling kept increasing on increasing the concentration of methyl cellulose and reached a plateau at 0.15 wt%, after which no change was observed on increasing the methyl cellulose concentration further. From these results, it can be concluded that methyl cellulose expedites the kinetics of collective motion of microtubules by increasing the probability of snuggling of the gliding microtubules.

Here, it should be mentioned that, I observed no considerable effect of methyl cellulose on the velocity of microtubules [Figure 2.12 A] in the present experimental conditions and viscosity of buffer also did not change appreciably on changing the concentration of the methyl cellulose [2.12 (B)] within the range studied.

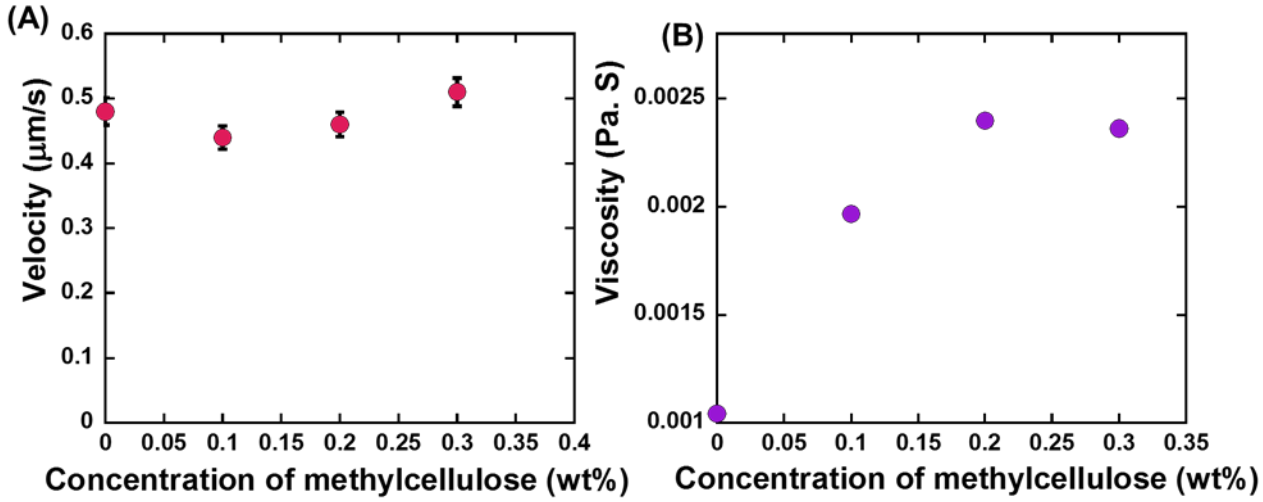

Figure 2.12: Effect of methyl cellulose concentration on the (A) velocity of gliding microtubules and (B) buffer viscosity.

It is to note that, the force that drives the microtubules comes from kinesins through consumption of the energy of ATP hydrolysis. The diffusion of kinesin driven microtubules is much faster compared to that driven by thermal forces. Therefore, in our work the thermal force induced diffusion has negligible effect on the movement of microtubules and the time scale of phase transition of microtubules should be governed by the active movement of microtubules, influence of depletion force and mutual interaction of the dynamic microtubules.

2.2.7 Role of microtubule associated proteins in the collective motion of microtubules

In cell, the dynamics of microtubules is regulated by a number of factors including some associated proteins known as microtubule associate protein (MAP)[46].The MAPs, e.g. Tau, MAP1, MAP2, MAP etc. can induce weak interactions between microtubules and enhance the stability of the assembly of microtubules likewise, the association constant (Ka) [47] of MAPs is ~107 M^{-1}. Therefore, to investigate the role of MAPs on the collective motion of microtubules driven by kinesins, I performed experiments by incorporating MAP4 in the gliding assay of microtubules in presence and absence of methyl cellulose.

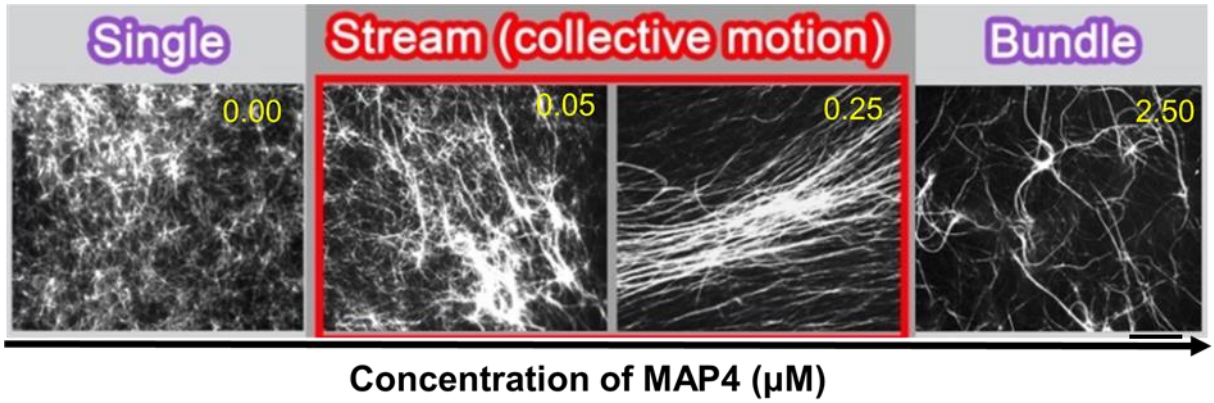

Figure 2.13: Effect of MAP4 on collective motion of microtubules driven by kinesins in absence of depletant (methycellulose). The yellow text refers to the concentration of MAP4 (μM) applied. Scale bar: 10 μm.

To understand the effect of MAP4 fragment on the evolution of collective motion, first I performed *in vitro* gliding assay in the presence of a wide range of MAP4 fragment (0. 5 to 2.50 μM) without methyl cellulose, at fixed kinesin and microtubule densities. The fluorescence images in Figure 2.13 show the behavior of microtubules at different MAP4 concentration. As, MAP4 can induce weak local interactions, microtubule filaments were bundled and generated stream like pattern at high MAP4 concentration. However, at too high concentration of MAP4, microtubules bundled to network like structure and such stream and/or bundle like assembly of microtubules were very unstable.

Next, to discuss the role of MAP4 in collective motion of microtubules I performed experiment in presence of 0.3 wt% methyl cellulose keeping the concentration of microtubules and kinesin same as mentioned above. The important thing we noticed here is the increase in stability of

the streams of the microtubules. To evaluate the influence of MAP4 in the orientation in maintaining the stability of microtubule streams, I compared nematic order parameter, *S* and density variance, D_f of microtubules with and without MAP4 fragment in the presence of 0.3 wt% methyl cellulose. In the presence of 0.25 μM MAP4 fragment, the *S* increased until 30 min and remained constant indicating a prolonged orientation of microtubules, which was in contrast to that observed in the absence of MAP4 fragment [Figure 2.14B]. Besides, in the presence of MAP4 fragment, the D_f increased and similar to the S remained constant showing the preservation of high density of microtubules in streams [Figure 2.14C].

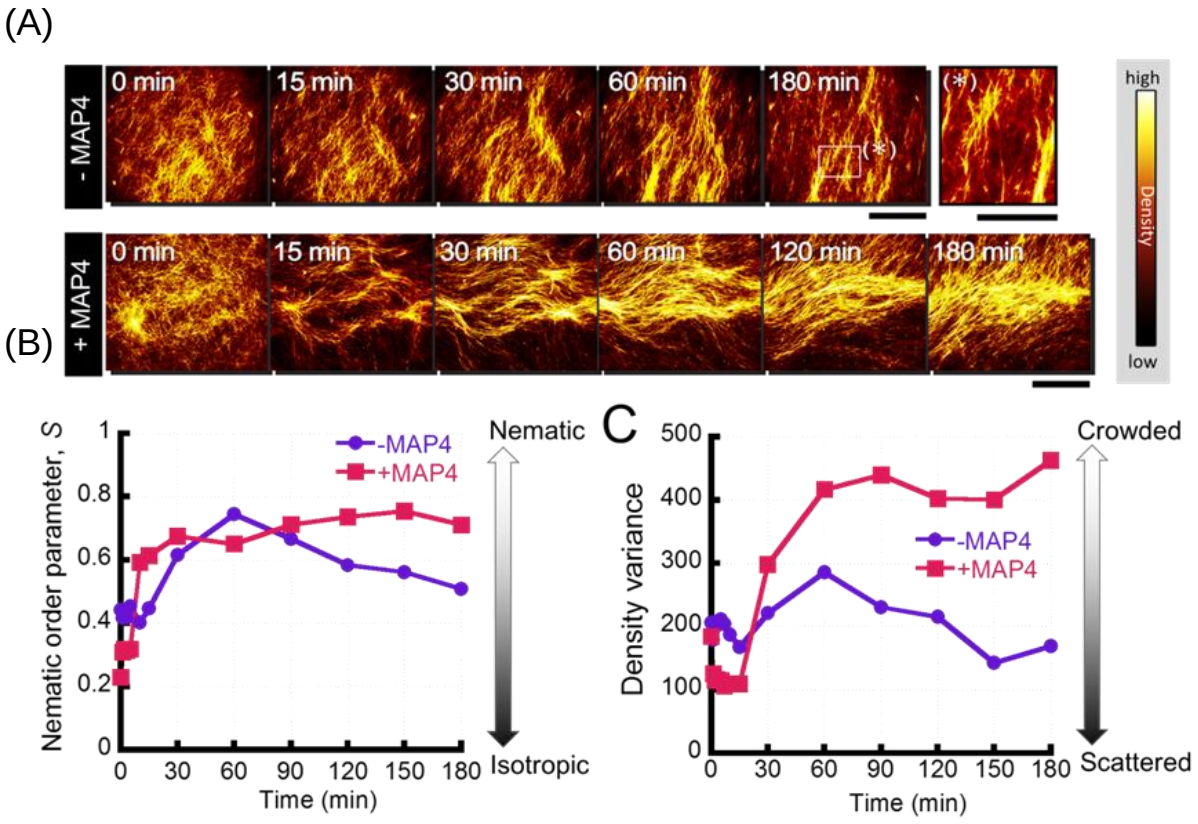

Figure 2.14: Stability of the streams of gliding microtubules. (A) Time course of the streams of microtubules in the absence and in the presence of MAP4 fragment. Color bar (right side) is fluorescence intensity of microtubules, which represents degree of density of microtubules. Analysis of stability of the streams by using (B) the nematic order parameter, *S* and (C) the density variance score. Scale bar: 20 μm.

To separately characterize the effect of methyl cellulose and MAP4 fragment on evolution of collective motion of microtubules, I performed *in vitro* gliding assay in the presence and absence of 0.25 μM MAP4 fragment, which were carried out both with and without 0.3 wt%

methyl cellulose at low kinesin and microtubule densities. The previous experimental results suggests that the probability of snuggling is the key issue which regulates the dynamics of collective motion of microtubules. So, I calculated the interaction probabilities among microtubules and found that the snuggling probability was 17.9 % in the absence of both MAP4 fragment and methyl cellulose, which increased to 35.0 % when 0.25 μM MAP4 fragment was present only. On the other hand, snuggling probability dramatically increased to 62.3 % in the presence of 0.3 wt% methyl cellulose but without MAP4fragment. However, presence of both the MAP4 fragment and methyl cellulose further brought a little increase in the snuggling probability (67.8 %).

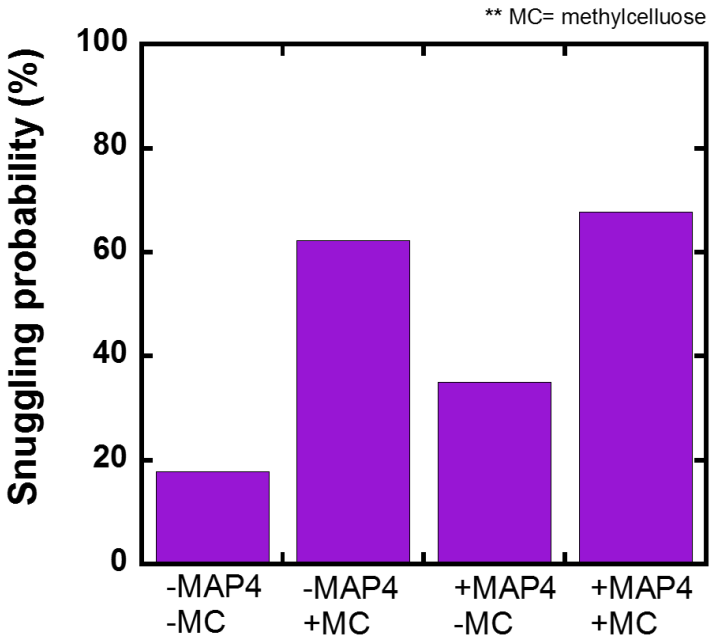

Figure 2.15: Effect of MAP4 fragment and MC on the behaviour of gliding microtubules. Probability of snuggling was evaluated in the presence or absence of MAP4 fragment without and with 0.3 wt% MC. Kinesin concentration was fixed at 500 nM. (+) and (-) indicate 'presence' and 'absence', respectively.

These results clearly reveal that it is the methyl cellulose, which mainly influences the collision event of the microtubules. Although MAP4 fragments can generate the streams and improve the stability of the streams, it has less pronounced effect on mutual interaction between microtubule filaments compared to that of methyl cellulose. Therefore, it can be concluded that depletion force due to methyl cellulose and weak attractive interaction induced by MAP4 fragment can together ensure high stability of microtubule streams and both interactions can be useful for demonstrating collective motion of microtubules on kinesin coated surface.

2.2.8 Investigation of the structure of the microtubule assemblies in collective motion

Besides the kinetic study, I also investigated the structure of the microtubule assemblies in the nematic phase (microtubules in the collective motion) using a confocal laser scanning microscope. The outcome, shown in Figure 2.16, reveals that the nematic phase of microtubules is a two dimensional structure comprised of overlapping bundles of microtubules. However, changes in the structural organization of microtubule assemblies in the nematic phase in response to the changes in concentration of the microtubules and methyl cellulose is unclear at this moment, understanding of which requires detail investigation in future.

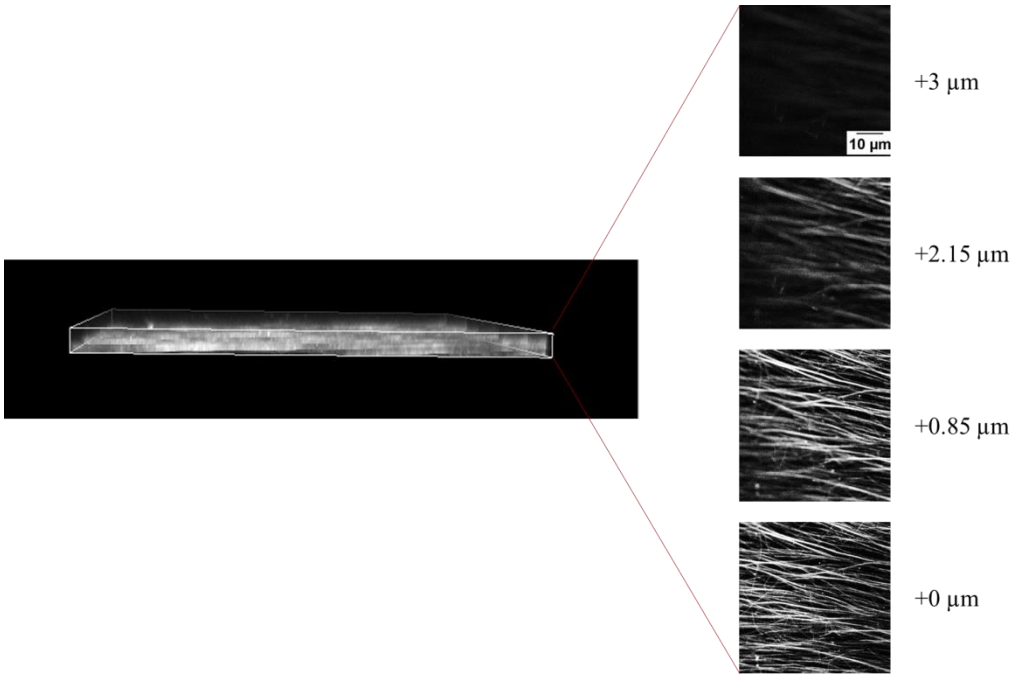

Figure 2.16: Two-dimensional structure of the microtubule assemblies in the nematic phase. The images were captured using a confocal laser scanning microscope. The values at the right to the images indicate the height, i.e. focus position along Z-axis.

2.3 Conclusions

In conclusion, I demonstrated the first-ever collective motion and stream pattern formation by microtubules on a kinesin coated surface using depletion force induced by a depletent methyl cellulose. This method offers a simple and universal technique to investigate the coordinated behaviour of self-propelled objects using biomolecular motor systems. I have also explored the kinetics of collective motion of microtubules driven by kinesins. I unveiled how the concentration of microtubules and depletion force affect the ensemble behavior of microtubules driven by kinesins. These results disclosed that both the concentration of microtubules and the depletant (methyl cellulose) have crucially important roles in the kinetics of collective motion of the kinesin driven microtubules. A minimum concentration of microtubules or methyl cellulose is required to allow the emergence of collective motion of microtubules and to cause a transition from an isotropic to a nematic phase. For low concentrations of methyl cellulose (e.g., <0.05 wt%) no collective motion of microtubules emerged even for high concentrations of microtubules. On the other hand, even for the relatively higher concentrations of methyl cellulose (e.g., 0.3 wt%), we observed no collective motion when the concentration of microtubules was low (1 μM). A minimum concentration of methyl cellulose (0.1 wt%) can induce the phase transition of microtubules if the concentration of microtubules is ≥10 μM. Conversely, for the microtubules, a minimum concentration (3 μM) is required for the phase transition for any of the concentration of methyl cellulose investigated. Importantly the time required to cause such a phase transition is also found affected by the concentration of microtubules and the methyl cellulose employed in the gliding assay. This work offers a better understanding of the collective motion of kinesin driven microtubules, which consequently would be useful in understanding the coordinated behavior of other self-propelled systems in nature. At the same time, this will be helpful in understanding not only the collective behaviour of self-propelled objects such as birds, animals or fishes, but also may provide new insight into emergent structures obtained through a non-equilibrium process[53-55]. Moreover, recently microtubule/kinesin system has attracted attention in the field of molecular robotics as the smallest self-propelled objects[56-57]. Molecular robots, relying on a large number of collectively moving self-propelled objects such as gliding microtubules, enables parallel processing in transporting a large number of small cargos and assembling building blocks into an ordered structure. Therefore, ideas obtained from the present study on collective motion of gliding microtubules are expected to expand the boundaries in the field of molecular robotics.

2.4 Experimental

2.4.1 Preparation and labelling of proteins

Tubulin was purified from porcine brain using a high-concentration PIPES buffer (1 M PIPES, 20 mM EGTA, and 10 mM $MgCl_2$; pH was adjusted to 6.8 using KOH) [49]. The high-concentration PIPES buffer and BRB80 buffer were prepared using PIPES from Sigma, and the pH was adjusted using KOH. Kinesin-1 consisting of the first 575 amino acid residues of human kinesin-1 was prepared by partially modifying the expression and purification methods described in literature[50]. Rhodamine-labelled microtubules were obtained by polymerizing a mixture of rhodamine-labelled tubulin (RT) and non-labelled tubulin (WT) (RT: WT = 4:1; final tubulin concentration, 55.6 μM) at 37 °C in the presence of 1 mM GTP according to the standard technique. The solution containing the microtubules was then diluted with motility buffer (80 mM PIPES, 1 mM EGTA, 2 mM $MgCl_2$, 0.5 mg mL^{-1} casein, 1 mM DTT, 10 μM paclitaxel and ~1% DMSO; pH 6.8).

2.4.2 *In vitro* gliding assay of microtubules

A flow cell with dimensions of 5.0×5.0×0.15 mm^3 (W×L×H) was assembled from two cover glasses of sizes (5×7) mm^2 and (40×50) mm^2 (MATSUNAMI), and a double-sided tape was used as the spacer. First the surface of the flow cell was coated with casein buffer (80 mM PIPES, 1 mM EGTA, 1 mM $MgCl_2$ and ~0.5 mg mL^{-1} casein; pH 6.8) and incubated for 3 min. Then 3 μL of kinesin-1 solution (~80 mM PIPES, 1 mM EGTA, 1 mM $MgCl_2$, 0.5 mg mL^{-1} casein, 1 mM DTT, 10 μM paclitaxel/DMSO, ~1% DMSO; pH 6.8) was applied to the flow cell and incubated for 1 min to bind the kinesin to the casein coated surface of the flow cell through non-specific interaction. The flow cell was washed with 5 μL of motility buffer (80 mM PIPES, 1 mM EGTA, 1 mM $MgCl_2$, 0.5 mg mL^{-1} casein, 1 mM DTT, 10 mM paclitaxel and ~1% DMSO; pH 6.8). Next, 3 μL of microtubule solution of a prescribed concentration was applied to the flow cell and incubated for 2 min, followed by washing with 5.0 μL of motility buffer. Then, 10 μL of 10 mM adenosine tri-phosphate (ATP) buffer containing methyl cellulose of a prescribed concentration (~80 mM PIPES, 1 mM EGTA, 1 mM $MgCl_2$, 0.5 mg mL^{-1} casein, 1 mM DTT, 10 μM paclitaxel/DMSO, 0-0.3 wt% methyl cellulose, ~1% DMSO; pH 6.8) was added to the flow cell. The flow cell was placed inside the inert chamber after the

addition of ATP and humid nitrogen gas was passed through the chamber to remove oxygen from the chamber[51, 52]. The time of ATP addition was set as 0 min, and microtubules were monitored under a fluorescence microscopy. All these experiments were performed at room temperature. Next, where the MAP4 fragments were used, the ATP buffer was applied to the flow cell after application of 0.25 μM MAP4fragment and subsequent wash with motility buffer. All the aforementioned experiments were performed at room temperature.

2.4.3 Microscopic image capture

The samples were illuminated with a 100 W mercury lamp and visualised with an epi-fluorescence microscope (Eclipse Ti; Nikon) using an oil-coupled Plan Apo 60×1.40 objective (Nikon). Filter blocks with UV-cut specifications (TRITC: EX540/25, DM565, BA606/55; GFP-HQ: EX455-485, DM495, BA500-545; Nikon) were used in the optical path of the microscope to allow for visualisation of samples while eliminating the UV portion of the radiation and minimising the harmful effects of UV radiation on the samples. Images and movies were captured using a cooled CMOS camera (Neo sCMOS; Andor) connected to a PC. To capture a field of view for more than several minutes, ND filters (ND4, 25% transmittance) were inserted into the illuminating light path of the fluorescence microscope to avoid photobleaching.

2.4.4 Analysis of the microscopic image

Quantitative analysis of collective motion of microtubule

The orientation of microtubules was calculated in terms of nematic order parameter (*S*), which was calculated according to the following equation by using Image J plugin, orientation J (http://bigwww.epfl.ch/demo/orientation/).

$$S = \frac{1}{N}\sqrt{\left(\sum_{i=0}^{180} R_i \cos 2\Theta_i\right)^2 + \left(\sum_{i=0}^{180} R_i \sin 2\Theta_i\right)^2}$$

where N refers to total number of microtubules in the frame, R_i is frequency of the angle of individual microtubules Θ_i (i = 0 to 180). The range of Θ_i was fixed from 0° to 180° based on the symmetry of horizontally or vertically aligned microtubules with respect to the X-axis. Since the microtubules in the nematic phase were oriented along the X-axis, we fixed the

director for both the isotropic and nematic phase along the X-axis and measured the nematic order parameter of microtubules in the XY plane.

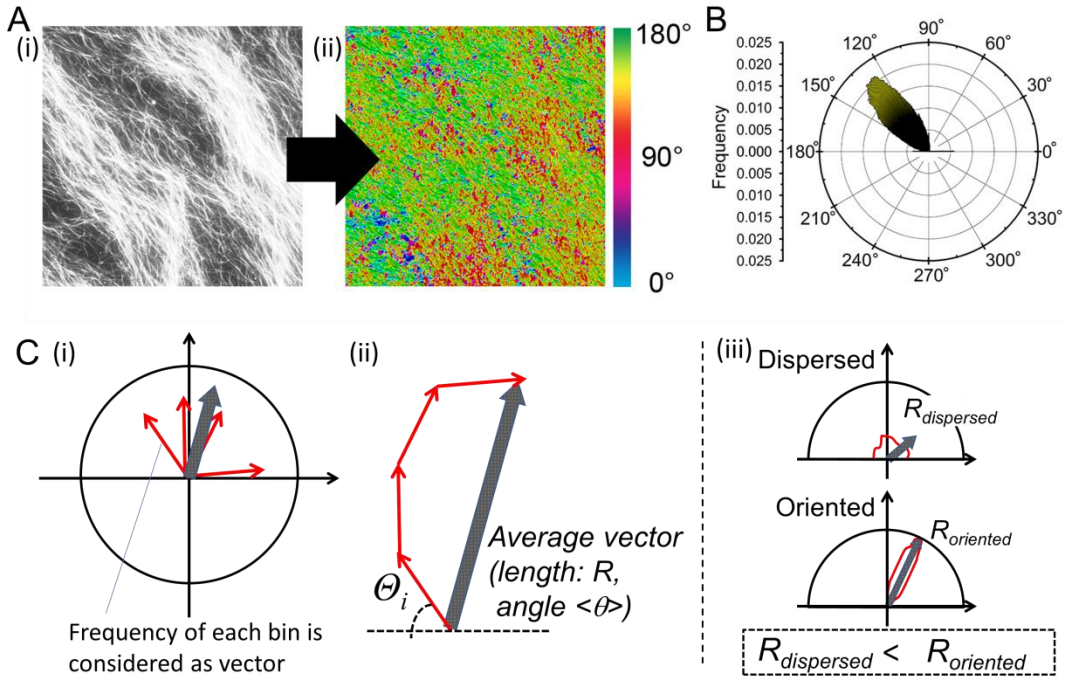

Figure 2.17 Analysis method of the angles and degree of orientation of microtubules. (**A**) (i) Fluorescent microscopic image of microtubules. (ii) Color map representing the distribution of microtubule orientation angles. (**B**) Circular histogram of orientation angles of microtubules obtained from a fluorescent microscopic image of microtubules in (A). (**C**) Directional analysis method. (i) Here each bin in the circular histogram is considered as a vector (length: R_i, angle: Θ_i). (ii) Average vector (length: R, mean orientation angle $<\theta>$) was used for evaluation of orientation direction and degree of orientation. (iii) Relationship between R and degree of orientation. If distribution of microtubules angles is dispersed, R becomes smaller ($R_{\text{dispersed}}$) than that of high oriented microtubules (R_{oriented}).

Analysis of the density of the microtubules in the streams

Density variance is calculated by the following equations:

Density variance $= \frac{1}{N} \sum_{i=1}^{n} (P_i - P_{ave})^2 \quad (eq. 2)$

for all tiles A_i (i = 1 to n) covering a frame. P_i is an estimated microtubule number in tile A_i

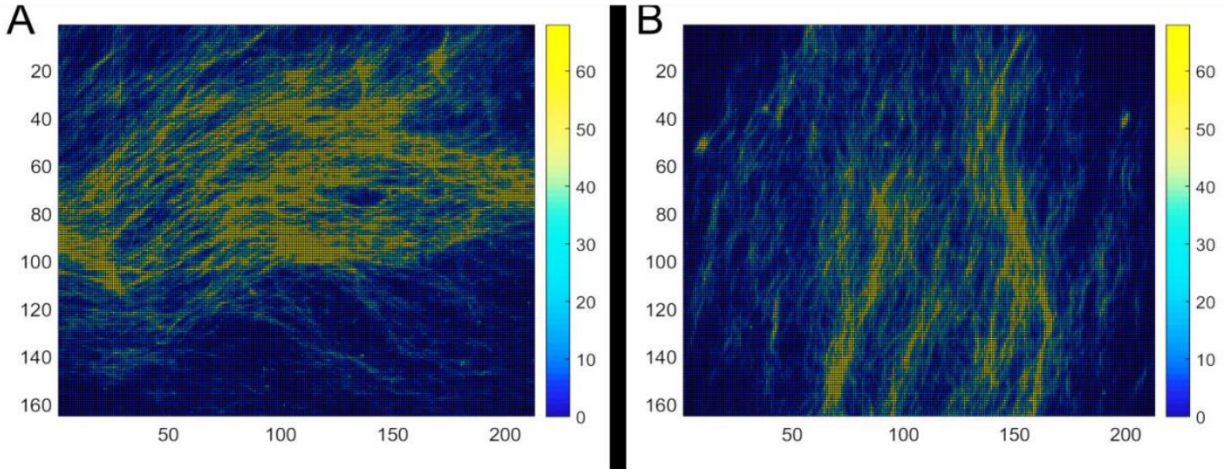

Figure 2.18: Distribution of estimated microtubule numbers at the time 90 min in microtubule gliding assay with MAP4 fragment (A) and without MAP4 fragment (B).Yellow: higher density, Blue: lower density. Density fluctuation, Df is calculated by the distribution of microtubule density or the numbers of microtubules per tiles covering a movie frame.

P_{ave} is average microtubule density when assuming the total number of microtubules are equally distributed over the frame, that is, P_{ave} = ∑(observed microtubule numbers /n.) $(eq. 3)$

The number of microtubule in a tile is estimated by quadratic function f of average signal intensity x available from pixels in a tile:

$$f(x) = ax^2 + bx + c, \qquad a = -0.045, b = 6.2, c = -4.5$$

We fitted unknown coefficients a, b and c by fitting a curve to the experimental data observed by high-resolution microscopy. The signal intensity is saturated around the number of microtubules over 60. In this work, 68 is chose as the maximum number of microtubules experimentally observed.

2.4.5 Determination of depletion force induced by methyl cellulose

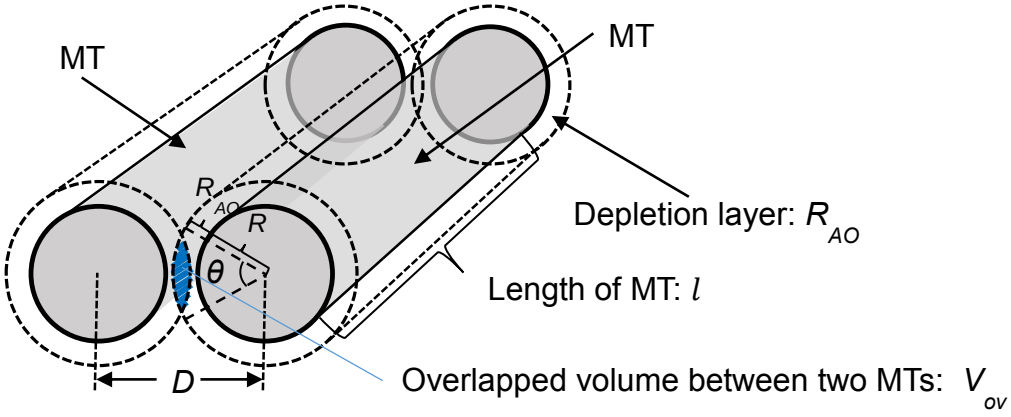

Let us considered two microtubules were immersed in 0.3 wt% methyl cellulose solution. Each microtubules was assumed as cylinder with radius R_{MT} =12.5 nm surrounded by depletion layer of radius R_{AO}.. The depletion force between two microtubules induced by 0.3 wt% methyl cellulose was calculated using A-O model. The radius of gyration (*Rg*) of 140 kDa methyl cellulose is ~30 nm. Perhaps, R_{AO} was determined as $2Rg/\sqrt{9} = 33.85$ nm.

Now the excluded volume of the associated microtubules V_{ex} is calculated by, $V_{ex}=V_{total}-Vov$

Where, *Vov* between two microtubules is $Vov = (R+R_{AO})^2 \times (\theta - \sin\theta) \times l$ …...……*eqn 1* The total volume of microtubules with excluded layer, $V_{total} = 2 \times 2\pi \times (R+R_{AO})^2 \times l$.....*eqn 2* So, the excluded volume, $Vex = Vtotal - Vov = (R+R_{AO})^2 (4\pi - (\theta - \sin\theta)) \times l$…….. ……..*eqn3*

The depletion force $F_{dep} = - P\Delta Vex$……*eqn4*

However, in equation 3, there is θ , which can be transformed into the following equation,

$\theta = \cos^{-1}\frac{D}{2}(R + RAO)$…….*eqn 5*

Finally, equation 3 can be written as,

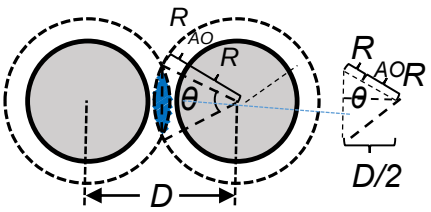

$$V_{ex} = (R + RAO)^2 \cdot \left(\cos^{-1}\frac{D}{2(R+RAO)} - \sin\cos^{-1}\frac{D}{2(R+RAO)}\right) \cdot l$$……..eqn 5

To differentiate Vex with respect to D, $(\cos^{-1}t)$' and $(\sin(\cos^{-1}t))$' are calculated.

$$\left(\cos^{-1}\frac{D}{2(R+RAO)}\right)' = -\frac{1}{2(R+RAO)}\cdot\frac{1}{\sqrt{1-(\frac{D}{2(R+RAO)})^2}} \quad \text{……eqn7}$$

$$\left(\sin\cos^{-1}\frac{D}{2(R+RAO)}\right)' = \cos\left(\cos^{-1}\frac{D}{2(R+RAO)}\right)\left(\frac{1}{2(R+RAO)}\cdot\frac{1}{\sqrt{1-(\frac{D}{2(R+RAO)})^2}}\right)$$

$$= \frac{D}{2(R+RAO)}\left(\frac{1}{2(R+RAO)}\cdot\frac{1}{\sqrt{1-(\frac{D}{2(R+RAO)})^2}}\right) \text{…….eqn 8}$$

From equation 7 and 8,

$$\Delta V_{ex} = \frac{1}{2}(R+RAO)\cdot\frac{1}{\sqrt{1-(\frac{D}{2(R+RAO)})^2}}\cdot\left(1-\frac{D}{2(R+RAO)}\right)$$

If $D \sim 2R + R_{AO}$ = 57.85 nm, then ΔV_{ex} = 2.18 × 10^{-13} nm^{-2}

Here, molecular weight of methyl cellulose =140000 Da,

Polymerization degree, N = 740,

Radius of gyration, R_g = 30 nm,

Depletion layer thickness, $R_{AO} = 2Rg/\pi^{1/2}$,

Concentration of methyl cellulose = 0.000214 M (=0.3 wt%)

$P = 0.000214\times4.04\times10^{-21}\times.02\times10^{-23}$

$= 0.52$ N m^{-2}

So, depletion force $F_{dep} = -P\Delta V_{ex}$

=0.11 pN or 28.10 k_BT μm^{-1}

2.5 References

1. T. Vicsek, *Nature*, 2001, **411**, 421.

2. T. Vicsek, and A. Zafeiris, *Phys. Rep.*, 2012, **517,** 71-140.

3. J. K. Parrish, S. V. Viscido, and D. Grünbaum, *Biol. Bull*., 2002, **202**, 296-305.

4. K. Kruse, J. F. Joanny, F. Julicher, J. Prost, and K. Sekimoto, *Phys. Rev. Lett.*, 2004, **92,** 078101 (1-4).

5. M. Loose, E. Fischer-Friedrich, J. Ries, K. Kruse, and P. Schwille, *Science*, 2008, **320**, 789–792.

6. I. D. Couzin, J. Krause, N. R. Franks, and S. A. Levin, *Nature*, 2005, **433**, 513–516.

7. I. H. Riedel, K. Kruse, and J. A. Howard, *Science*, 2005, **309**, 300–303.

8. C. Dombrowski, L. Cisneros, S. Chatkaew, R. E. Goldstein, and J. O. Kessler, *Phys. Rev. Lett.*, 2004, **93**, 098103 (1-4).

9. A. Czirok, E. Ben-Jacob, I. Cohen, and T. Vicsek, *Phys. Rev. E*, 1996, **54**, 1791–1801.

10. F. J. Nedelec, T. Surrey, A. C. Maggs, and S. Leibler, *Nature,* 1997, **389**, 305–308.

11. C. W. Reynolds, *Comp. Graph.*, 1987, **21**, 25-34.

12. T. Vicsek, A. Czirok, E. Ben-Jacob, I. Cohen, and O. Shochet, *Phys. Rev. Lett.*, 1995, **75**, 1226-1229.

13. I. D. Couzin, *Trends. Cogn. Sci*., 2008, **13**, 36-43.

14. P. Kraikivski, R. Lipowsky, and J. Kierfeld, *Phys. Rev. Lett*., 2006, **96**, 258103 (1-4).

15. H. Levine, W. J. Rappel, and I. Cohen, *Phys. Rev. E*, 2000, **63**, 017101 (1-4).

16. G. Gregoire, and H. Chate, *Phys. Rev. Lett*., 2004, **92**, 025702 (1-4).

17. F. Ginelli, F. Peruani, M. Bär, and H. Chate, *Phys. Rev. Lett*., 2010, **104**, 184502 (1-4).

18. K. H. Nagai, Y. Sumino, R. Montagne, I. S. Aranson, and H. Chate, *Phys. Rev. Lett*., 2015, **114**, 168001 (1-6).

19. V. Schaller, C. Weber, C. Semmrich, E. Frey, and A. R. Bausch, *Nature*, 2010, **467**, 73-77.

20. Y. Sumino, K. H. Nagai, Y. Shitaka, Y. Tanaka, K. Yoshikawa, H. Chate, and K. Oiwa, *Nature*, 2012, **483**, 448-452.

21. T. Sanchez, D. T. N. Chen, S. J. DeCamp, M. Heymann, and Z. Dogic, *Nature*, 2012, **491,** 431-435.

22. Y. Liu, Y. Guo, J. M. Valles, Jr. and J. X. Tang, *Proc. Natl. Acad. Sci. USA*, 2006, **103**, 10654-10659.

23. Y. Guo, Y. Liu, R. Oldenbourg, J. X. Tang and J. M. Valles, Jr, *Phys. Rev. E*, 2008, **78**, 04910

24. S. Köhler, O. Lieleg and A. R. Bausch, *PLoS ONE*, 2008, **3**, e2736..

25. A.C. Reymann, J. L. Martiel, T. Cambier, L. Blanchoin, R. Boujemaa-Paterski and M. Théry, *Nat. Mater*., 2010, **9**, 827-832

26. D. Popp, A. Yamamoto, M. Iwasa and Y. Maéda, Biochem. *Biophys. Res. Comm*., 2006, **351**, 348-353

27. D. Marenduzzo, K. Finan and P. R. Cook, *J. Cell Biol.*, 2006, **175**, 681-686.

28. T. Sanchez, D. Welch, D. Nicastro and Z. Dogic, *Science*, 2011, **333**, 456-459

29. T. Sanchez, D. T. N. Chen, S. J. DeCamp, M. Heymann and Z. Dogic, *Nature*, 2012, **431**, 491-435

30. G. M. Whitesides, and B. Grzybowski, *Science*, 2002, **295**, 2418-2421.

31. M. Fialkowski, K. J. M. Bishop, R. Klajn, S. K. Smoukov, C. J. Campbell, and B. A. Grzybowski, *J. Phys. Chem. B*, 2006, **110**, 2482-2496.

32. M. C. Cross, and P. C. Hohenberg, *Rev. Mod. Phys*., 1993, **65**, 851-1123.

33. Y. Jeune-Smith and H. Hess, *Soft Matter*, 2010, **6**, 1778-1784.

34. S. Asakura, and F. Oosawa, *J Chem Phys*, 1954, **22**, 1255–6.

35. B. G¨otzelmann, R. Evans and S. Dietrich, *Phys. Rev. E*, 1998, **57,** 6785.

36. D. J. Needleman, M. A. Ojeda-Lopez, U. Raviv, K. Ewert, et al. *Phys Rev Lett*, 2004, **93**, 198104.

37. M. Hosek, J. X. Tang. *Soft Matter Phys*, 2004, **69**, 051907.

38. A. W. C Lau, A. Prasad, Z. Dogic, *Epl-Europhys Lett*, 2009, **87**, 48006.

39. F. Huber, D. Strehle, J. Schnauss, J. Kas, *New J Phys*, 2015, **17**, 043029.

40. M Barun, Z Lansky, F Hilitsky, Z. Dogic, S. Diez, *Bioessays*, 2006, **38**, 474.

41. R. Phillips, J. Kondev, and J. Theriot, Physical Biology of the Cell, Garland Science Publishing, United Kingdom, 2008, 524-529.

42. F. Hilitski, A. R. Ward, L. Cajamarca, M. F. Hagan, G. M. Grason and Z. Dogic, *Phys. Rev. Lett*., 2015, **114**, 138102

43. D. Inoue, T. Nitta, A. M. R. Kabir, K. Sada, J. P. Gong, A. Konagaya, and A. Kakugo, *Nat. Commun*., 2016, **7**, 12557:1-10.

44. K. V. Mardia, and P. E. Jupp, *Directional Statistics*, John Wiley and Sons Ltd., England, 2000, 57-82.

45. R. Rezakhaniha, A. Agianniotis, J. T. C. Schrauwen, A. Griffa, D. Sage, C. V. C. Bouten, F. N. Van de vosse, M. Unser, and N. Stergiopulos, *Biomech. Model. Mechanobiol.*, 2012, **11**, 461-473.

46. B. V. Vaart, A. Akhmanova, A. Straube, *Biochem. Soc. Trans*. 2009, **37**, 1007.

47. I. Theurkauff, C. Cottin-Bizonne, J. Palacci, C. Ybert, L. Bocquet, *Phys. Rev. Lett.* 2012, **108**, 268303.

48. W. O. Hancock, Protein-based Nanotechnology: Kinesin–Microtubule-driven Systems for Bioanalytical Applications, Wiley-VCH Verlag GmbH & Co. KGaA, 2007.

49. M. Castoldi, and A. V. Popov, Protein Expres. Purif, 2003, 32, 83-88.

50. R. B. Case, D. W. Pierce, H. B. Nora, L. H. Cynthia, and R. D. Vale, *Cell*, 1997, **90**, 959-966.

51. A. M. R. Kabir, D. Inoue, A. Kakugo, A. Kamei, and J. P. Gong, *Langmuir*, 2011, **27**, 13659-13668.

52. A. M. R. Kabir, D. Inoue, A. Kakugo, K. Sada, and J. P. Gong, *Polym. J.*, 2012, **44**, 607-611.

53. G. M. Whitesides, B. Grzybowski, Science, 2002, **295**, 2418-2421.

54. M. Fialkowski, K. J. M. Bishop, R. Klajn, S. K. Smoukov, C. J. Campbell and B. A. J. Grzybowski, Phys. Chem. B, 2006, **110**, 2482-2496.

55. M. C. Cross and P. C. Hohenberg, Rev. Mod. Phys., 1993, 65, 851-1123.

56. S. Murata, A. Konagaya, S. Kobayashi, H. Saito, M. Hagiya, New Generat. Comput., 2013, **31**, 27-45.

57. Hagiya M., Konagaya A., Kobayashi S., Saito H. and Murata S., Acc. Chem. Res.,2014, **47**, 1681-1690.

Chapter 3

Rigidity of active cytoskeletal filaments governs the mode of their collective motion

Abstract

I have regulated the mode of collective motion of gliding microtubules by changing their rigidity. Relatively rigid microtubules generate a large-scale spiral pattern and enhance local polarization in their movement, whereas local streams are formed due to the collective motion of flexible microtubules. Rigidity of microtubules is found directly correlated to the extent of noise in their movement, which in turn affects the mode of their collective motion. This work has experimentally supported the theoretical models of collective motion by showing how the self-organization of self-propelled particles is governed by the mechanical property of individuals.

3.1 Introduction

Collective motion is a fascinating example of coordinated behavior of self-propelled objects in nature such as animals, flocks of birds, cells and bacteria, which is associated with formation of large scale patterns[1-10]. The detailed study on collective motion may provide us insight into the emergent structures, and functions, which consequently will allow us obtaining information about how to assemble a large number of collectively moving self-propelled objects to more ordered structures with a view to application in nanotechnology. The *in silico* works have provided mechanistic details on generation of different mode of collective motion[11-17]. For instance, Vicsek model has suggested that the density of moving agents and noise in their movement are important parameters that can regulate the mode of collective motion[11]. Later on, Nagai group has reported that the mode of collective motion[12] also depends on the persistence in the movement of the self-propelled particles. However, these theoretical models are still lacking proper experimental verification. In recent years biomolecular motor systems F-actin/myosin and microtubule/dynein or microtubules/kinesin have emerged as ideal candidates for experimentally demonstrating the collective motion and different type of pattern formation through *in vitro* gliding assay[18-22].

In the chapter 2, I have demonstrated collective motion of microtubules driven by kinesin and investigated the roles of some physiochemical properties (i.e. concentrations of microtubule and depletion force) on the kinetics of collective motion. In this chapter I will describe, how the mechanical property i.e. rigidity of microtubules influences their collective motion. I investigated the collective motion of microtubules by varying their rigidity and found that, the flexible microtubules generate local streams and rigid microtubules generate large spiral pattern through collective motion. My analysis of single microtubule motility suggested that the change in rigidity of microtubules has a profound influence on their persistence length and noise of movement. These experimental findings support the theoretical predictions and offer a simple approach to control the mode of collective motion of self-propelled particles only by changing their physical property.

3.2 Results and discussion

In the previous chapter, I have demonstrated the collective motion of the microtubules, where the microtubules were prepared from tubulin using guanosine-5′-triphosphate (GTP) [Figure 3.1]. The collective motion was demonstrated using an *in vitro* gliding assay and stream like pattern was observed in the collective motion of microtubules.

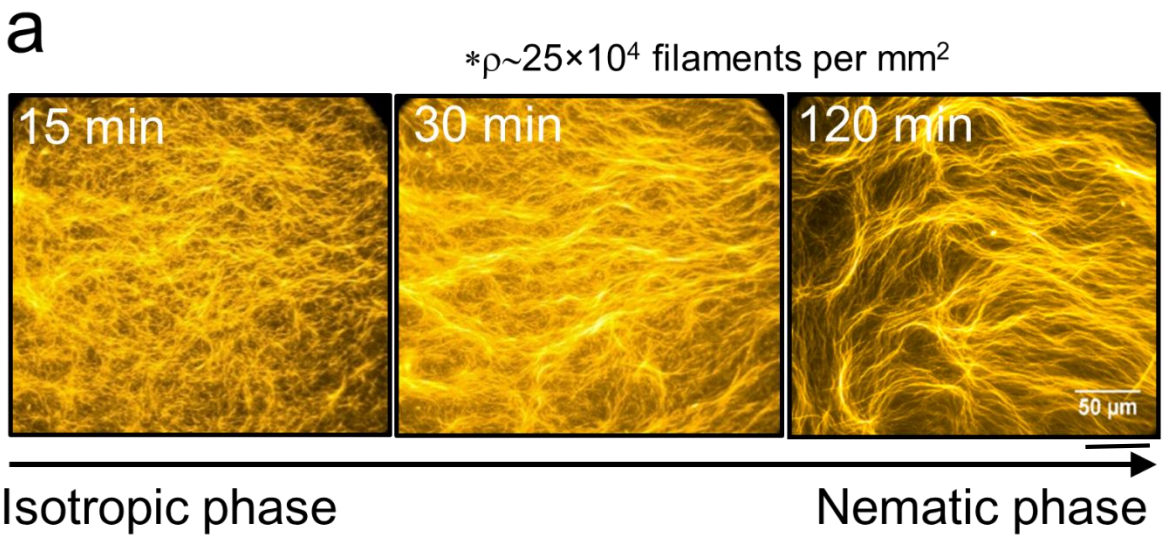

Figure 3.1: Time-lapse fluorescence images showing emergence of stream pattern by the collective motion of GTP-microtubules. Scale bar: 50 µm.

GTP-microtubules are structurally flexible[23, 24] and the flexural rigidity of taxol stabilized GTP-microtubules is $32\pm2\times10^{-24}$ Nm^2. To study the influence of the mechanical property of microtubules on their collective motion, next I performed collective motion of microtubules by varying their rigidity. For this, I polymerized tubulins using GMPCPP (guanosine-5'-[(α,β)-methyleno] triphosphate). It is reported, GMPCPP-microtubules are structurally rigid than GTP-microtubules and its flexural rigidity is $62\pm2\times10^{-24}$ Nm^2 [23, 24].

3.2.1 Collective motion of rigid microtubules

Collective motion of GMPCPP-microtubules was demonstrated using the same experimental setup as used previously in the study of collective motion of GTP-microtubules. The density of GMPCPP- microtubules in the motility assay was $\sim22\times10^4$ filaments per mm^2. By adding ATP buffer, motility of the microtubules was initiated on the kinesin carpet at room temperature (25 ^oC). The microtubules were monitored under a fluorescence microscopy.

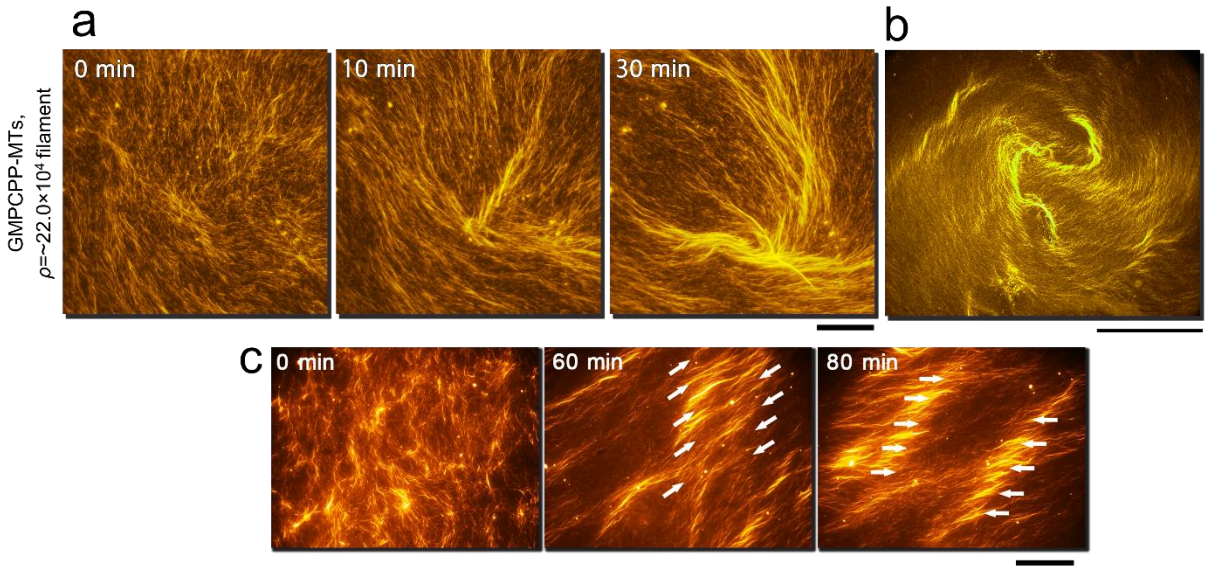

Figure 3.2: Collective motion of rigid microtubules. Time-lapse fluorescence images showing emergence of spiral pattern (a) in the collective motion of rigid microtubules, the full view of spiral pattern captured after 120 min of addition of ATP (b), and density-wave of microtubules in the spiral pattern (c). Scale bar for a, c is 50 μm and for b is 500 μm respectively.

Just after initiation of motility, most of the microtubules showed polarity in their motility by approaching towards the center of the flbhuow cell and constructed a spiral pattern [Figure 3.2a]. Over time, this spiral pattern spanned over the entire flow cell and generated a large spiral pattern [Figure 3.2b] with diameter of ~3 mm. The microtubules in the spiral pattern also exhibited density wave like motion [Figure 3.2c].

3.2.2 Tuning the mode of collective motion by changing microtubules rigidity

I have demonstrated the collective motion of microtubules by changing their mechanical property (rigidity) and formation of different modes of patterns are obtained. The flexible microtubules (GTP-microtubules) generate nematic local streams in collective motion, while the rigid microtubules (GMPCPP-microtubules) assemble to a polar spiral pattern.

The diversity in orientation of microtubules in random, streams and spiral patterns was differentiated by calculating the circularity of microtubules in each phase. The circularity is defined as the spatial correlation of the moving microtubules in a circular pathway.

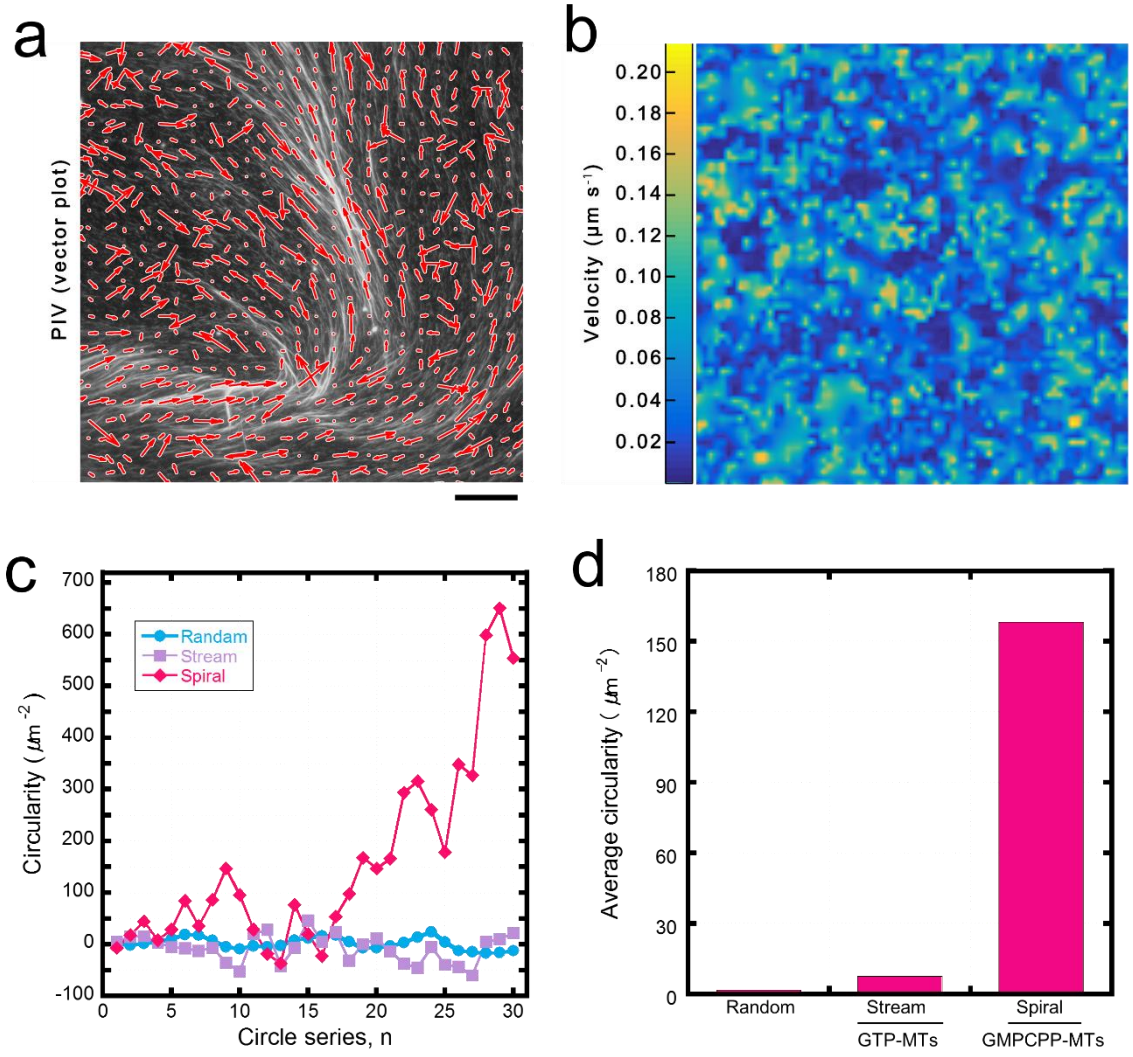

Figure 3.3: Estimation of circularity of microtubules in collective motion. The (a) vector profile and (b) color map of velocity of GMPCPP-microtubules in collective motion estimated from PIV analysis. The circularity profile (c) and average circularity (d) of microtubules after 30 min of ATP addition. Scale bar: 5 μm.

The circularity of the microtubules in different patterns (random, stream, spiral) was estimated using PIV (particle image velocimetry) method[25]. In this technique, the velocity vector profile of microtubules was determined first (as shown in Figure 3.3a). The detailed of the determination of circularity analysis is given in experimental section. The circularity of microtubules in spiral and stream pattern were determined and found that the microtubules in spiral pattern attained the highest circularity. As expected due to circular orientation of microtubules in the spiral pattern, a large average value of circularity for spiral pattern was observed [Figure 3.3d]. In contrary, in the stream pattern the direction of alignment of microtubules was linear with less spatial circular coherency than that in spiral pattern. Such

alignment of microtubules might be attributed to the smaller circularity value for microtubules in streams [Figure 3.3d]. Thus, the circularity analysis provides us an idea in differentiating the orientation of microtubules in different phases.

Here, by changing the mechanical property (rigidity) of individual microtubules, I obtained completely two different modes of collective motion leading to formation of different patterns. Next, I have investigated the role of length of microtubules and concentration on their collective motion.

3.2.3 Effect of length and concentrations of flexible microtubules on their collective motion

I investigated in details the collective motion of flexible microtubules by changing the length and concentration of microtubules. I prepared GTP-microtubules by varying their lengths from very short to the long length. The average length (mean ± standard deviation) of microtubules of short, middle and long length GTP-microtubules were ~2.04±0.80, ~15.63±9.69, and ~39.32±15.53 μm respectively.

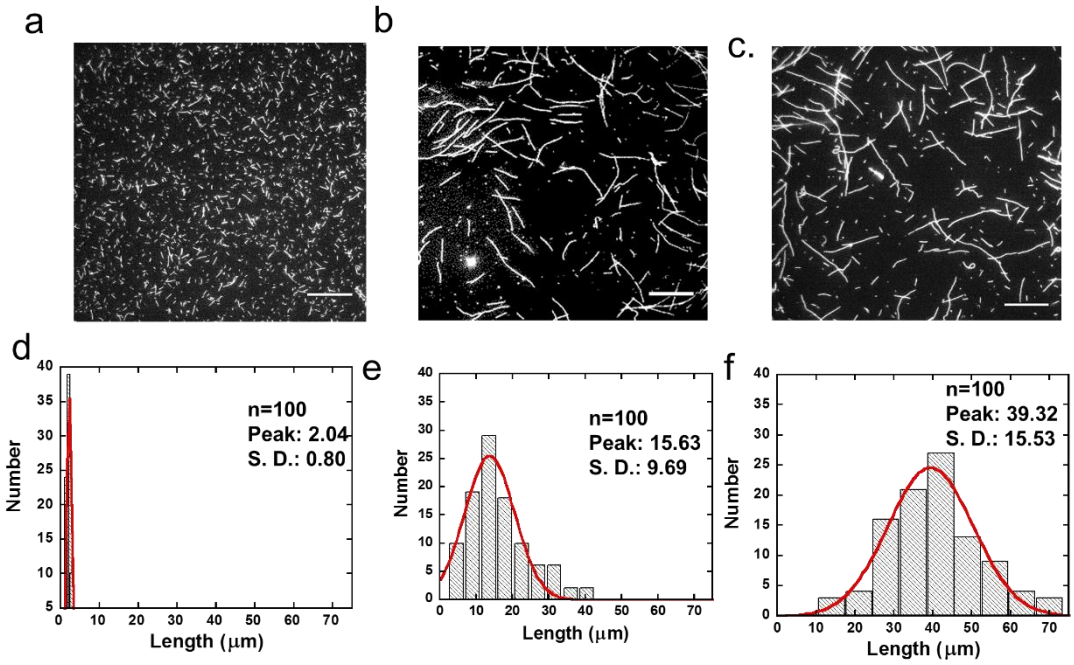

Figure 3.4: Fluorescence images (a, c) and corresponding Gaussian distribution (d-f) of length of short, middle, and long length GTP-microtubules. Scale bar: 5 μm.

Then experiments were performed by varying the density of microtubules over a wide range (0.90 - 25 $\times 10^4$ filaments per mm^2). It was found that, at high density (at or above ~15×10^4

filaments per mm^2) irrespective of lengths, GTP-microtubules generate stream like pattern.

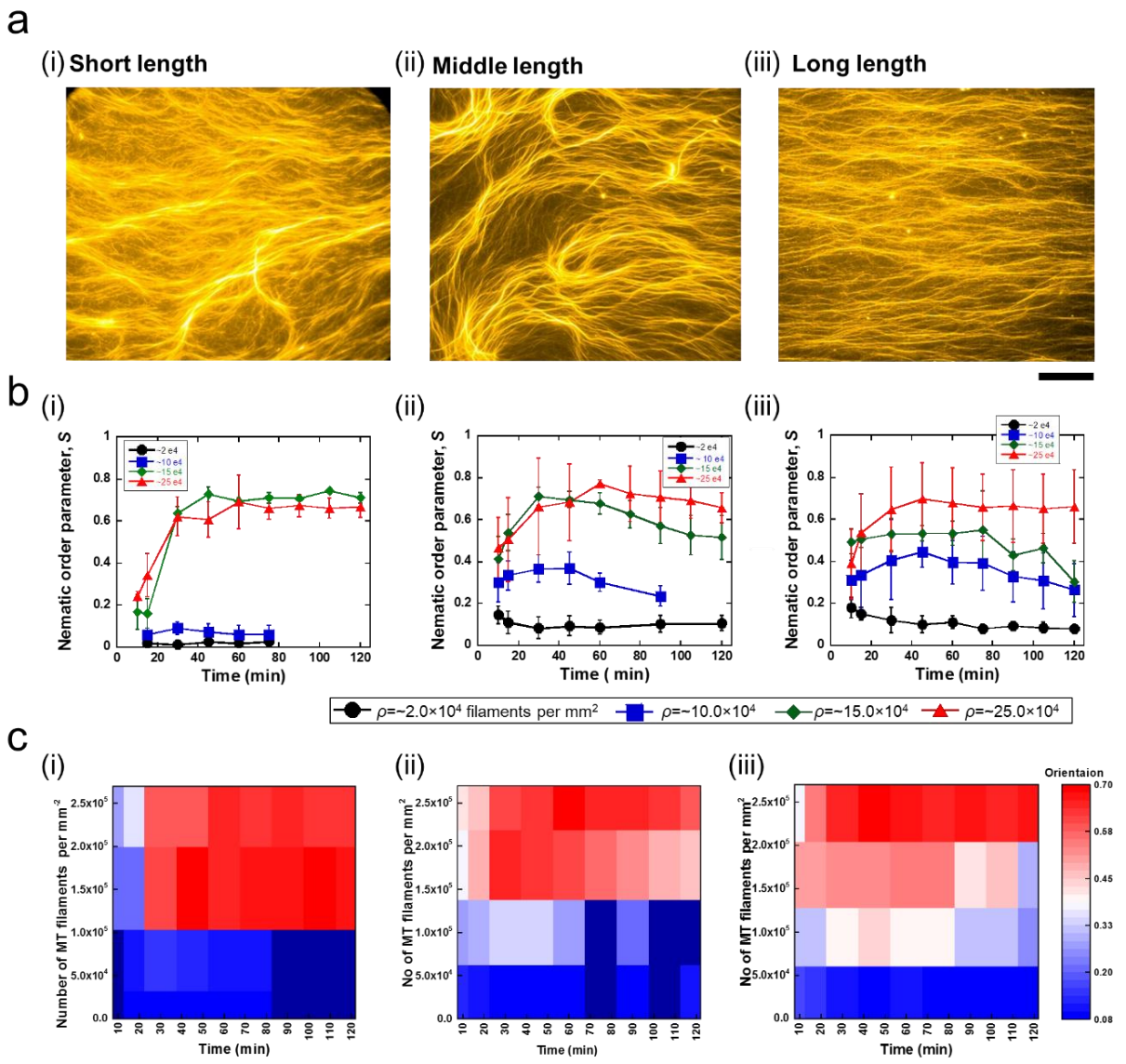

Figure 3.5: Effect of microtubule length on the collective motion. (a) Fluorescence images of short, middle, and long length GTP-microtubules in collective motion. Images were captured after 60 min of ATP addition. Scale bar: 25 μm. (b) Change of the orientation of (i.) short, (ii.) middle, and (iii.) long length GTP-microtubules with time. Here (a), (b), (c), and (d) corresponds to ~2.0, ~10.0, ~15.0 and ~25.0 ×10^4 microtubules per mm^2 (c) Heat maps showing the nematic order parameter of microtubules at different observation time as a function of microtubule concentration.

The orientation of microtubules at different time was further quantified by calculating nematic order parameter of the microtubules, *S* through analyzing their fluorescence microscopy images using 'Image *J* plugin Orientation *J*' [26, 27]. The value of *S* ranges between 0 and 1, where S=0 or 1 represents random or ordered/aligned orientation of the microtubules respectively. For

lower density, the order parameter was close to zero and remained steady all over the observation period. When the density was increased the order parameter for orientation of microtubules increased. Therefore, the upsurge of order parameter towards ~1 reveals that at high density with time the collective motion of microtubules took place which caused a phase transition from isotropic to nematic state [Figure: 3.5b]. The phase transition kinetics can be more clearly understood from the heat maps showing the distribution of orientation of microtubules at different time with respect to surface density [Figure 3.5c]. Initially, just after ATP addition (0 min), no ordered orientation of microtubules was observed for any of the concentrations of microtubules of all lengths. For this observation time, the heat map entirely represents random orientation of the microtubules [blue region]. At high concentration (~ 25×10^4 filaments per mm^2) at about 25 min after addition of ATP, nematic phase can be detected [red region] for short length microtubules [Figure 3.5c i.]. In contrast, for middle length microtubules the phase transition kinetics in collective motion was little sluggish (e.g., 30 min) [Figure 3.5 (c) ii.]. A clear separation of the random isotropic and ordered nematic phase could be easily observed from the heat maps, for long length GTP-microtubules. After ~15 min of ATP addition, orientation order of microtubules reached to plateau. Thus, the phase transition is faster in collective motion of long length GTP-microtubules. Based on the above discussion, the role of microtubules length in their collective motion can be clearly visualized. The length of GTP-microtubules may not affect the spatial pattern formation but significantly change their phase transition kinetics.

3.2.4 Effect of length and concentration of rigid microtubules on their collective motion

A detailed study on the collective motion of rigid microtubules was carried out by changing the length and concentration of the microtubules. First, the effect of concentration of GMPCPP-microtubules on the emergence of collective emotion was investigated. The concentration of microtubules was varied from 1.0 to 5.0 μM keeping the concentration of kinesin same. The fluorescence images of microtubules captured after 60 min of addition of ATP is presented in Figure 3.6. From the fluorescence images, the influence of concentration of microtubule on the emergence of spiral pattern can be understood well. At lower concentration, the orientation of microtubules was random. These experimental results were further justified by the circularity analysis of microtubules using PIV.

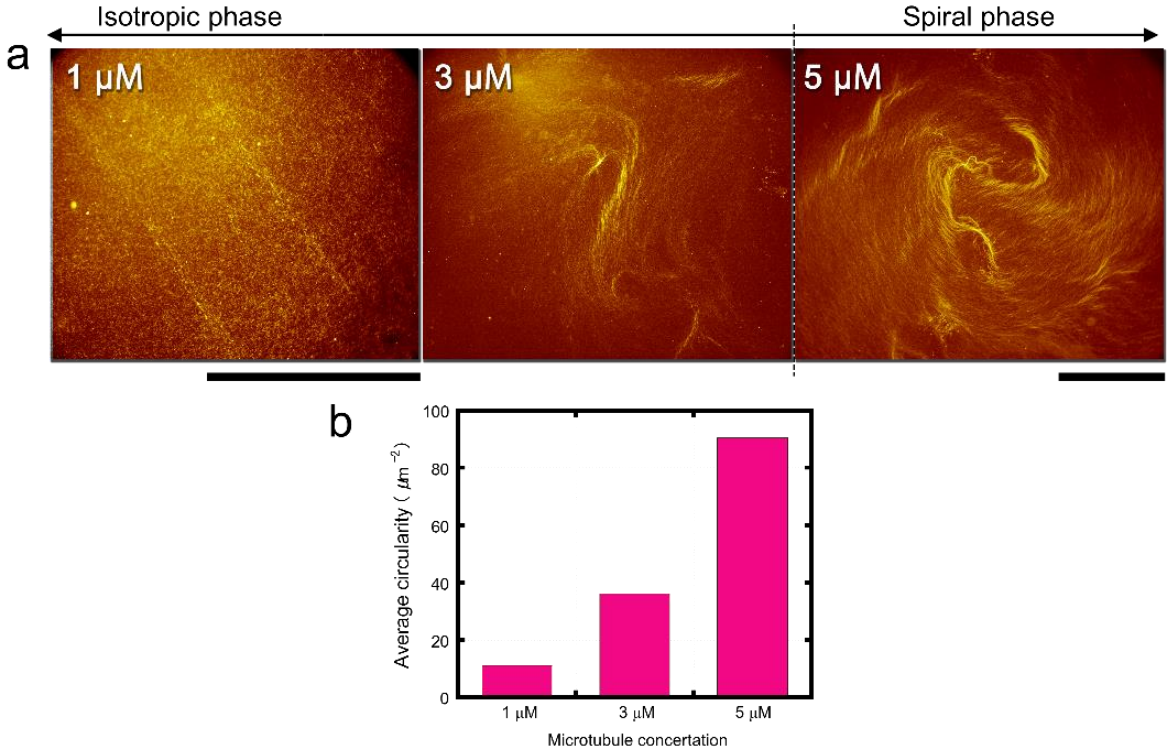

Figure 3.6: (a) Effect of concentration of microtubules on the collective motion of microtubules. Scale bar: 200 μm. (b) The average circularity of microtubules at every condition.

Next, using rigid microtubules of two different lengths: short (average ± standard deviation) (4.19±2.05 μm) and long (average ± standard deviation) (12.75±7.35 μm), the effect of length of microtubule on their collective motion was studied.

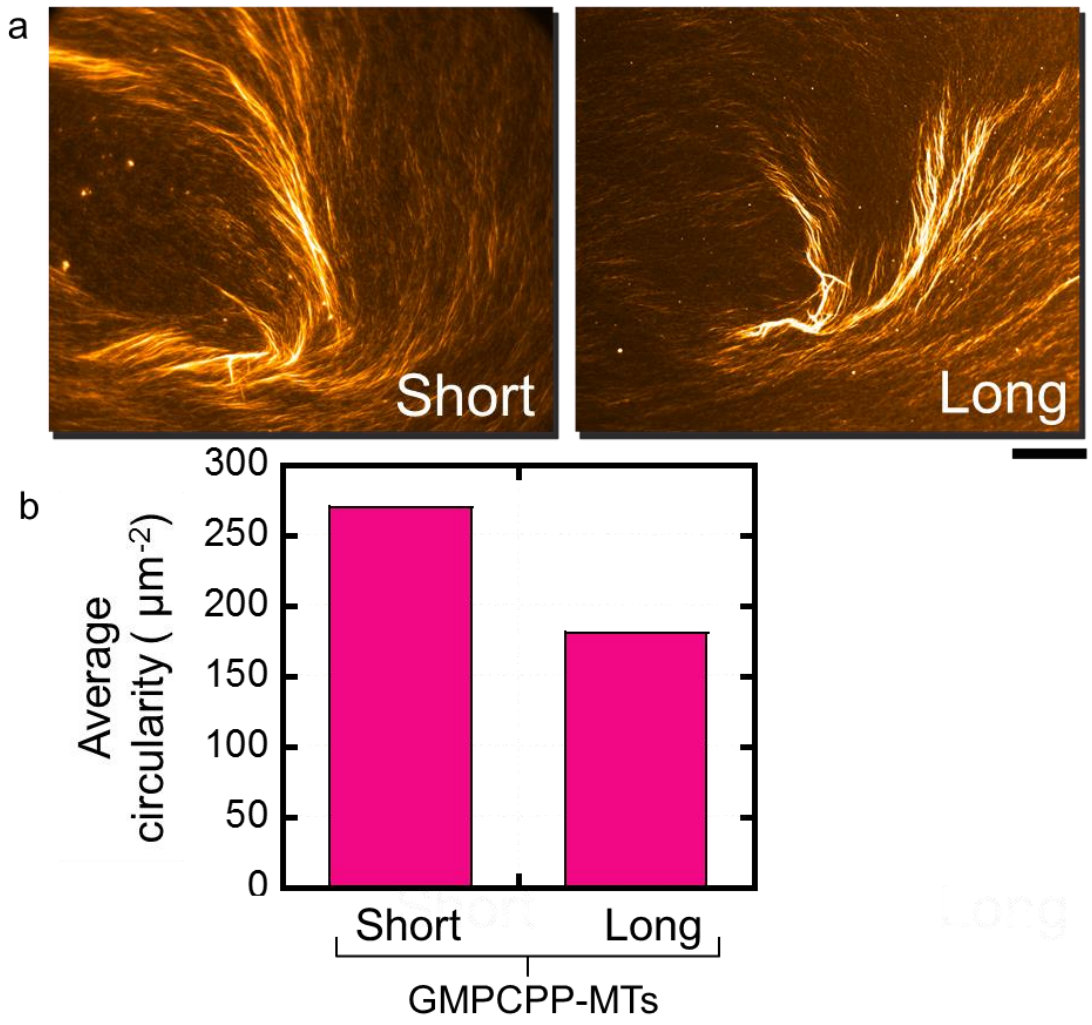

Figure 3.7: Collective motion of short and long length rigid microtubules. (a) Fluorescence images showing orientation of short and long length GMPCPP-microtubules in collective motion (b) Average circularity of spiral pattern shown in figure a. The images were captured after 60 min of ATP addition. Scale bar: 20 μm.

In the fluorescence images of microtubules shown in Figure 3.7, the generation of spiral patterns in collective motion of both short and long length microtubules can be observed. In the PIV analysis, no considerable difference in average circularity of long and short length microtubules was found. This implies that length of microtubules may not affect the mode of collective motion. The effect of motor protein concentration on spiral pattern formation was also investigated and it was found that the motor protein concentration has no influence on collective motion of rigid microtubules.

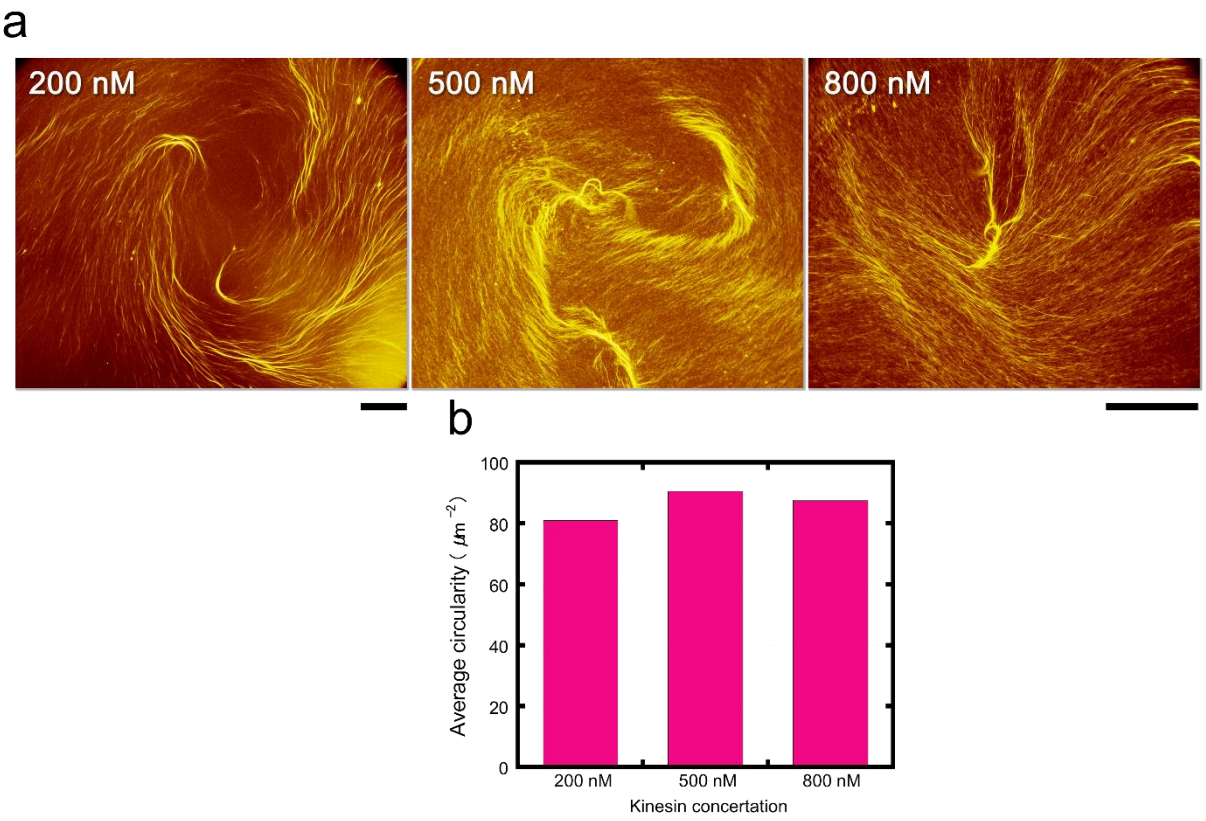

Figure 3.8: Effect of concentration of kinesin on collective motion of GMPCPP- microtubules. Emerged spiral pattern of microtubules at different kinesin concentrations (a). Scale bar: 500 μm. The estimated average circularity of microtubules in the spiral patterns (b).

3.2.5 Mechanism behind tuning of the mode of collective motion: experimental verification of theoretical approaches

The aforementioned experimental results suggest that, the mechanical property of microtubules influences the mode of collective motion and pattern formation by the microtubules. For instance, rigid microtubules generated spiral pattern and flexible microtubules oriented to local streams. In order to explore the mechanism behind governing the mode of collective motion upon changing the mechanical property, I investigated the behavior of single microtubule filaments. In the motility assay of microtubules, two different types of interactions such as snuggling and crossing over occur. The snuggling is the most important event in generation of collective motion and I have found that there is no major difference in snuggling probability for long and short GTP and GMPCPP-microtubules. The distribution of snuggling angle also demonstrates similar phenomenon.

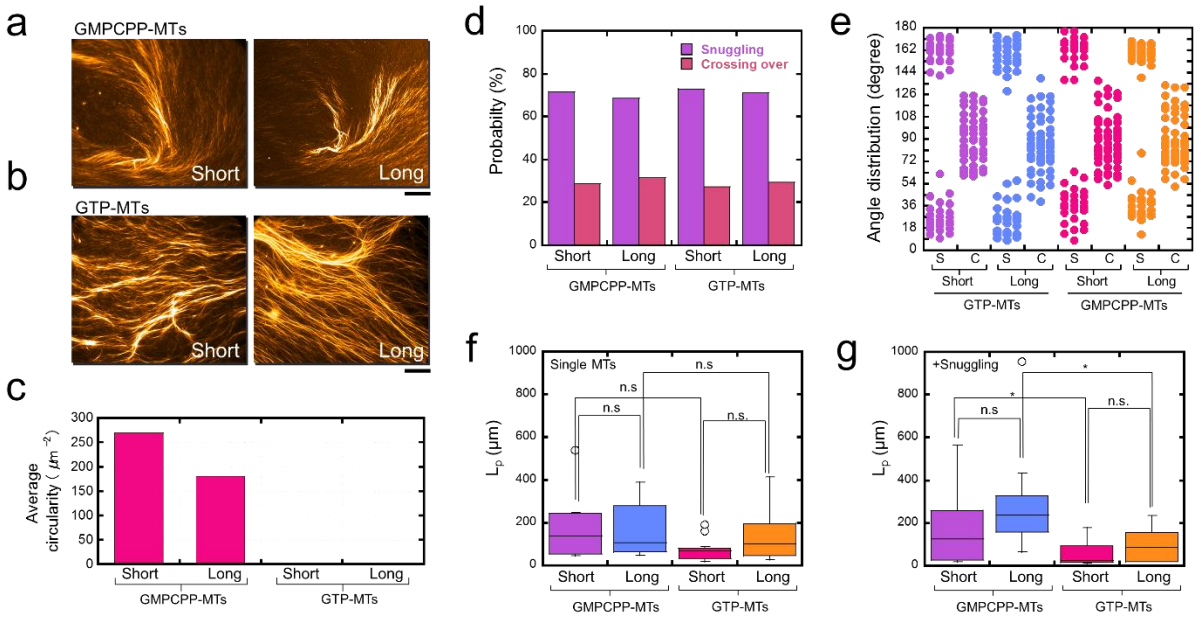

Figure 3.9: The formation of (a) spiral, (b) stream pattern by microtubules of different rigidity. Scale bar: 100 μm. The average circularity of microtubules for each pattern (c). Analysis of single microtubule filaments (d) interaction probability, (e) distribution of snuggling angle, (f) persistence angle and (g) snuggling length of microtubules respectively.

A substantial difference was observed for the persistence length and snuggling length of microtubules upon change in rigidity. The snuggling length was measured from the trajectory of single filaments undergoing snuggling during their motility. The amount of noise in movement of microtubules in different modes of their collective motion was also determined and presented in Figure 3.10. The noise was estimated by counting the events of derailment of microtubules from the average route in their collective motion. The experimental analysis reveals that as the rigidity of microtubules increases, the amount of noise decreases and vice versa.

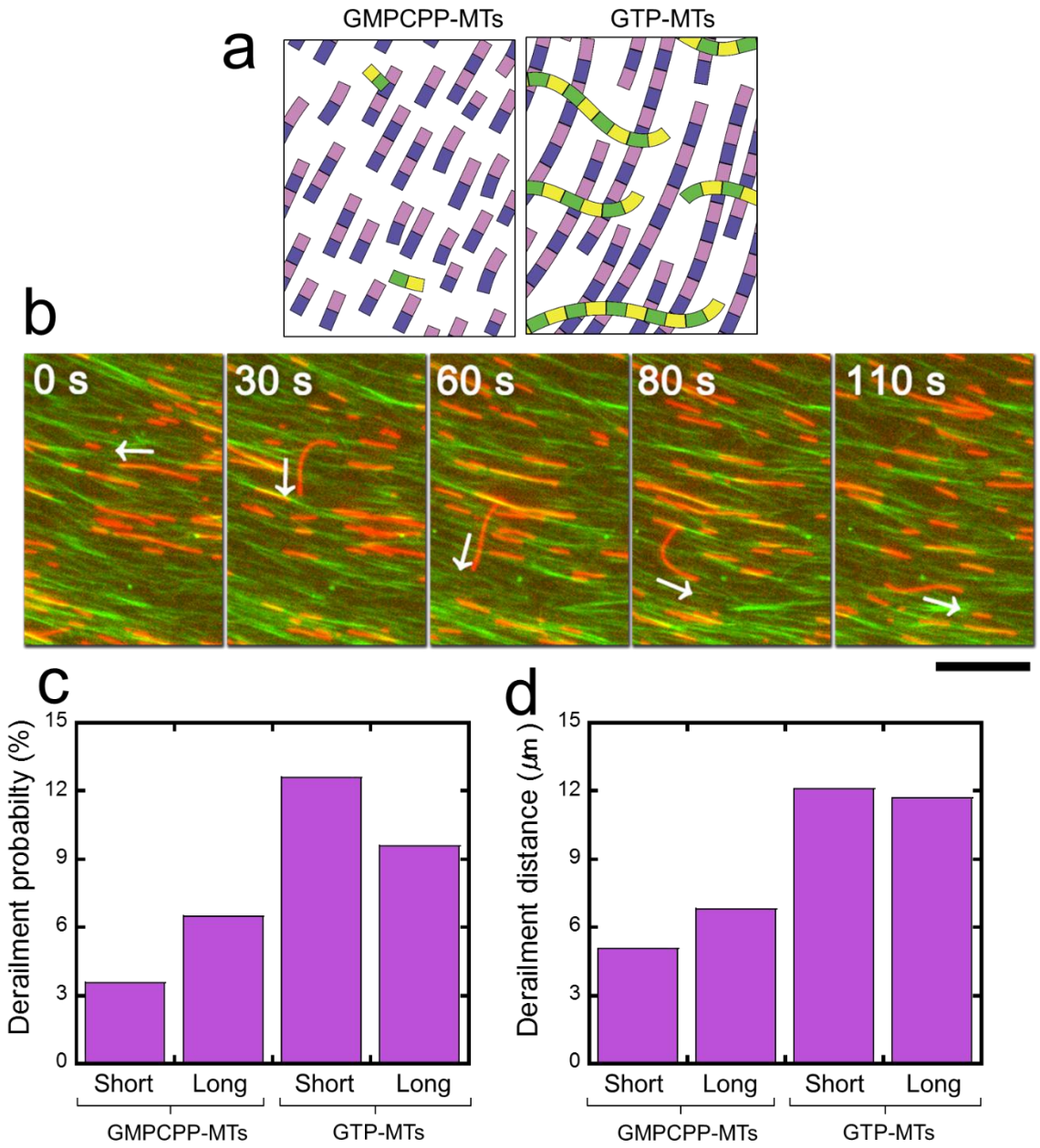

Figure 3.10 The extent of noise (derailment) of microtubule movement is regulated by microtubules mechanical property. A schematic diagram (a) and fluorescence images showing derailment of microtubule in collective motion. Scale bar: 10 μm. (c) The extent of derailment, and the length of (c) derailment of microtubules in their collective motion.

The previous theoretical model suggested some postulates on the mode of collective motion of moving agents considering the properties of individuals. the famous model of 'self-propelled particles' by Vicsek cited that the density of moving agents and noise are important parameters that control the phase transition of moving objects from disorder to ordered state[11]. Nagai group has reported that, the persistence length of moving objects plays an important role in generation

of large structures like, vortex pattern[12]. However, these postulates are lacking proper experimental verification.

My experimental results directly support these postulates. I have found differences in persistence length and snuggling length in two different modes of collective motion i.e; in spiral and stream. In addition, the amount of noise is also different in the two patterns. In more ordered polar spiral pattern, the extent of noise is less than in the stream patterns. In a generic sense, the mechanical property of microtubules can govern the mode of collective motion, which supports the theoretical approaches taken to describe the role of moving objects in the mode of their collective motion. This work approaches to the concept of programing the self-organization of cytoskeletal filaments by simply changing their mechanical property. This may not only provide us with a method to program the active-self organization of self-propelled particles but also will be helpful to understand the dynamics of active matters in nature.

3.3 Conclusions

In conclusion, I have demonstrated collective motion of microtubules, which leads to the emergence of streams and large spiral patterns in collective motion of microtubules driven by kinesin. The microtubules in stream pattern are in nematic orientation, whereas polarized orientation of microtubules is found in spiral pattern. Microtubules with different structural rigidity show differences in their motile behavior, more specifically, in their persistence length, snuggling length, and amount of noise in collective motion. According to the theoretical predications, these parameters are very important to control the mode of collective motion of moving objects. This work thus provides an experimental verification of the existing theoretical models and offer a new approach to control the mode of collective motion of self-propelled systems by changing the rigidity of individuals.

3.4 Experimental

3.4.1 Preparation and labelling of proteins

Tubulin was purified from porcine brain using a high-concentration PIPES buffer (1 M PIPES, 20 mM EGTA, and 10 mM $MgCl_2$; pH was adjusted to 6.8 using KOH) [28]. The high-concentration PIPES buffer and BRB80 buffer were prepared using PIPES from Sigma, and the pH was adjusted using KOH. Kinesin-1 consisting of the first 575 amino acid residues of human kinesin-1 was prepared by partially modifying the expression and purification methods described in literature[29]. Rhodamine-labelled microtubules were obtained by polymerizing a mixture of rhodamine-labelled tubulin (RT) and non-labelled tubulin (WT) (RT: WT = 4:1; final tubulin concentration, 55.6 μM) at 37 °C in the presence of 1 mM GTP according to the standard technique. The solution containing the microtubules was then diluted with motility buffer (80 mM PIPES, 1 mM EGTA, 2 mM $MgCl_2$, 0.5 mg mL^{-1} casein, 1 mM DTT, 10 μM paclitaxel and ~1% DMSO; pH 6.8).

3.4.2 *In vitro* gliding assay of microtubules

A flowcell with dimensions of 5.0×5.0×0.15 mm^3 (W×L×H) was assembled from two cover glasses of sizes (5×7) mm^2 and (40×50) mm^2 (MATSUNAMI), and a double-sided tape was used as the spacer. First the surface of the flowcell was coated with casein buffer (80 mM PIPES, 1 mM EGTA, 1 mM $MgCl_2$ and ~0.5 mg mL^{-1} casein; pH 6.8) and incubated for 3 min. Then 3 μL of kinesin-1 solution (~80 mM PIPES, 1 mM EGTA, 1 mM $MgCl_2$, 0.5 mg mL^{-1} casein, 1 mM DTT, 10 μM paclitaxel/DMSO, ~1% DMSO; pH 6.8) was applied to the flowcell and incubated for 1 min to bind the kinesin to the casein coated surface of the flowcell through non-specific interaction. The flowcell was washed with 5 μL of motility buffer (80 mM PIPES, 1 mM EGTA, 1 mM $MgCl_2$, 0.5 mg mL^{-1} casein, 1 mM DTT, 10 mM paclitaxel and ~1% DMSO; pH 6.8). Next, 3 μL of microtubule solution of a prescribed concentration was applied to the flowcell and incubated for 2 min, followed by washing with 5.0 μL of motility buffer. Then, 10 μL of 10 mM adenosine tri-phosphate (ATP) buffer containing methylcellulose of a prescribed concentration (~80 mM PIPES, 1 mM EGTA, 1 mM $MgCl_2$, 0.5 mg mL^{-1} casein, 1 mM DTT, 10 μM paclitaxel/DMSO, 0-0.3 wt% methylcellulose, ~1% DMSO; pH 6.8) was added to the flowcell. The flowcell was placed inside the inert chamber after the addition of ATP and humid nitrogen gas was passed through the chamber to remove oxygen from the chamber[30, 31]. The time of ATP addition was set as 0 min, and microtubules were monitored

under a fluorescence microscopy. All these experiments were performed at room temperature..

3.4.3 Microscopic image capture

The samples were illuminated with a 100-W mercury lamp and visualised with an epifluorescence microscope (Eclipse Ti; Nikon) using oil-coupled Plan Apo 60× 1.40 and dry Plan Flour 10×0.30 objectives (Nikon). Filter blocks with UV-cut specifications (TRITC: EX540/25, DM565, BA606/55; GFP-HQ: EX455-485, DM495, BA500-545; Nikon) were used in the optical path of the microscope to allow for visualisation of samples while eliminating the UV portion of the radiation and minimising the harmful effects of UV radiation on the samples. Images and movies were captured using a cooled CMOS camera (Neo sCMOS; Andor) connected to a PC. To capture a field of view for more than several minutes, ND filters (ND4, 25% transmittance) were inserted into the illuminating light path of the fluorescence microscope to avoid photobleaching.

3.4.4 Analysis of the microscopic image

Quantitative analysis of collective motion of microtubule

The orientation of microtubules was calculated in terms of nematic order parameter (*S*), which was calculated according to the following equation by using Image J plugin, orientation J (http://bigwww.epfl.ch/demo/orientation/)

$$S = \frac{1}{N}\sqrt{\left(\sum_{i=0}^{180} R_i \cos 2\Theta_i\right)^2 + \left(\sum_{i=0}^{180} R_i \sin 2\Theta_i\right)^2}$$

where N refers to total number of microtubules in the frame, R_i is frequency of the angle of individual microtubules Θ_i (i = 0 to 180). The range of Θ_i was fixed from 0° to 180° based on the symmetry of horizontally or vertically aligned microtubules with respect to the X-axis. Since the microtubules in the nematic phase were oriented along the X-axis, we fixed the director for both the isotropic and nematic phase along the X-axis and measured the nematic order parameter of microtubules in the XY plane.

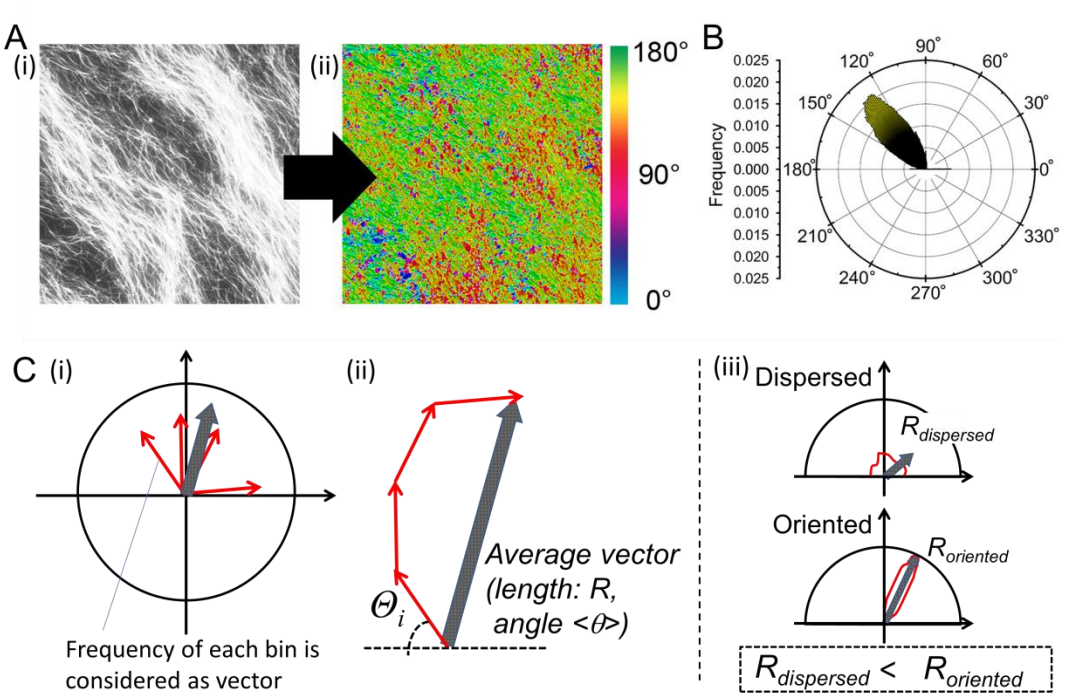

Figure 3.10: Analysis method of the angles and degree of orientation of microtubules. (**A**) (i) Fluorescent microscopic image of microtubules. (ii) Color map representing the distribution of microtubule orientation angles. (**B**) Circular histogram of orientation angles of microtubules obtained from a fluorescent microscopic image of microtubules in (A). (**C**) Directional analysis method. (i) Here each bin in the circular histogram is considered as a vector (length: R_i, angle: Θ_i). (ii) Average vector (length: R, mean orientation angle $<\theta>$) was used for evaluation of orientation direction and degree of orientation. (iii) Relationship between R and degree of orientation. If distribution of microtubules angles is dispersed, R becomes smaller ($R_{\text{dispersed}}$) than that of high oriented microtubules (R_{oriented}).

Circularity Analysis:

The circularity was analyzed using the following equation

$$Circulation\,[\mu m^2] = \sum_{i}^{N} \left(\frac{[\boldsymbol{V}_{MT,i}][\boldsymbol{d}_{field,i,n}]\cos\theta_i}{[\boldsymbol{V}_{av}]} \right)$$

Where V_{MT}, i is the velocity vector of MTs at point *i*. $d_{field,\,i,\,n}$ represents field vector at point *I* in n^{th} field circle and θ is the angle between $V_{MT,\,i}$ and $d_{field,\,i,\,n.}$ V_{av} is the average velocity of MTs. N is the number of the velocity vectors aligning with N^{th} field circle.

3. 5 References

1. T. Vicsek, *Nature*, 2001, **411**, 421.
2. T. Vicsek, and A. Zafeiris, *Phys. Rep.*, 2012, **517,** 71-140.
3. J. K. Parrish, S. V. Viscido, and D. Grünbaum, *Biol. Bull*., 2002, **202**, 296-305.
4. K. Kruse, J. F. Joanny, F. Julicher, J. Prost, and K. Sekimoto, *Phys. Rev. Lett.*, 2004, **92,** 078101 (1-4).
5. M. Loose, E. Fischer-Friedrich, J. Ries, K. Kruse, and P. Schwille, *Science*, 2008, **320**, 789–792.
6. I. D. Couzin, J. Krause, N. R. Franks, and S. A. Levin, *Nature*, 2005, **433**, 513–516.
7. I. H. Riedel, K. Kruse, and J. A. Howard, *Science*, 2005, **309**, 300–303.
8. C. Dombrowski, L. Cisneros, S. Chatkaew, R. E. Goldstein, and J. O. Kessler, *Phys. Rev. Lett.*, 2004, **93**, 098103 (1-4).
9. A. Czirok, E. Ben-Jacob, I. Cohen, and T. Vicsek, *Phys. Rev. E*, 1996, **54**, 1791–1801.
10. F. J. Nedelec, T. Surrey, A. C. Maggs, and S. Leibler, *Nature*, 1997, **389**, 305–308.
11. T. Vicsek, A. Czirok, E. Ben-Jacob, I. Cohen, and O. Shochet, *Phys. Rev. Lett*., 1995, **75**, 1226.
12. K. H. Nagai, Y. Sumino, R. Montage, I. S. Aranson, and H. Chate, *Phys. Rev. Lett*., 2015, 114, 16801 (1-6).
13. F. Gineli, F. Perusni, M. Bar, and H. Chate, *Phys. Rev. Lett.*, 2010, 184502 (1-4).
14. A. Czirók, and T. Vicsek, *Statistical Mechanics of Biocomplexity*, 1999, Springer Berlin / Heidelberg, 152–164.
15. I. D. Couzin, J. Krause, R. James, G. D. Ruxton, and N. R. Franks, *J. Theor. Biol.*, 2002, **218**, 1.

16. F. Cucker, and E. Mordecki, *J. Math. Pure. Appl.*, 2008, **89**, 278-296.

17. F. Cucker, and S. Smale, *IEEE. T. Automat. Contr*., 2007, **52**, 852–862.

18. V. Schaller, C. Weber, C. Semmrich, E. Frey, and A. R. Bausch, *Nature*, 2010, **467**, 73-77.

19. Y. Sumino, K. H. Nagai, Y. Shitaka, Y. Tanaka, K. Yoshikawa, H. Chate, and K. Oiwa, *Nature*, 2012, **483**, 448-452.

20. T. Sanchez, D. T. N. Chen, S. J. DeCamp, M. Heymann, and Z. Dogic, *Nature*, 2012, **491,** 431-435.

21. D. Inoue, B. Mahmot, A. M. R. Kabir, T. I. Farhana, K. Tokuraku, K. Sada, A. Konagaya, and A. Kakugo, Nanoscale, 2015, **7**, 18054-18061.

22. A. Saito, T. I. Farhana, A. M. R. Kabir, D. Inoue, A. Konagaya, K. Sada, and A. Kakugo, *RSC Adv*., 2017, **7**, 13191-13197

23. J. Mickey, J. Howard, *J. Cell Biol.* 1995, **130**, 909.

24. S. Wada, A. M. R. Kabir, M. Ito, D. Inoue, K. Sada, and A. Kakugo, *Soft Matter*, 2015, **11**, 1157-1163.

25. W. Thielicke, and E.J. Stamhuis, 2014, PIV lab – Towards User-friendly, Affordable and Accurate Digital Particle Image Velocimetry in MATLAB. Journal of Open Research Software 2(1):e30, DOI: http://dx.doi.org/10.5334/jors.bl

26. K. V. Mardia and P. E. Jupp, Directional Statistics, *John Wiley and Sons* Ltd., England, 2000, 57-82.

27. R. Rezakhaniha, A. Agianniotis, J. T. C. Schrauwen, A. Griffa, D. Sage, C. V. C. Bouten, F. N. van de Vosse, M. Unser and N. Stergiopulos, *Biomech. Model. Mechanobiol*., 2012, **11**, 461-473.

28. M. Castoldi, and A. V. Popov, Protein Expres. Purif, 2003, 32, 83-88.

29. R. B. Case, D. W. Pierce, H. B. Nora, L. H. Cynthia, and R. D. Vale, *Cell*, 1997, **90**, 959-966.

30. A. M. R. Kabir, D. Inoue, A. Kakugo, A. Kamei, and J. P. Gong, *Langmuir*, 2011, **27**, 13659-13668.

31. A. M. R. Kabir, D. Inoue, A. Kakugo, K. Sada, and J. P. Gong, *Polym. J.*, 2012, **44**, 607-611.

Chapter 4

Effect of external mechanical stimuli on collective motion of microtubules

Abstract

The collective motion of self-propelled objects, e.g.; animals, microorganisms, cytoskeleton is a ubiquitous and fascinating self-organization phenomenon. Nowadays, *in vitro* motility assay is being considered as model system to experimentally investigate various aspects of group behavior and pattern formation by self-propelled objects. In an *in vitro* motility assay, cytoskeletal filaments (F-actin and microtubule) are propelled by biomolecular motors (myosin and kinesin or dynein). When a high density of cytoskeletal filaments is maintained, they are capable to align spontaneously and self-organize into large scale patterns through collective motion. In this chapter, I have investigated the effect of external mechanical stimuli, applied as indentation stress, on collective motion of microtubules. I have found that, in response to indentation stress collectively moving microtubules generate an ultra large (diameter ~5 mm) vortex pattern. Spatial orientation of microtubules in the vortex pattern depends on the extent of indentation stress, which is also correlated to indentation length, indenter size, and shape. This work provides an approach to ensemble group of nanoscale self-propelled particles to a microscale pattern, which offers a new approach to control the group behavior of self-propelled particles and expand their applications in the field of nanotechnology.

4.1 Introduction

The coordinated behavior of the self-propelled particles, emerged from the interactions among individuals is referred as collective motion. The large scale patterns of collectively moving objects such as, human crowds, animals, birds, cells, bacteria, to subcellular cytoskeletal filaments in the nature have fascinated us and drawn attention to explore the emergent functions in collective motion. One of spectacular behaviors of collectively moving objects is their responsiveness towards any external perturbation or stimulation. For instance, schools of fish are able to move in a rather orderly fashion or change direction abruptly. Due to the presence of a nearby predator, the same fish can swirl like a vehemently stirred fluid. However, such natural phenomena still lacks proper *in vitro* study. In recent years biomolecular motor systems; microtubule/dynein or microtubule/kinesin have emerged as ideal candidates for demonstrating the collective motion of self-propelled particles through *in vitro* gliding assay[1-14]. Recently, the microtubule filaments are reported as mechanosensor, which reorient their configuration to an energetically preferred orientation in response to external mechanical stimuli. *In vivo* results reveal that in plant cell two dimensionally aligned microtubules reorient parallel to the direction of tensile stress [15]. In animal cell, with cyclic stimulus, the microtubule network rearranges and develops characteristic angle to the stretch direction, which ultimately regulates the morphology of the cell[16]. Recently, regulation of the directionality of kinesin driven microtubules has been demonstrated *in vitro* by applying mechanical stress[17]. The response of microtubules moving in collective motion, to single step and cyclic stretching stimuli has been investigated and orientation of microtubules has been observed[18]. In this chapter, I will investigate in-detail the response of collectively moving microtubules to external mechanical stimuli applied as indentation stress. For this, an *in vitro* motility assay of microtubules was demonstrated on an elastomeric substrate; polydimethyl siloxane (PDMS) and indentation stress was applied to it. A mechanical chamber named ‘indentation chamber’ was constructed for this purpose. An ultra-large vortex of ~5 mm in diameter was formed by collectively moving microtubules due to application of indentation stress[18]. A detailed study on the vortex formation and influence of different parameters related to indentation have been investigated. This work provides a new method for controlling the collective motion of self-propelled systems, which might enable us to obtain desired large scale patterns and cooperative work from huge a number of self-propelled particles.

4.2 Results and discussion

4.2.1 Experimental setup used to apply indentation stress on microtubules

The response of group of self-propelled microtubules to external mechanical stimuli, applied as indentation stress, was investigated by employing a newly developed experimental set up named as 'indentation chamber'. The detailed specification of the chamber is as follows:

Design of indentation chamber

The indentation chamber was constructed with a view to apply indentation stress and to investigate the responsiveness of microtubules moving in groups.

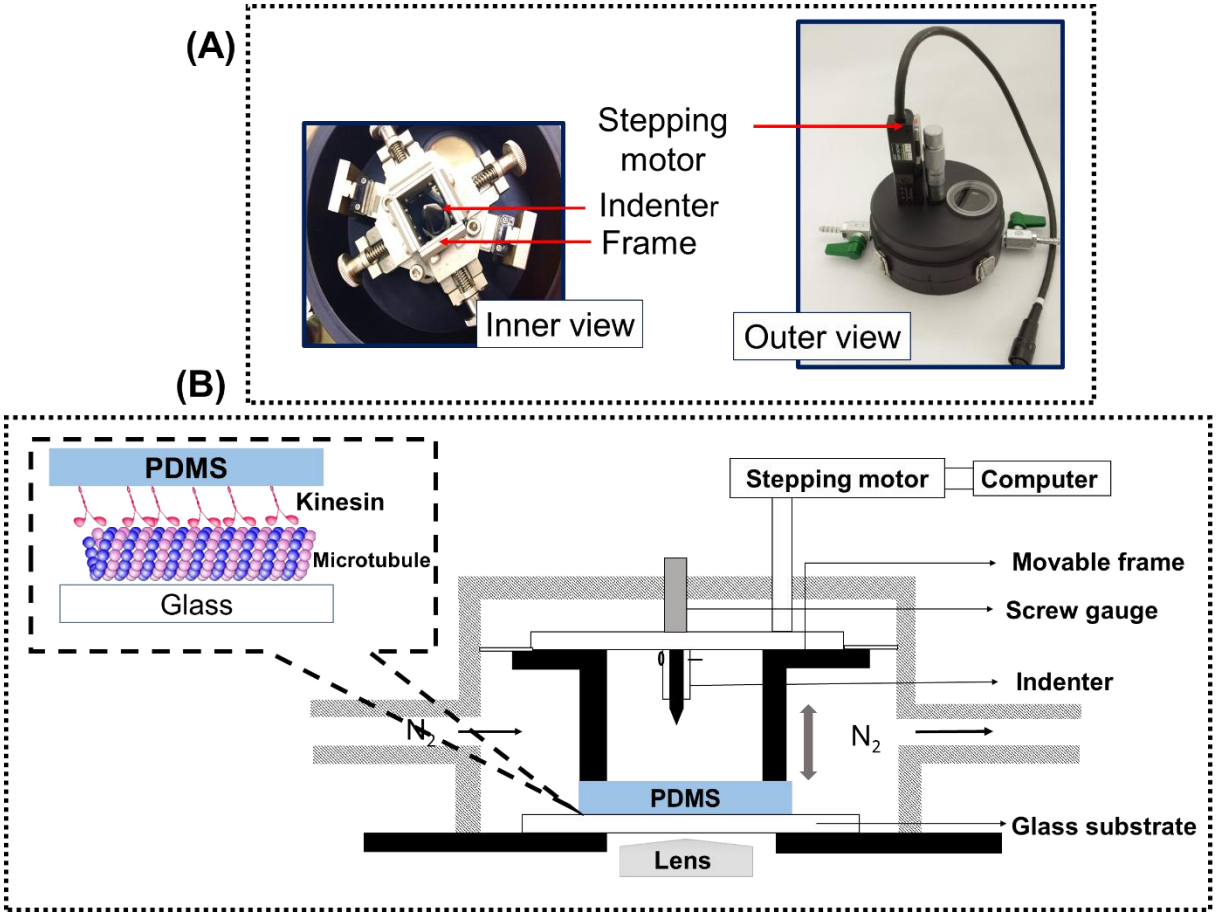

Figure 4.1: Images (A) and schematic diagram (B) of the indentation chamber. The illustration of the motility assay of microtubules/kinesin on PDMS substrate is shown in inset of (B).

The motility assay was prepared on PDMS mounted on four movable frames fixed upon a movable stage [Figure 4.1]. The upward-downward movements of the movable stages was

controlled by using a stepping motor connected to a computer. The indenter that indents the motility assay substrate was placed below PDMS at center of the chamber.

Specification of the indentation chamber

The indentation stress was applied to the PDMS using the indenter. I have used indenters of two different shapes: speheroconical and flat triangular tip filament. I have also used sperohocincal indenters of different diameters, i.e., 0.5, 2.0, and 4.0 mm. The indentation length and indentation speeds were controlled using the stepping motor. The stepping motor allowed maximum 13 mm depth indentation.

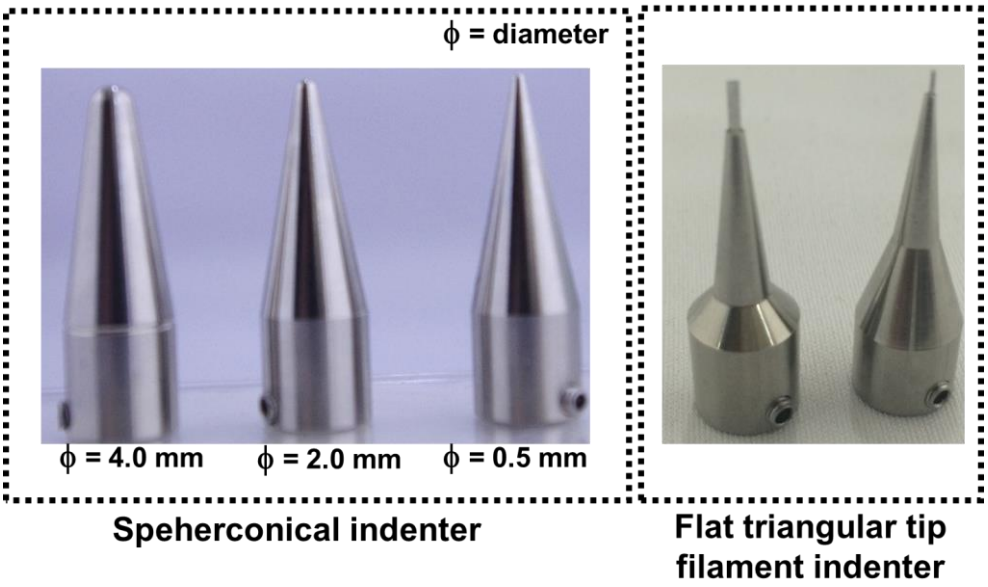

Figure 4.2: Images of the indenters used to apply indentation stress.

Application of indentation stress

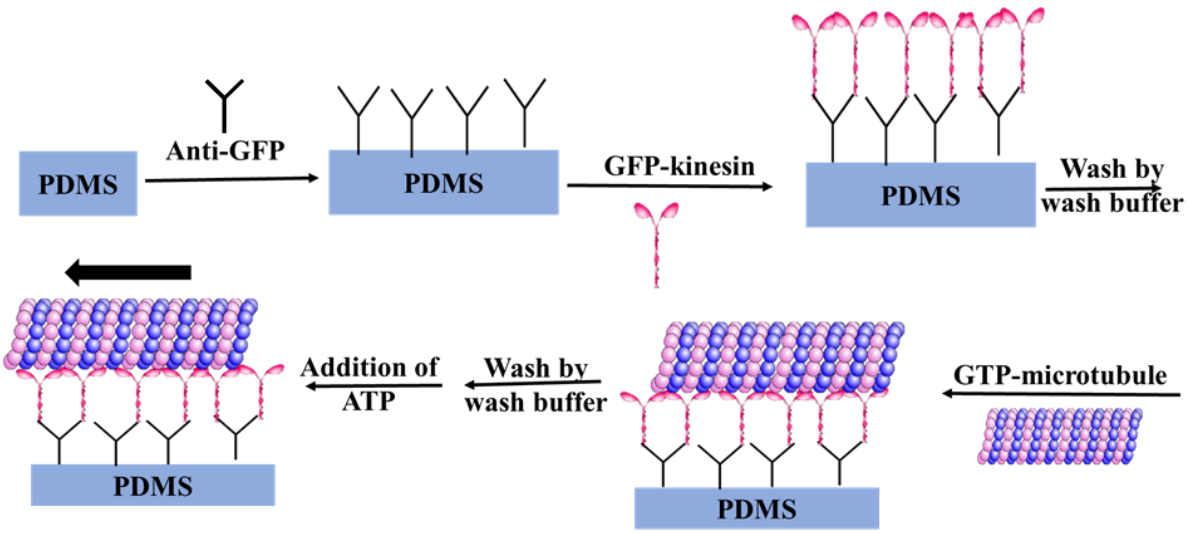

Figure 4.3: Illustration of preparation of motility assay on PDMS substrate.

Before applying indentation stress, a motility assay of high-density microtubules was prepared on the PDMS. The dimension of the PDMS was 5 × 15 × 0.05 mm^3 (length × width × height) and the assay was prepared according to scheme 4.3. [Detail is annexed in experimental section]

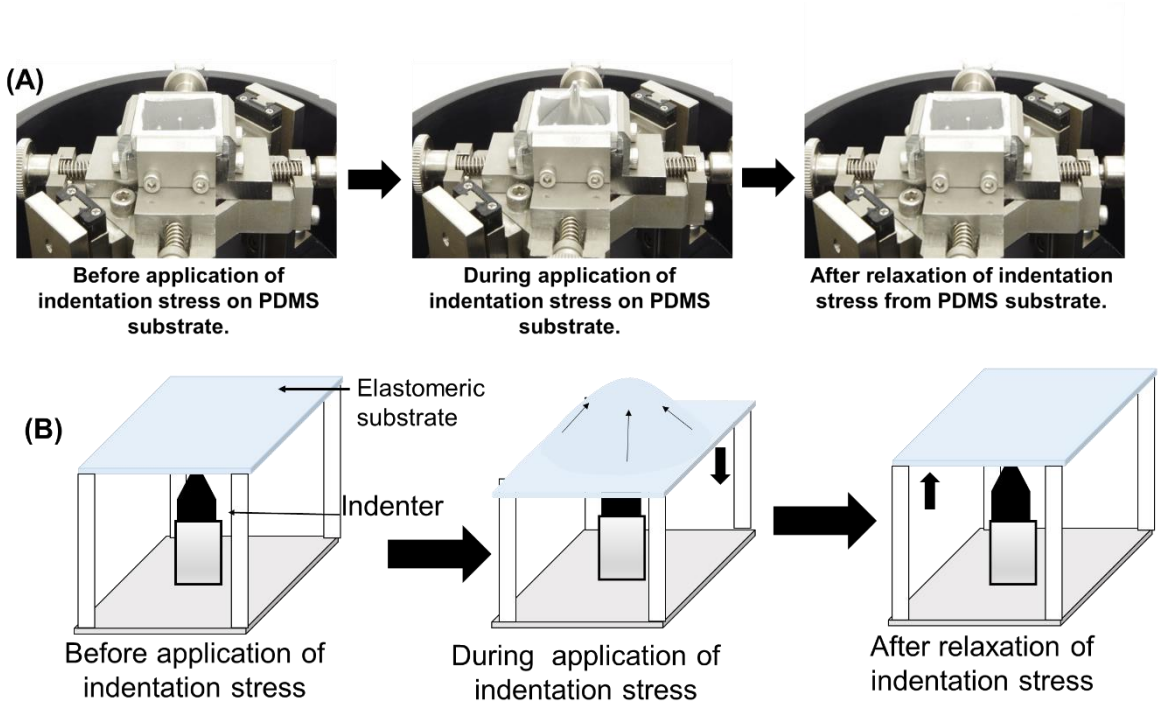

Figure 4.4: Image (A) and schematic diagram (B) of application of indentation stress on the PDMS substrate.

The indentation stress was applied by indenting the PDMS substrate from the bottom. The stage holding the movable frames was pushed down towards the indenter tip to a desired distance to apply indentation stress. The indenting length, and duration of application of indentation were controlled using the computer controlled stepping motor. The indentation stress was retained for 5 seconds.

4.2.2 Response of microtubules in collective motion to indentation stress

First, I prepared a high-density motility assay to observe the collective motion of microtubules driven by kinesin. Microtubules were prepared by polymerizing tubulins in presence of GTP (guanosine tri-phosphate). Initially, on addition of ATP (adenosine tri-phosphate) buffer the microtubules started moving randomly at a constant velocity of 180 nm s^{-1} without showing any directional preference.

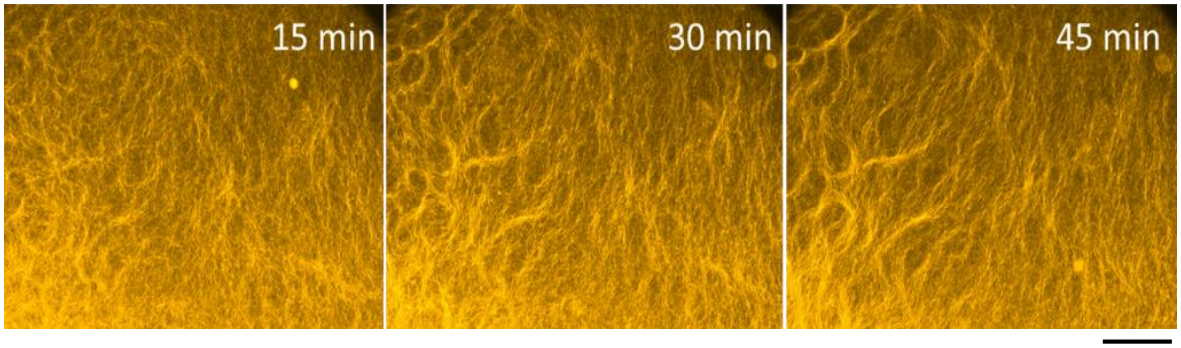

Figure 4.5: Time-lapse fluorescence image of microtubules showing emergence of collective motion on PDMS substrate. Scale bar: 100 μm.

Within 30 min after the addition of ATP, microtubules gradually formed local streams [Figure 4.5]. Next, I applied indentation to the motility assay substrate as shown in Figure 4.4. The diameter of the indenter tip was 4.0 mm and the indentation length was 5 mm. The indentation was maintained for 5 sec.

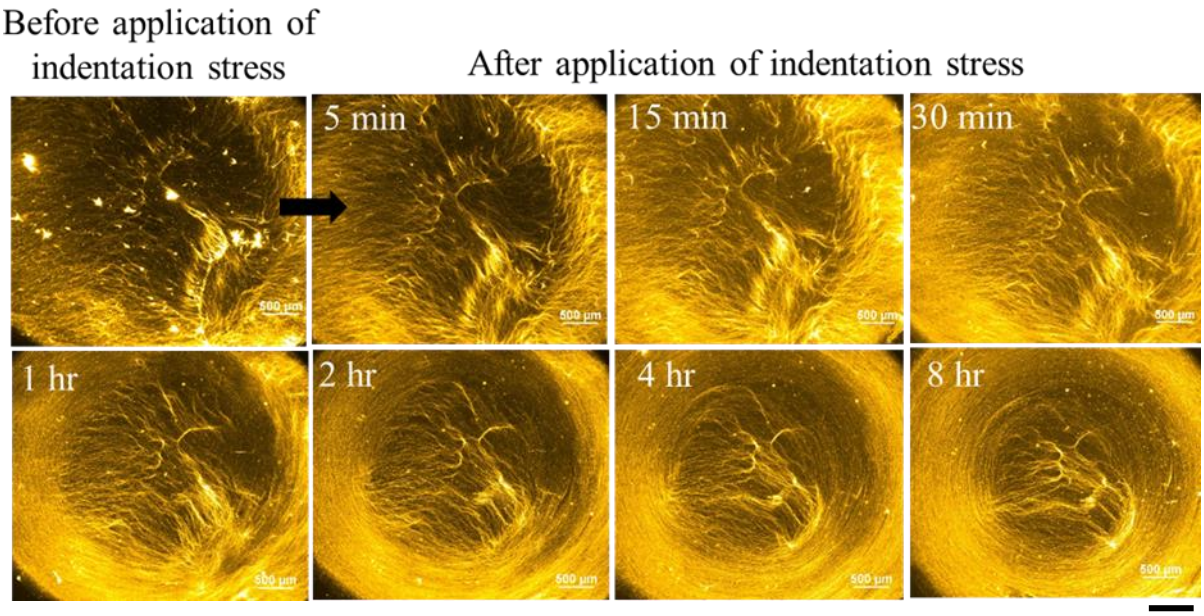

Figure 4.6: Time-lapse fluorescence images of orientation of microtubules after indentation. Scale bar: 500 μm.

The time lapse images [Figure 4.6] show that, the microtubules in the stream pattern started to change their spatial orientation due to the indentation stress and within ~2 hours aligned themselves to an ultra large vortex pattern of almost ~5 mm diameter. It is interesting that, at the central part of the vortex, the microtubules were oriented in stream pattern. Next, to characterize the vortex pattern, I analyzed the nematic order parameter of the microtubules.

4.2.3 Characterization of the vortex pattern

The vortex pattern of microtubules was characterized considering the spatial orientation of microtubules at different time and location of the flow cell after application of indentation stress. The orientation of microtubule was quantitatively analyzed using nematic order parameter, *S* [detail in experimental] which can be calculated using the following equation[19].

$$S = \frac{1}{N}\sqrt{\left(\sum_{i=0}^{180} R_i \cos 2\Theta_i\right)^2 + \left(\sum_{i=0}^{180} R_i \sin 2\Theta_i\right)^2}$$

Where, N refers to total number of microtubules in the frame, R_i is frequency of the angle of individual microtubules,

Θ_i (i = 0 to 180). The range of Θ_i was fixed from 0° to 180° based on the symmetry of horizontally or vertically aligned microtubules with respect to the x axis.

The order parameter was calculated from the fluorescence images of collectively moving microtubules captured at different time after application of indentation stress. Several regions of interest (ROI), from center to periphery were selected to calculate the order parameter of orientation of microtubules at different space as shown in Figure 4.7.

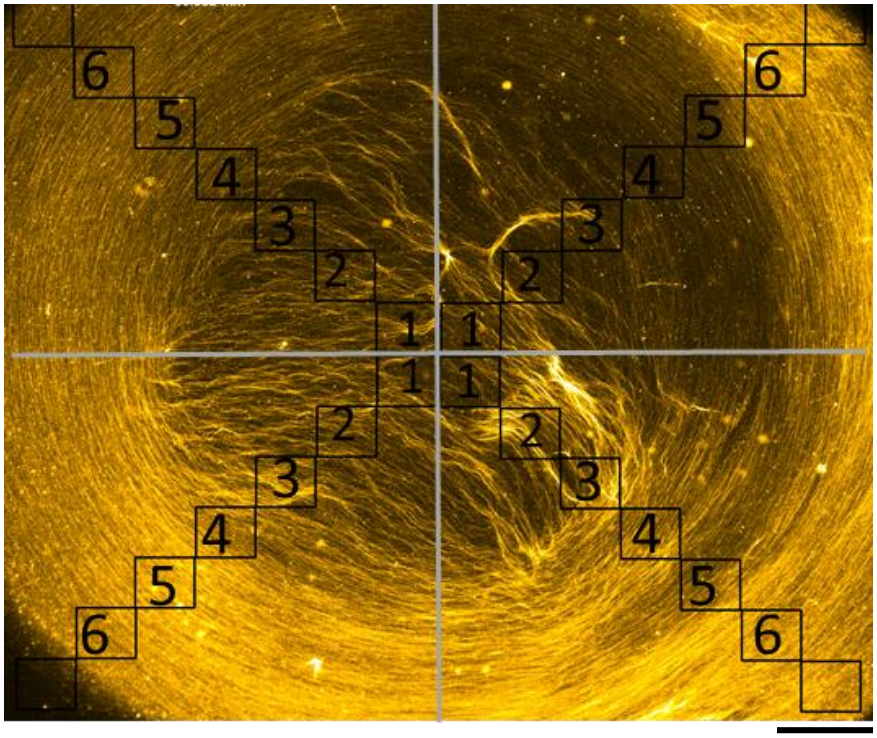

Figure 4.7: Fluorescence image of an ultra-large vortex pattern after 2 hours of application of indentation stress. The squares represent the selected ROI, from center to periphery of vortex pattern in this study. The ROIs were used for quantitative analysis. Scale bar: 500 μm.

In Figure 4.7, fluorescence image of an ultra-large vortex pattern of microtubules captured after 2 hours of applying 5 mm indentation stress is presented. The vortex pattern was divided into 4 equal parts and in each portion six ROIs of same area were chosen and denoted as 1,2,3,4, 5, and 6 from center to periphery. The size of each ROI was 100×120 pixel. Nematic order parameter of microtubules in each region was calculated from every part and finally the average was calculated. The time-lapse fluorescence images of formation of vortex [Figure 4.6] were used to measure the change of order parameter with time. The profile of change of order parameters of microtubules as a function of time is presented in Figure 4.8, from which the change of orientation of microtubule with time upon application of indentation stress can be

understood. The analysis revealed that, at the center part, [region 1 and 2] the value of order parameter was less compared to the regions towards periphery. On contrary, from center to periphery the degree of orientation of microtubules increased with time. Near the periphery, the order parameter was higher and at 120 minute reached the steady sate. The comparative value of order parameter at region 5 and 6 attributed to the similar order of orientation of microtubules at periphery. From the Figure 4.7, it can be observed that the ROI 1, 2 and 3 were selected from the center part, where motile microtubules generate stream pattern. The higher values of order parameter at periphery (ROI 5, 6) indicate that the orientation of microtubules at the vortex array was more nematic than in the stream pattern (ROI 1, 2, 3).

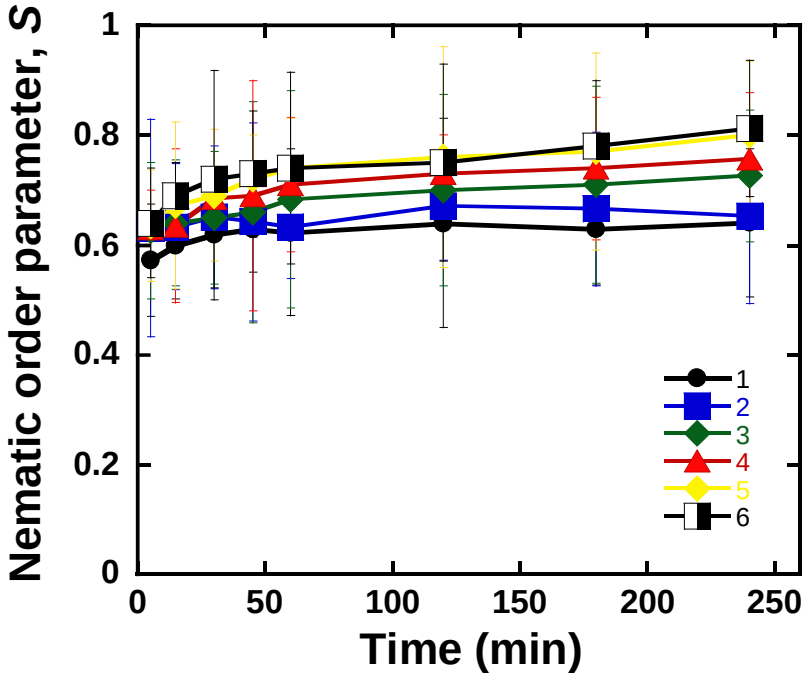

Figure 4.8: Change of nematic order parameter of microtubules with time. Here 1, 2, 3, 4, 5, 6, 7 indicates the corresponding ROI shown in Figure 4.7.

The above experimental results reveal that the application of indentation stress on microtubules generate two different modes of collective motion. At the center, the collectively moving microtubules generate stream pattern, while for the rest of the part, collectively moving microtubules oriented to vortex pattern in response to the stress. A model was speculated to explain such orientation of microtubules due to application of indentation by considering the stretching of PDMS substrate. The model is illustrated in Figure 4.9A and the fluorescence image of orientation of microtubules are presented in Figure 4.9B.

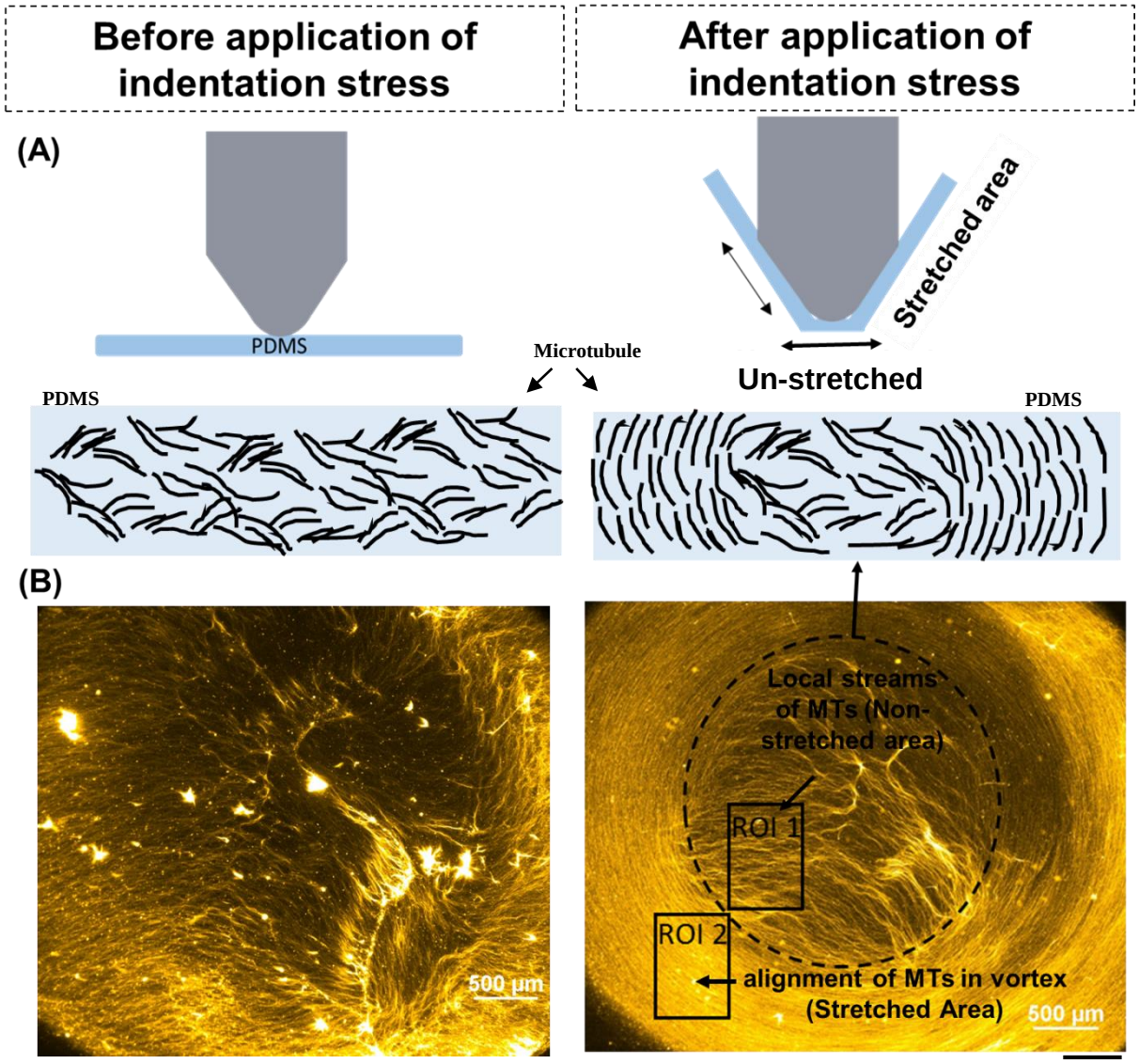

Figure 4.9: Schematic diagram showing the stretching of PDMS upon indentation (A) and orientation of microtubules before and after indentation (B). Fluorescence images of orientation of microtubules before and after indentation. Scale bar: 500 µm.

The indenter used in above experiment was speheroconical in shape and geometry of indenter was wide (4 mm) and smooth. We can assume that the area of PDMS experiencing indentation remains un-stretched. However, the surrounding area becomes stretched. Due to such imbalance in stretching stress, two regions having different stress field can be emerged which probably contributed to different orientation of microtubules. This concept is in agreement with experimental result where local stream pattern was observed in center part or un-stretched region and vortex pattern was generated on the surroundings or the stretched region.

The boundary between these two regions was dynamic. The size of the inner boundary (dotted circle in Figure 4.10) with time was estimated which shown in Figure 4.10B. It was observed that the inner boundary diameter decreased with time, which attributed to the modulation of the directionality of motile microtubules in the streams and rearrangement of their orientation to vortex array induced by collectively moving microtubules in the vortex pattern.

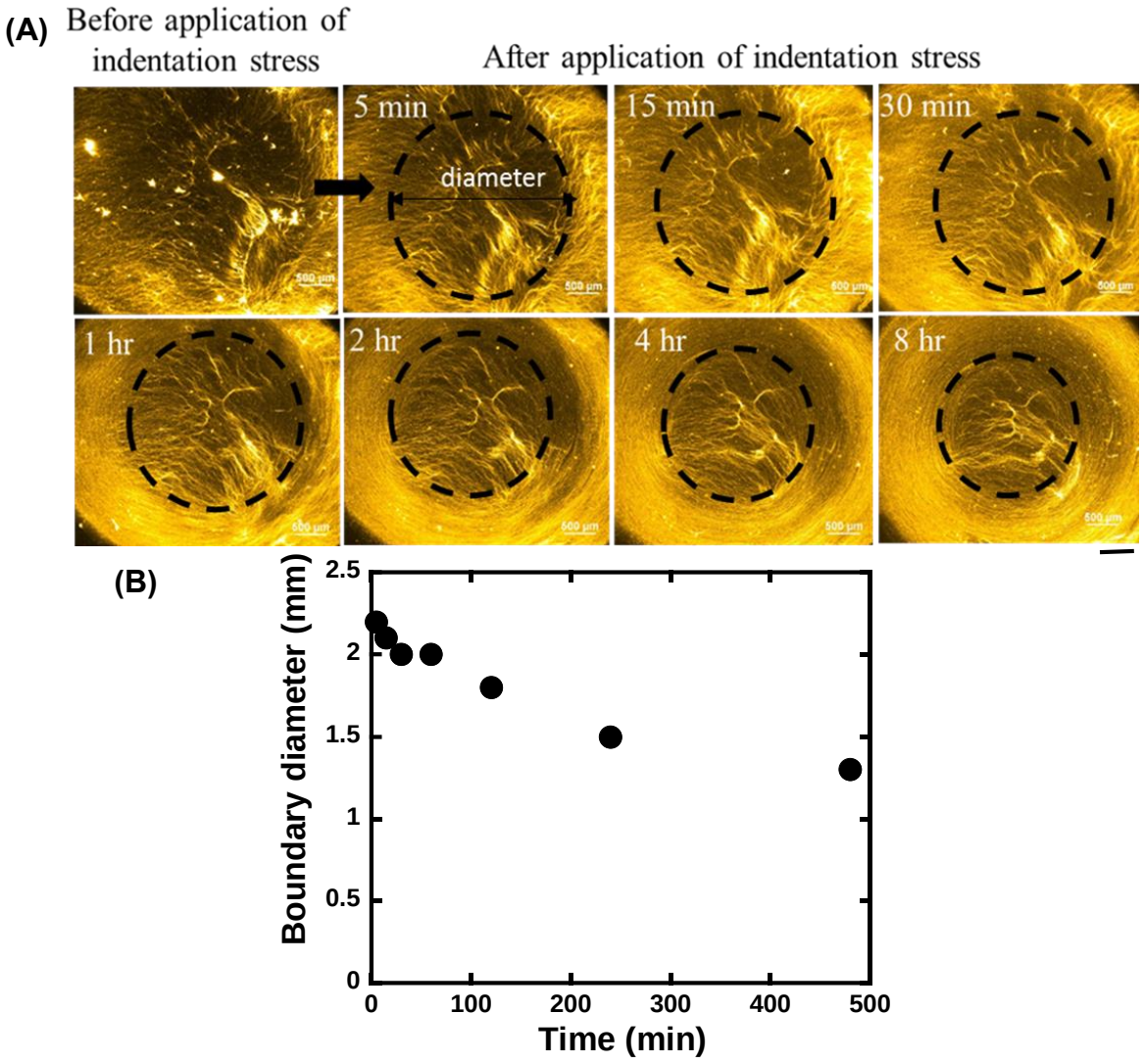

Figure 4.10: (A) Fluorescence images of collectively moving microtubules showing decrease of inner boundary of the vortex pattern (dotted line), and (B) change of diameter of inner boundary with time. Scale bar: 500 µm.

So far, emergence of an ultra large vortex pattern of collectively moving microtubules in response to mechanical (indentation) stress was discussed. In addition, I also performed experiments where indentation stress was applied on microtubules exhibiting random motion. However, instead of vortex pattern formation only detachment of microtubules was observed

in this case. Such observation suggests that, the formation of vortex pattern depends on both cooperative behavior of microtubules and application of indentation stress. According to contact mechanics for nanoindentation, the applied force and induced stress field during indentation depend on a number of parameters that include; indentation depth, the contact diameter and shape of the indenter[20]. So, the influences of these parameters on vortex formation deserve systematic investigation.

4.2.4 Effect of depth of indentation on orientation of collectively moving microtubules

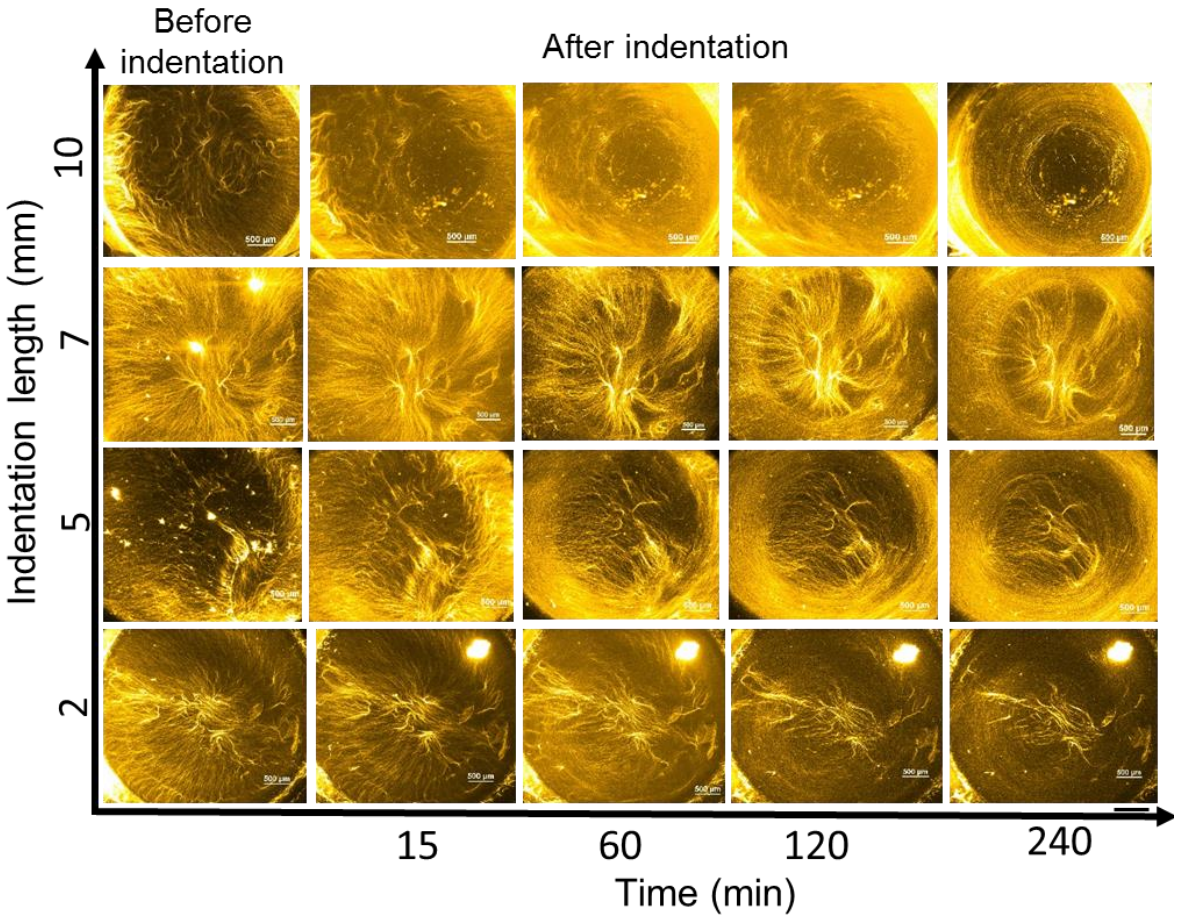

Figure 4.11: Fluorescence images of collectively moving microtubules before and after application of indentation stress with different indentation length of 2, 5, 7, and 10 mm. Scale bar: 500 µm.

In order to evaluate the dependency of formation of vortex pattern on the indention length, experiments were carried out by applying indentation of different lengths; e.g. 2, 5, 7, 9, and 10 mm. In each experiment, the collective motion of microtubules was investigated prior to applying indentation.

After 1 hour of addition of ATP-buffer, indentation stress was applied to the collectively moving microtubules as described in section 4.1. The fluorescence images of orientation of microtubules in the vortex pattern formed in case of different indentation lengths are shown in Figure 4.11. For 2.0 mm indentation, vortex pattern was not observed to form while for 5 and 7 mm (moderate) indentation, an ultra-large vortex pattern was observed. At very high indentation (10 mm), the vortex pattern emerged within 1 hour of application of indentation. However, detachment of microtubules at the center part was observed here.

The extent of stress field induced by indentation may be different from one region to another for different indentation length, which probably affected the dynamics of vortex pattern formation. However, the degree of alignment of microtubules in the vortex pattern can be more clearly understood by comparing the change of nematic order parameter, with time at different indentation depth. In order to calculate order parameter of microtubules after indentation, first a boundary was fixed between two regions with different orientation of microtubules (vortex and stream). Two ROIs of same area were selected from both regions and order parameter of microtubules with time in these regions was calculated [Figure 4.13]

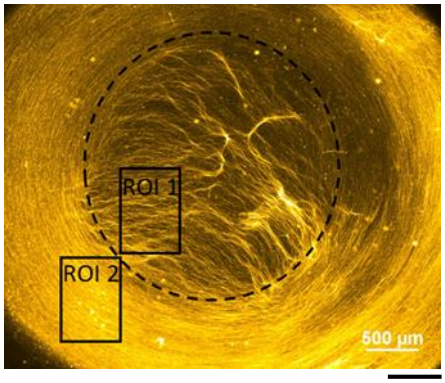

Figure 4.12: Selection of ROI to calculate nematic order parameter with time two region separated through an imaginary boundary. Scale bar: 500 µm.

The time-lapse fluorescence images of collectively moving microtubules for different indentation length [Figure 4.11] were used to calculate the order parameters presented in Figure 4.13.

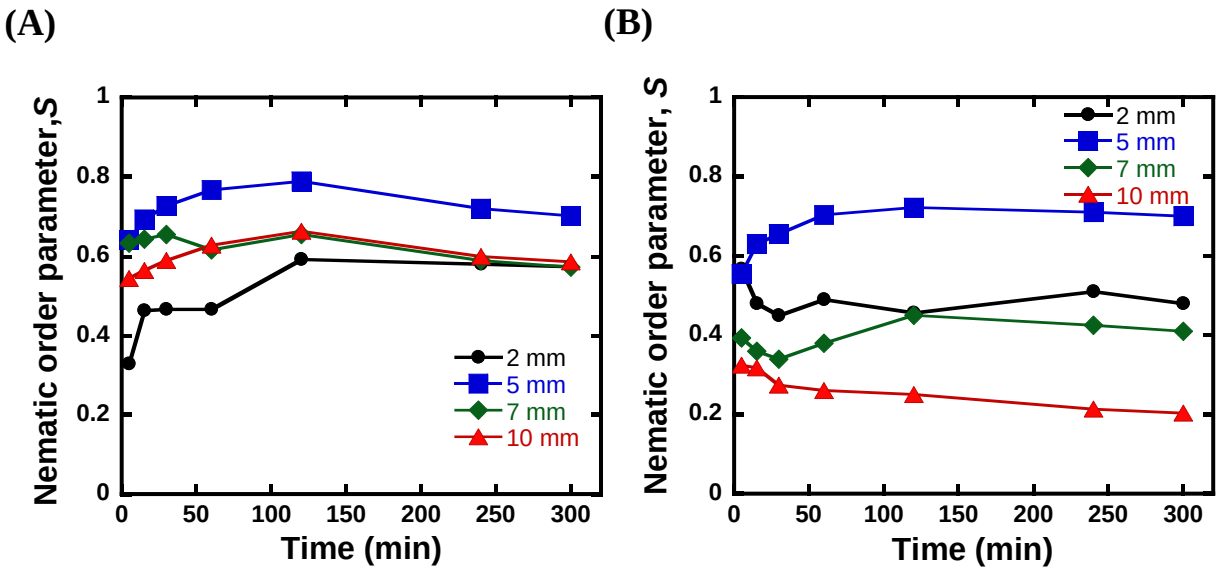

Figure 4.13: Change of nematic order parameter of microtubules with time at different indentation length (2 to 10 mm), where (A) is for vortex part (ROI: 2) and (B) is for center part (ROI: 1).

The change of degree of orientation of microtubules can be understood from Figure 4.13 where (A) and (B) represents change of *S*at vortex and center part respectively. Both in vortex and center region the highest value of order parameter was obtained for 5 mm indentation. Therefore, this is the best condition to obtain an ultra large vortex pattern. At 10 mm indentation, order parameter value decreased at center. The possible reason for this could be the detachment of microtubules at center in this case. The relation between orientations of microtubules to applied indentation can be better understood from Figure 4.14 where change of order parameter with indentation length is presented.

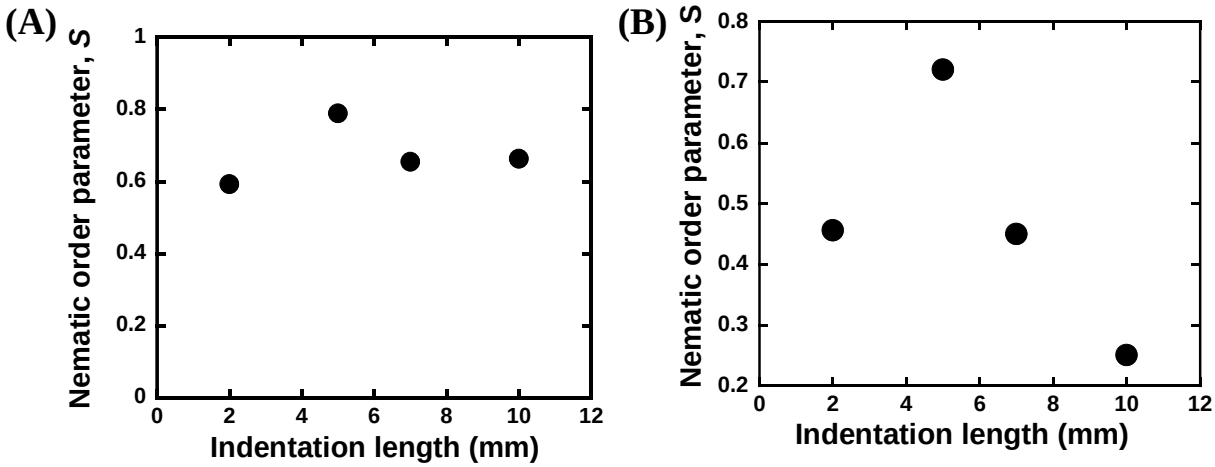

Figure 4.14: Change of order parameter of microtubules at (A) vortex and (B) center region with time.

From Figure 4.13A, we can observe that within 120 min, the order parameters attained a saturated value. In Figure 4.14, the order parameter obtained at 120 min, was plotted for different indentation length. Both in vortex (Figure 4.14A) and in center (Figure 4.14B) the highest value of order parameter was obtained at 5 mm indentation. Almost same value of *S*was observed at the vortex region for 7 and 10 mm indentation. The lower value for center region at 10 mm indentation agrees with the phenomena of detachment of microtubules. Therefore, the orientation of microtubules after application of indentation stress depends on the depth of indentation.

4.2.5 Effect of effective indenter diameter on collective motion of microtubules

The previous experimental results revealed that, deformation of PDMS substrate due to indentation plays a key role in the orientation of microtubule. To investigate further, experiments were performed by changing diameter of the indenter to 0.5 mm and 2.0 mm. Before applying indentation, first the collective motion of microtubules was investigated. Here the indentation length was 5 mm for each experiment. Emergence of an ultra-large vortex pattern was observed for both indenters. To compare the orientation of microtubules in the vortex pattern, fluorescence images of microtubules were captured after 1 hour of application of indentation stress (Figure 4.15).

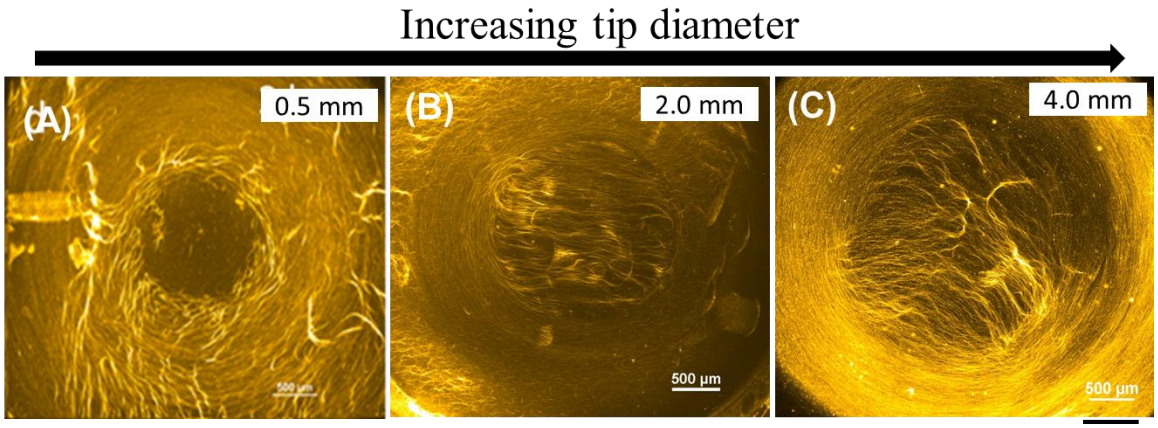

Figure 4.15: Fluorescence images of collectively moving microtubules at 1 hour after application of stress. The indenter diameter increases from 0.5 mm to (A) to (C) 4.0 mm. Scale bar: 500 µm.

From Figure 4.15, differences in the orientation of microtubules in the vortex pattern can be observed clearly. The detachment of microtubules from center part is noticeable when the

indenter diameter was 0.5 mm (Figure 4.15A). A change in dynamics of vortex formation was also observed with the change of indenter size [Figure 4.15 and 4.17].

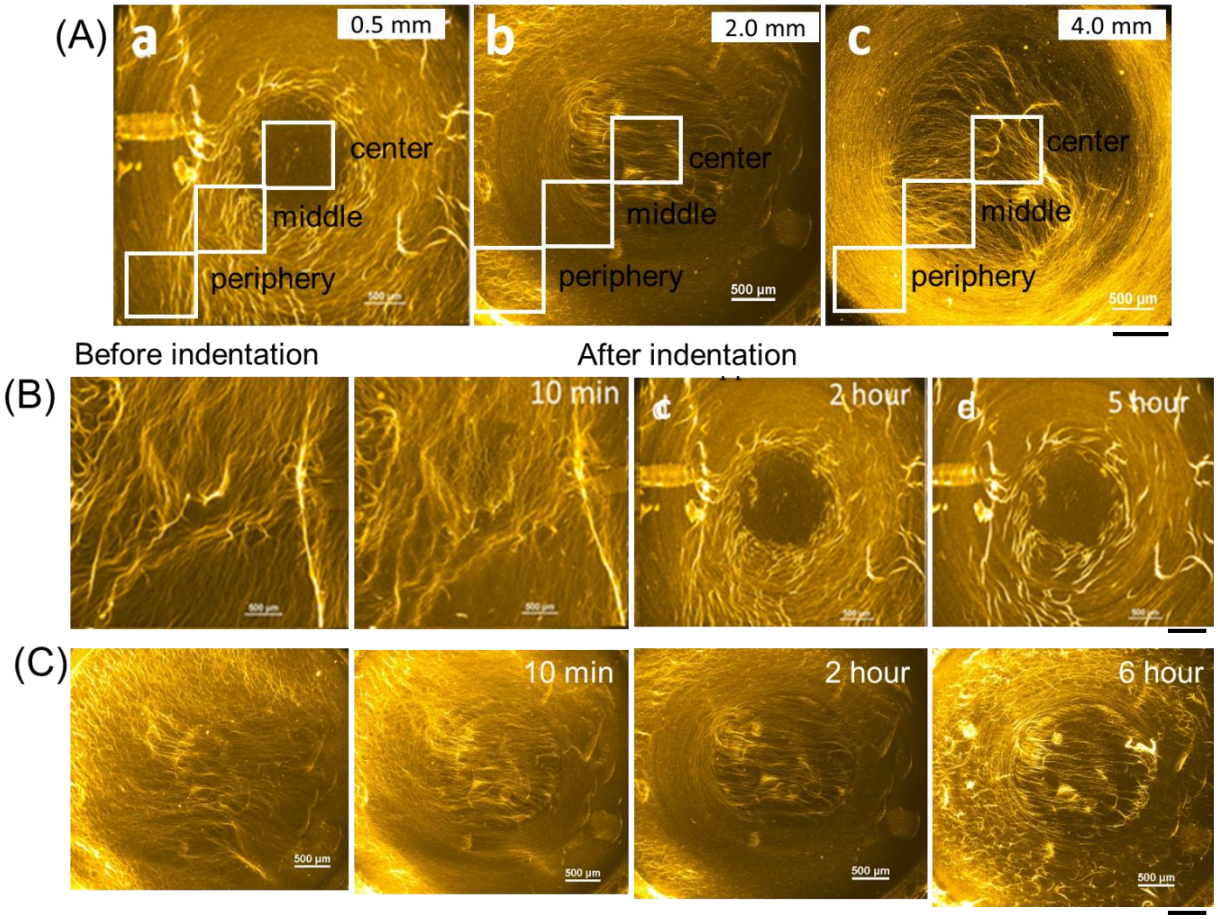

Figure 4.16: (A) Selection of ROI from center to the periphery of the vortex patterns obtained through using (a) 0.5, (b) 2.0, and (c) 4.0 mm diameter indenter. Time-lapse fluorescence images of collectively moving microtubules before and after indentation using indenter with diameter of (B) 0.5 mm, and (C) 2.0 mm. Scale bar: 500 µm.

In case of indenter with 4.0 mm diameter, the microtubules in the vortex pattern were more oriented than other events. All these findings can be justified by analyzing order parameter. To analyze the degree of orientation of microtubules in vortex pattern at different indenter diameter, three ROIs were chosen for every image from center to periphery [shown in Figure 4.16A]. Considering only the center part where the indentation stress was applied, it is obvious that in case of 0.5 mm tip (small) diameter almost all microtubules detached while, for 4.0 mm (large) diameter microtubules show collective motion in local streams. The increase in nematic order parameter is the evidence of the increasing order alignment of microtubules with increasing indenter diameter.

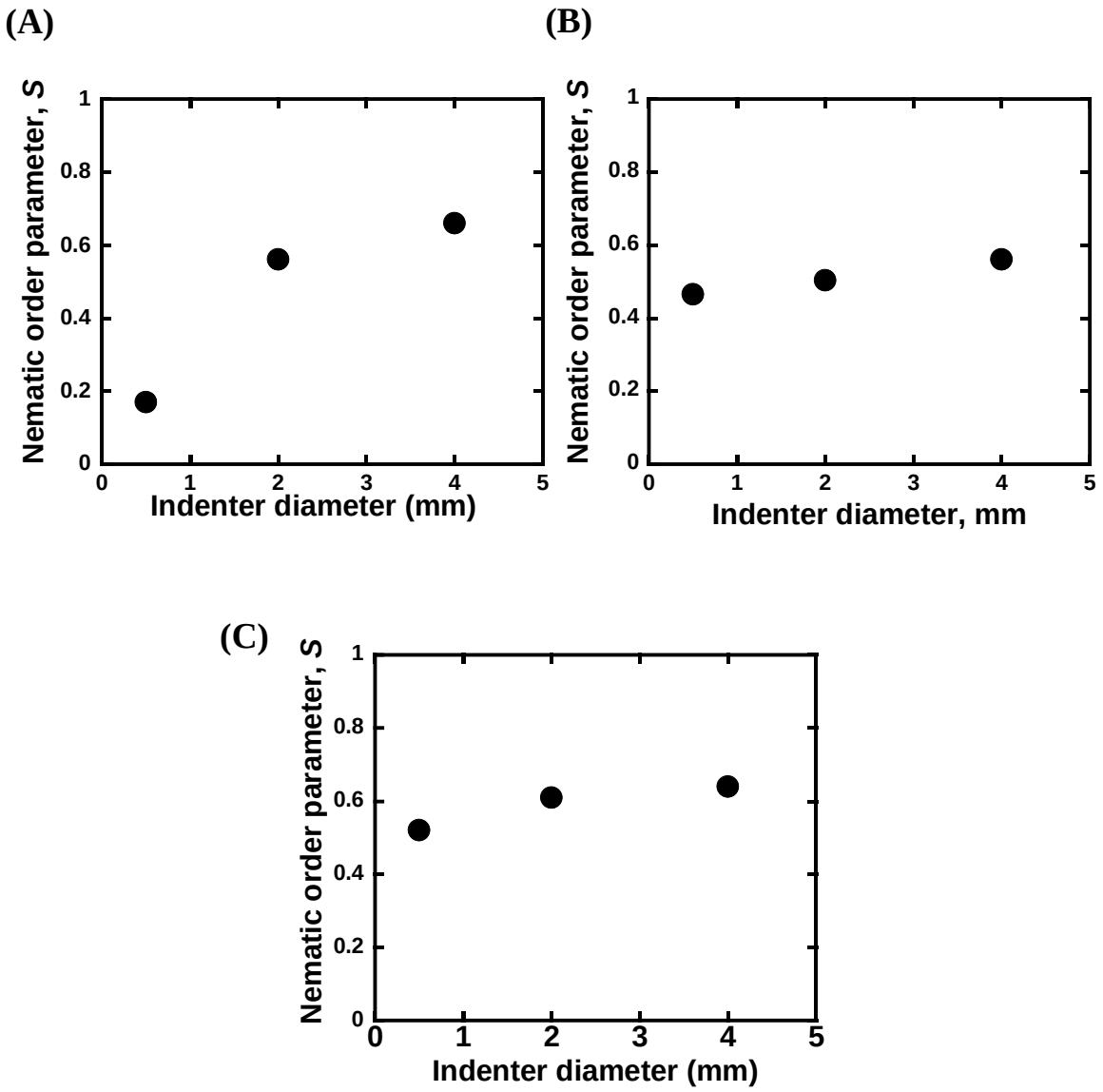

Figure 4.17: A profile of change of order parameter at (A) center, (B) middle, and (C) periphery of the vortex pattern with change in indenter diameter.

At the equidistant positions from center (Figure 4.17B), nematic order parameter for orientation of microtubules were almost same for all indenters. The orientation of microtubules was almost similar at the middle part of the vortex pattern. Although, at the periphery, well-ordered arrangement of microtubules in vortex array can be noticed for large tip (Figure 4.17C). Change of alignment of microtubules with time for different tip diameters can be more clearly understood from the correlation of nematic order parameters with time for different indenter as shown in Figure 4.18. The order parameter was determined from the fluorescence images of microtubules after indentation. With time the magnitude of order parameter increased, which

indicates the ordered arrangement of microtubules in vortex. The time-lapse fluorescence images shown in Figures 4.7 and 4.16 also support this finding.

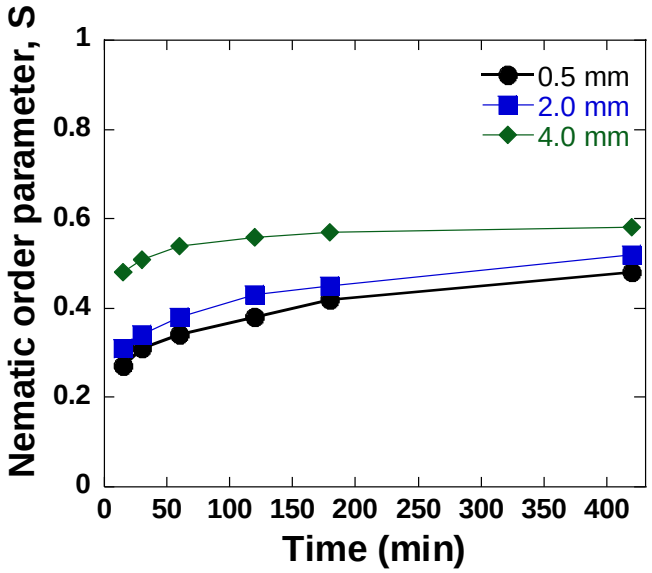

Figure 4.18: Change of nematic order parameter of microtubules with time for different indentation diameter. The values (0.5, 2.0 and 4.0 mm) written in right corner indicate the tip diameter of indenter.

The collectively moving microtubules can sense applied stress field and according to that can change their moving direction. It can be assumed that change in geometry of indenter tip might have tuned the degree of induced stress field, which ultimately controlled the directionality of collectively moving microtubule. As a result, vortex pattern having different alignment of microtubules correlating to time was observed.

Next, I performed experiments by using an indenter of a different shape (filament indenter having a triangular flat tip) to elucidate the role of indenter shape on the organization of microtubules upon application of indentation stress.

4.2.6 Effect of shape of indenter on the collective motion of microtubules

Before applying indentation stress, collective motion of the microtubules was studied. On addition of ATP, microtubules started moving randomly, without showing any specific directional preference. The collisions between microtubules increased with time and collective motion emerged. These collectively moving microtubules ultimately formed stream like pattern.

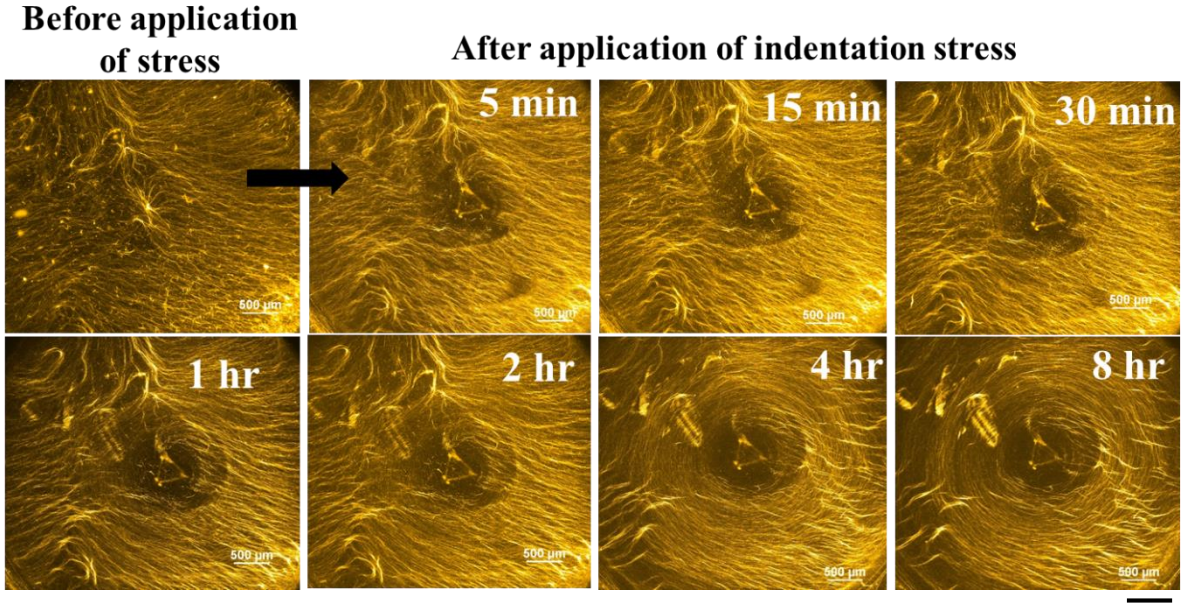

Figure 4.19: Fluorescence images of collectively moving microtubules before and after application of indentation stress. Scale bar: 500 µm.

The indentation was then applied on the collectively moving microtubules on the PDMS substrate**.** As a result, a vortex pattern was obtained (Figure 4.19). Initially, microtubules in the vortex were disordered. With time, disordered parts were gradually organized into the vortex pattern and microtubules in vortex exhibited collective motion. However, despite the change of shape of indenter tip an ultra-large vortex pattern was observed upon indentation. This result indicates that, emergence of an ultra large vortex pattern by microtubules in a kinesin based motility assay is a generic phenomenon and depends on depth of indentation, but not on the size and shape of the indenter.

4.2.7 Response of collectively moving microtubules to cyclic indentation

Next, with a view to study the effect of mode of indentation stress to vortex formation, I applied cyclic indentation stress on collectively moving microtubules. The stress was applied by

repeated indentation keeping the time difference between each indentation very low (5 sec). First, experiments were performed where indentation stress was applied consecutively in three cycles. In each cycle, first, the stress was applied, retained for 5 sec then released and waited for 5 sec. After waiting for 5 sec, again indentation was applied. In this manner, three cycles of indentation was applied before starting observation. The experiments were carried out for two different indentation length: 2 mm and 5 mm. the 2 mm indentation length was not sufficient for the emergence of an ultra large vortex. For the 5 mm indentation, well ordered ultra-large vortex pattern was observed. Here, the indenter diameter was 4 mm.

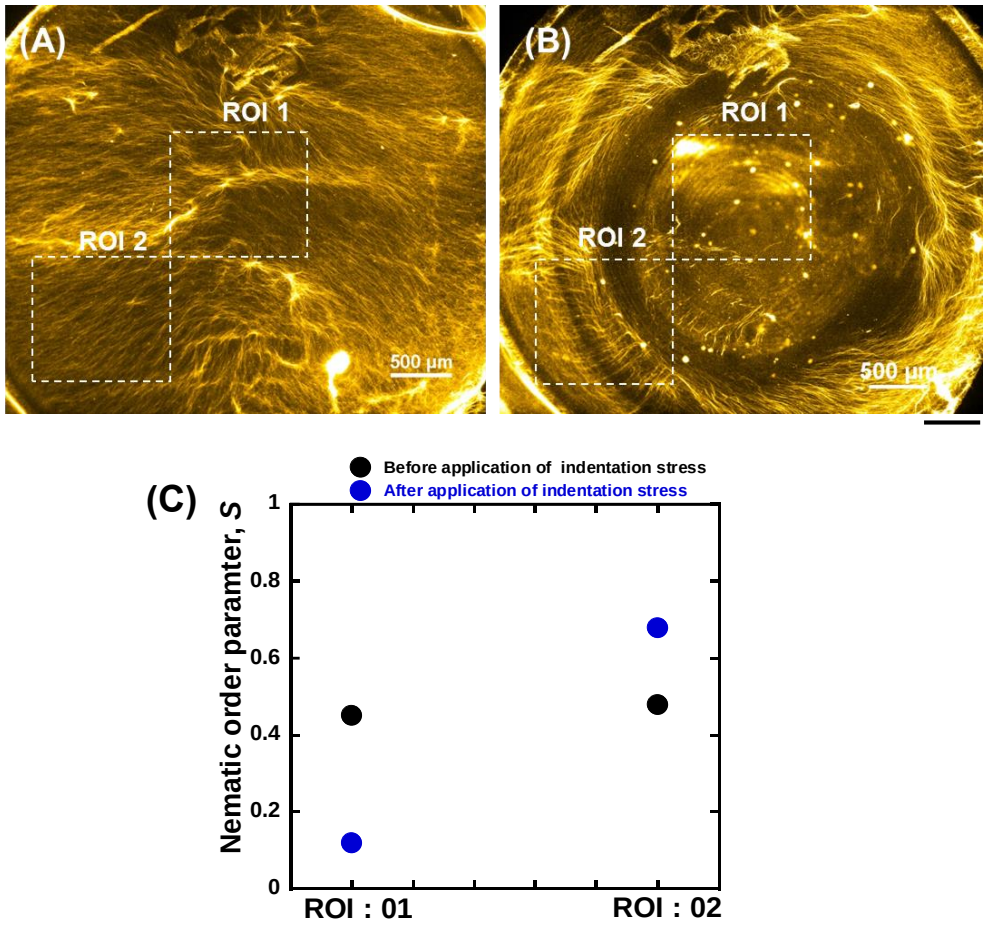

Figure 4.20: Fluorescence images of orientation of microtubules (A) before and (B) after 3 hours of application of indentation stress. (C) The corresponding order parameters in ROI: 1 and ROI: 2 before and after indention. Scale bar: 500 µm.

In both case of, low [2 mm] and moderate [5 mm] indentation, formation of ultra large vortex pattern was observed which resembles with previous result obtained in case of single step indentation. For 2 mm indentation, within 15 min of indentation, the microtubules started orienting in vortex pattern and by 3 hours a stable vortex pattern was emerged (Figure 4.20).

However, 5 mm indentation most of the microtubules detached from center part and microtubules around the vacant region immediately arrange themselves in vortex array within 15 min (Figure 4.21). Therefore, simultaneous application of indentation stress do not alter the mode of pattern formation.

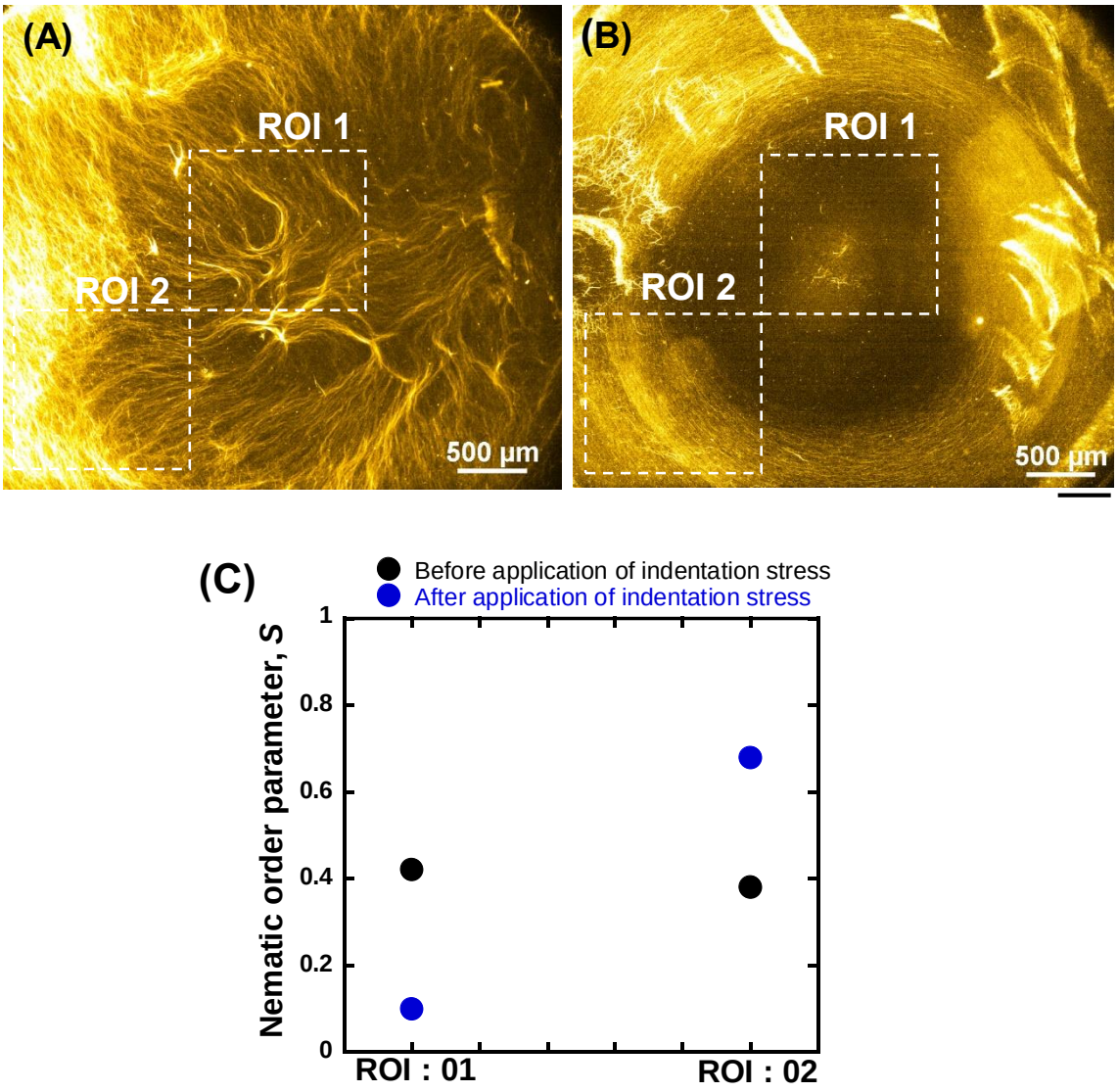

Figure 4.21: Fluorescence images of orientation of microtubules (A) before and (B) after 1 hour of application of indentation stress. (C) The corresponding order parameters in ROI: 1 and ROI: 2; before and after indention. Scale bar: 500 µm.

4.2.8 Response of microtubules in vortex pattern to stretching stress

So far, I have demonstrated formation of a vortex pattern by applying indentation stress to microtubules in collective motion. Next, I investigated whether other mode of external stress, e.g; uniaxial stretching can affect the collective motion of microtubules in the vortex. In this section, I will focus on the responsiveness of motile microtubules in vortex to external stretching stress. To study the effect of uniaxial stretching stress on collectively moving microtubules in vortex pattern first indentation stress was applied according to the section 4.1. Next after generation of a stable vortex pattern, uniaxial stress was applied to the PDMS surface by stretching as shown in Figure 4.22.

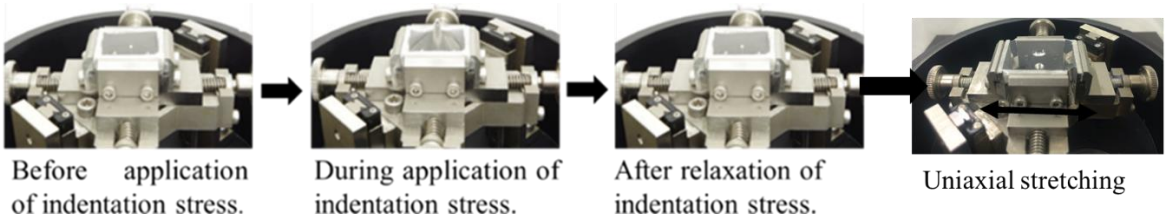

Figure 4.22: Application of uniaxial stretching followed by indentation stress of PDMS substrate.

(I) Effect of indentation stress on collective motion of microtubules

First, I investigated the collective motion of microtubules and after the phase transition from random to stream like pattern, I applied 5 mm indentation to the motility assay substrate.

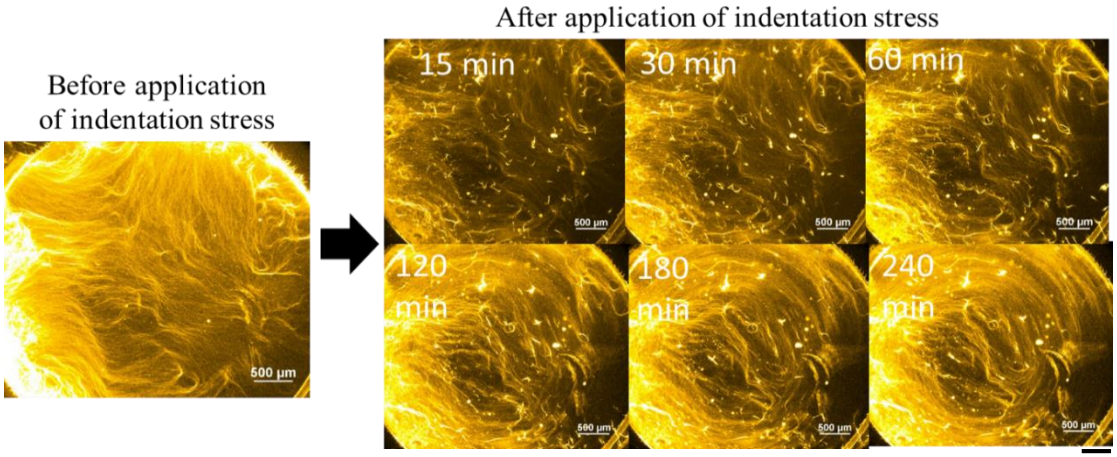

Figure 4.23: Fluorescence images of collectively moving microtubules before and after application of indentation (indentation length **5 mm**). Scale bar: 500 µm.

The orientation of microtubules with time after application of the indentation stress can be observed from Figure 4.23. After 2 hours of application of indentation, the collectively moving microtubules reoriented to vortex pattern. From previous study, it is known that four to five hours is enough for the formation of a stable ultra large vortex pattern. In the previous section, the effect of consecutive indentation stress on the microtubules oriented in vortex pattern was presented. The results indicated that once the microtubules formed stable vortex pattern, it might be not easy to perturb their orientation. So, I investigated the effect of uniaxial stretching stress on the stability of vortex pattern. I stretched the PDMS substrate after four hours of application of indentation stress.

(II) Effect of stretching stress on microtubules in a vortex pattern

The uniaxial stretching (52%, strain) was applied to the PDMS surface by stretching the substrate after the vortex formation. The orientation of microtubules in the vortex pattern before, during, and after application of stretching stress is presented in Figure 4.25. Although due to the application of stress the vortex pattern still exist but some distortion was observed along the stretching axis [Figure 4.25B]. The observation was continued for 90 min, but no characteristic change in pattern was observed. Then tensile stress was removed by compressing back PDMS, to original position. The fluorescence images of microtubule orientation after relaxation of tensile stress is presented in Figure 4.25C. After relaxation, the collectively moving microtubules regained the well-ordered vortex pattern, resembling to original one.

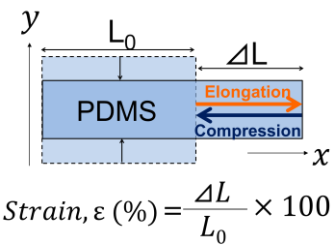

$$Strain, \varepsilon\ (\%) = \frac{\Delta L}{L_0} \times 100$$

Figure 4.24: Definition of stretch strain. Stretching strain, ε, where L_0 is initial length of substrate (15 mm) and ΔL is the change of length (7.8 mm) after applying strain.

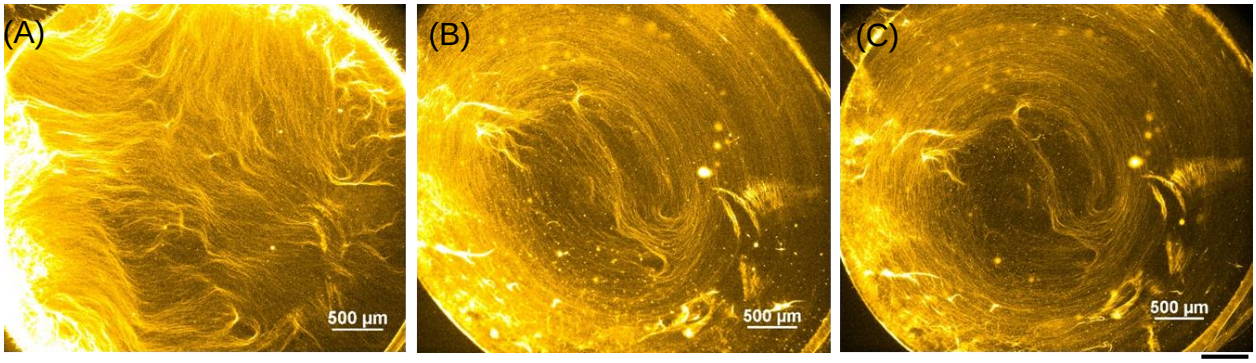

Figure 4.25: Orientation of microtubules in vortex pattern at different conditions (a) due to indentation stress, (b) after application and (c) relaxation of stretching stress. Scale bar: 500 µm.

The application of 52% tensile strain may not be enough to perturb the orientation of microtubules in the ultra large vortex pattern. It suggests that the ultra large vortex pattern emerged due to application of indentation stress is stable enough and microtubules are able to retain their moving directionality despite further application of mechanical stress.

The aforementioned experimental results describe that; the external mechanical stress can control the group behavior of microtubules and assemble a large number of motile units to a large structure. The application of indentation stress can employ two different force field to the microtubules. The stress induced at the region around the point of indentation depends on the geometry of the indenter and which ultimately regulate the spatial orientation of microtubules in the vortex pattern. In addition, the formation of vortex pattern directly depends on the depth of the indentation. The size and shape of indenters are important to control the dynamics of vortex formation [Figure 4.16]. Therefore, application of indentation stress to collectively moving microtubules not only allows generating a vortex pattern, but also provides us with a way to control the kinetics of vortex formation by changing the geometric parameters i.e, indenter shape and indentation extent. Combining with hard materials such as microscale structure of moving objects like the vortex of microtubules can construct 'smart materials' which can be used to construct molecular device. For instance, the swimming bacteria can turn tiny gears, and build hybrid biological machines at the microscopic scale[25]. So, the ultra-large vortex pattern of microtubules can be a good option to prepare such hybrid biological machines.

4.3 Conclusions

In conclusion, I demonstrated the formation of an ultra large vortex pattern of microtubules by applying external mechanical stress as indentation stress. The emerged vortex pattern of microtubules was quite stable and retained their structural directionality even in presence of further mechanical perturbation i.e., cyclic indentation or uniaxial stretching. This study would allow us to understand the group behavior of self-propelled particles and their responses to external mechanical perturbation. I also investigated the influence of other parameters like, indenter shape, size, and length of indentation on the vortex formation. The experimental results suggested that the emergence of the vortex pattern was not dependent on the size and shape of the indenter, rather highly depended on the extent of indentation. In addition, it is also possible to control the orientation of microtubules and kinetics of vortex formation by tuning these parameters. This work provides a new approach to control the group behavior of self-propelled particles, which will widen the applications of self-propelled systems in nanotechnology.

4.4 Experimental

4.4.1 Preparation and labelling of proteins

Tubulin was purified from porcine brain using a high-concentration PIPES buffer (1 M PIPES, 20 mM EGTA, and 10 mM $MgCl_2$; pH was adjusted to 6.8 using KOH) [21]. The high-concentration PIPES buffer and BRB80 buffer were prepared using PIPES from Sigma, and the pH was adjusted using KOH. Kinesin-1 consisting of the first 575 amino acid residues of human kinesin-1 was[22]. Rhodamine-labelled microtubules were obtained by polymerizing a mixture of rhodamine-labelled tubulin (RT) and non-labelled tubulin (WT) (RT: WT = 4:1; final tubulin concentration, 55.6 μM) at 37 °C in the presence of 1 mM GTP according to the standard technique. The solution containing the microtubules was then diluted with motility buffer (80 mM PIPES, 1 mM EGTA, 2 mM $MgCl_2$, 0.5 mg mL^{-1} casein, 1 mM DTT, 10 μM paclitaxel and ~1% DMSO; pH 6.8).

4.4.2 *In vitro* motility assay on PDMS surface

A poly (dimethylsiloxane) (PDMS) substrate (12 × 12 × 0.05 mm^3, L × W × T; Fuso Rubber Industry Co., Ltd) was fixed to the movable frame of the stretch chamber. The PDMS surface was exposed to plasma for 1 min by a plasma etcher (SEDE-GE; Meiwafosis Co., Ltd.) to obtain a hydrophilic surface. Anti-GFP antibody (Invitrogen) at 0.01 mg mL^{-1} (10 μL) was applied to the PDMS surface. After incubation for 3 min, the PDMS surface was washed with 5 μL of casein solution (80 mmol L^{-1} PIPES, 1 mmol L^{-1} EGTA, 1 mmol L^{-1} $MgCl_2$, ~2 mg mL^{-1} casein; pH adjusted to 6.8 using HCl) and incubated for 2 min. Then, 10 μL of 200 nmol L^{-1} K560-GFP solution (~80 mmol L^{-1} PIPES, 1 mmol L^{-1} EGTA, 1 mmol L^{-1} $MgCl_2$, 0.5 mg mL^{-1} casein, 1 mmol L^{-1} DTT, 10 μmol L^{-1} paclitaxel/DMSO, ~1% DMSO; pH 6.8) was introduced and incubated for 3 min to bind the kinesin to the antibody. The PDMS surface was washed with 10 μL of motility buffer. Next, 10 μL of 5 μmol L^{-1} microtubule solution was introduced and incubated for 3 min, followed by washing with 20 μL of motility buffer; 5 μL of 0.25 μmol L^{-1} MAP4 was then introduced and incubated for 3 min, followed by washing with 20 μL of motility buffer. Then, 100 μL of 10 mmol L^{-1} ATP (~80 mmol L^{-1} PIPES, 1 mmol L^{-1} EGTA, 1 mmol $L^{-1}MgCl_2$, 0.5 mg mL^{-1} casein, 1 mmol L^{-1} DTT, 10 μmol L^{-1} paclitaxel/DMSO, 0.3 wt% methyl cellulose, ~1% DMSO; pH 6.8) was dropped on the cover glass (40 × 50 mm^2; MATSUNAMI) on the bottom of the stretch chamber. After closing the stretch chamber, humid nitrogen gas was passed through the chamber to remove any oxygen

from the chamber[23, 24]. After passing the nitrogen gas for 30 min, the stretcher part equipped with the PDMS substrate was lowered until it contacted the ATP buffer on the bottom cover glass. The time of ATP addition was set as 0 min, and microscopic observation was initiated. The aforementioned experiments were performed at room temperature.

4.4.3 Application of indentation stress.

PDMS substrate was fixed to the stage (15 mm x 15 mm x 0.05 mm). Indentation stress was applied to microtubules moving on PDMS substrate by using an indenter tip driven by computer controlled stepping motor as described in section 4.1.

4.4.4 Microscopic image capture

The samples were illuminated with a 100-W mercury lamp and visualized with an epifluorescence microscope (Eclipse Ti; Nikon) using a dry *S*Fluor 4 × 0.20 objective (Nikon). Filter blocks with UV-cut specifications (TRITC: EX540/25, DM565, BA606/55; GFP-HQ: EX455-485, DM495, BA500-545; Nikon) were used in the optical path of the microscope to allow for visualization of samples while eliminating the UV portion of the radiation and minimizing the harmful effects of UV radiation on the samples. Images and movies were captured using a cooled CMOS camera (Neo sCMOS; Andor) connected to a PC. To capture a field of view for more than several minutes, ND filters (ND4, 25% transmittance) were inserted into the illuminating light path of the fluorescence microscope to avoid photo bleaching.

4.4.5 Analysis of the microscopic image

Quantitative analysis of collective motion of microtubule

The orientation of microtubules was calculated in terms of nematic order parameter (*S*), which was calculated according to the following equation by using Image J plugin, orientation J (http://bigwww.epfl.ch/demo/orientation/)

$$S = \frac{1}{N}\sqrt{\left(\sum_{i=0}^{180} R_i \cos 2\Theta_i\right)^2 + \left(\sum_{i=0}^{180} R_i \sin 2\Theta_i\right)^2}$$

where N refers to total number of microtubules in the frame, R_i is frequency of the angle of individual microtubules Θ_i (i = 0 to 180). The range of Θ_i was fixed from 0° to 180° based on the symmetry of horizontally or vertically aligned microtubules with respect to the X-axis.

Since the microtubules in the nematic phase were oriented along the X-axis, the director was fixed for both the isotropic and nematic phase along the X-axis and measured the nematic order parameter of microtubules in the XY plane.

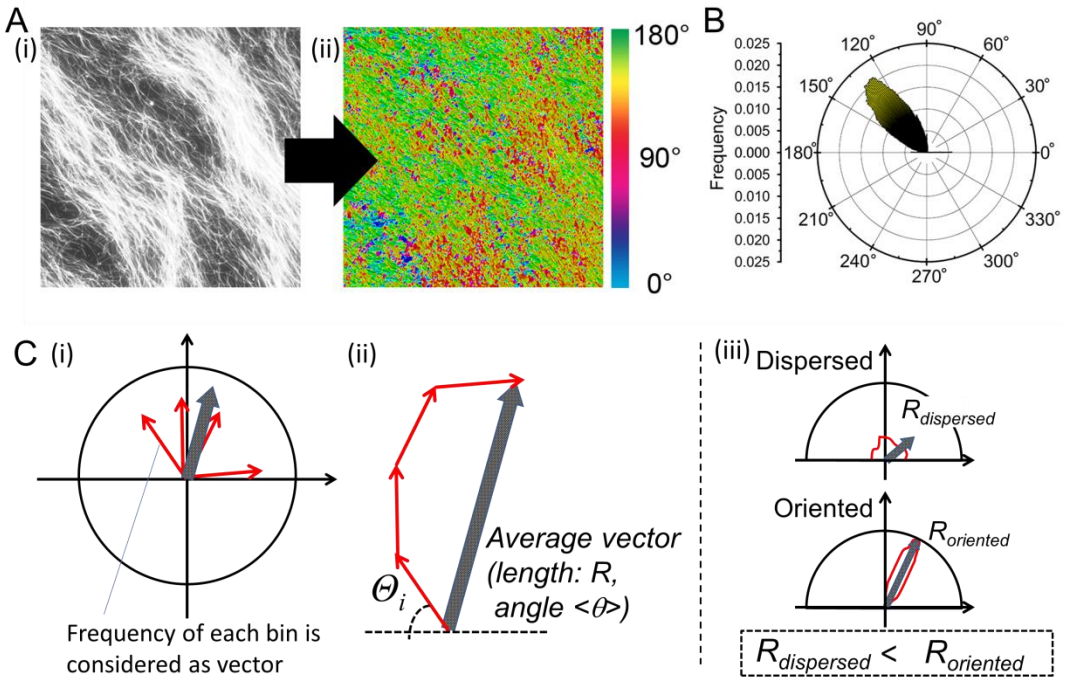

Figure 4.26: Analysis method of the angles and degree of orientation of microtubules. (**A**) (i) Fluorescent microscopic image of microtubules. (ii) Color map representing the distribution of microtubule orientation angles. (**B**) Circular histogram of orientation angles of microtubules obtained from a fluorescent microscopic image of microtubules in (A). (**C**) Directional analysis method. (i) Here each bin in the circular histogram is considered as a vector (length: R_i, angle: Θ_i). (ii) Average vector (length: R, mean orientation angle $<\theta>$) was used for evaluation of orientation direction and degree of orientation. (iii) Relationship between R and degree of orientation. If distribution of microtubules angles is dispersed, R becomes smaller ($R_{\text{dispersed}}$) than that of high oriented microtubules (R_{oriented}).

4.5 References

1. R. Brandt, and G Lee, *Cell Motil. Cytoskeleton*, 1994, **28**, 143–154.

2. R. Brandt, and G Lee, *J. Biol. Chem.*, 1993**, 268**, 3414–3419.

3. D. J. Needleman, M. A. Ojeda-Lopez, U. Raviv, K. Ewert, H. P. Miller, L. Wilson, and C. R Safinya,. *Biophys. J, 2005,* **89,** 3410–3423.

4. J. L. Ross, D. K. Fygenson, *Biophys. J.*, 2003**, 84**, 3959–3967.

5. J. L. Ross, C. D. Santangelo, V. Makrides, and D. K Fygenson,. *Proc. Natl Acad. Sci. USA*, 2004, **101**, 12910–12915.

6. J. L. Ross, H. Shuman, E. L. Holzbaur, and Y. E. Goldman, *Biophys. J.*, 2008**, 94**, 3115–3125.

7. R. Urrutia, M. A. McNiven, J. P. Albanesi, D. B. Murphy, and B. Kachar, *Proc. Natl Acad. Sci. USA*, 1991, **88,** 6701–6705.

8. T. Surrey, F. Nedelec, S. Leibler, and E. Karsenti, *Science*, 2001, **292**, 1167–1171.

9. V. Schaller, C. Weber, C. Semmrich, E. Frey, and A. R. Bausch, *Nature*, 2010, **467**, 73-77.

10. Y. Sumino, K. H. Nagai, Y. Shitaka, Y. Tanaka, K. Yoshikawa, H. Chate, and K. Oiwa, *Nature*, 2012, **483**, 448-452.

11. T. Sanchez, D. T. N. Chen, S. J. DeCamp, M. Heymann, and Z. Dogic, *Nature*, 2012, **491,** 431-435.

12. D. Inoue, B. Mahmot, A. M. R. Kabir, T. I. Farhana, K. Tokuraku, K. Sada, A. Konagaya, and A. Kakugo, Nanoscale, 2015, **7**, 18054-18061.

13. A. Saito, T. I. Farhana, A. M. R. Kabir, D. Inoue, A. Konagaya, K. Sada, and A. Kakugo, *RSC Adv*., 2017, **7**, 13191-13197

14. S. Robinson, A. Burian, E. Couturier, B. Landrein, M. Louveaux, E. D. Neumann, A. Peaucelle, A. Webber, and N. Nakayama, *J. Exp. Botany*, 2013, **64**, 4729-4744.

15. T. Iba, and B. E. Sumpio, *Microvas. Res. Nov*., 1991, **42**, 245-254.

17. D. Inoue, T. Nitta, A. M. R. Kabir, K. Sada, J. P. Gong, A. Konagaya, and A. Kakugo, Nat. Commun., 2016, **7**, 12557:1-10.

18. D. Inoue, Effect of Stepwise Feeding and External Mechanical Stimuli on Active Self-organization of Microtubules, 2015, Ph. D thesis, Hokkaido university.

19. K. V. Mardia, and P. E. Jupp, Directional Statistics, John Wiley and Sons Ltd., England, 2000, 57-82.

20. G. Feng, S. Qu, Y. Huang, and W. D. Nix, *Acta Materialia*, 2007, **55,** 2929–2938.

21. M. Castoldi, and A. V. Popov, Protein Expres. Purif, 2003, 32, 83-88.

22. R. B. Case, D. W. Pierce, H. B. Nora, L. H. Cynthia, and R. D. Vale, Cell, 1997, 90, 959-966.

23. A. M. R. Kabir, D. Inoue, A. Kakugo, A. Kamei, and J. P. Gong, *Langmuir*, 2011, **27**, 13659-13668.

24. A. M. R. Kabir, D. Inoue, A. Kakugo, K. Sada, and J. P. Gong, *Polym. J.*, 2012, **44**, 607-611.

25. A. Sokolova, M. M. Apodacac, B. A. Grzybowskic,, and I. S. Aransona, *PNAS*, 2010, **107**, 969–974.

Chapter 5

Concluding remarks

In this dissertation, I have summarized the studies on collective motion of microtubules driven by kinesin motor-proteins using *in vitro*. The collective motion of microtubules has been demonstrated via regulating mutual interactions among the gliding microtubules, by employing depletion force among them. The roles of concentration of microtubules and depletion force on the kinetics of collective motion of microtubules have been explored. An approach to control the mode of collective motion of gliding microtubules only by changing the mechanical rigidity of the microtubules has been presented. The response of collectively moving microtubules to external stress; e.g. mechanical stress has been descried.

In chapter 2, I have demonstrated the first-ever collective motion of microtubules on a kinesin coated surface using depletion force induced by a macromolecule (methyl cellulose) *in vitro*. It was reported previously that microtubule/kinesin, the most widely used biomolecular motor system was failed to exhibit collective motion and consequently formed no pattern which has been attributed to the intrinsic property of kinesin that is speculated to affect the behavior of individual microtubules and local interaction among them. In this work, employing methyl cellulose as depletant to induced depletion force, the snuggling probability by attractive collision between gliding microtubules has been raised, which consequently allowed emergence of collective motion and finally resulted in pattern formation by microtubules. I have also explored the kinetics of collective motion of microtubule and how the concentration of microtubules and depletion force affect the ensemble behavior of microtubules driven by kinesins was unveiled. The experimental results suggested that both the concentration of microtubules and the depletant (methyl cellulose) have important impacts on the kinetics of collective motion of the kinesin driven microtubule. A minimum concentration of the microtubules or methyl cellulose is required to allow the emergence of collective motion of microtubules and to cause a transition from an isotropic to a nematic phase. For low concentrations of methyl cellulose, no collective motion of microtubules emerged even for high concentrations of microtubules. On the other hand, even for the relatively higher concentrations of methyl cellulose, no collective motion was observed when the concentration of microtubules was low. A minimum concentration of methyl cellulose and microtubule is required for the phase transition in collective motion of microtubule. Importantly the concentration of

microtubules and the methyl cellulose employed in the gliding assay also affect the time required to cause such a phase transition. These findings offer a simple and universal technique to investigate the coordinated behaviour of self-propelled objects using biomolecular motor systems.

In chapter 3, based on the results of chapter 2, I have studied collective motion of microtubules having different mechanical property and found the emergence of streams and large spiral pattern by flexible GTP-microtubules and rigid GMPCPP-microtubule. The experimental analysis revealed that the mechanical property of microtubules has regulated the persistence length and extent of noise of movement of microtubule in the collective motion. Theoretical studies predict that these are the regulatory factors that can control the mode of collective motion. By experimentally verifying the theoretical models, I established a new approach to regulate the mode of collective motion of self-propelled biomolecular system by changing the mechanical property of individuals. This work offers a novel way to program the self-organization of self-propelled objects, which ultimately will help us to design programmable molecular robots.

In chapter 4, I demonstrated the formation of an ultra large vortex pattern by collectively moving microtubules in response to external mechanical stress subjected by indentation. The obtained programmed vortex pattern of microtubules is advantageous over the other unprogrammed patterns of microtubules in means of size, directionality, and stability. The experimental results also suggested that, the kinetics of the formation of vortex pattern and orientation of the microtubules in the vortex depends on the induced stress field, which is directly related to some geometric parameter, like indenter size, shape, and indentation depth. This study would allow us to understand the group behavior of self-propelled particles experiences external perturbation.

I have presented a system to study in-depth the collective motion of kinesin driven microtubules, which offers a better understanding of the coordinated behavior of other self-propelled systems in nature. At the same time, this will clarify the collective behaviour of self-propelled objects such as birds, animals or fishes, but also may provide new insight into emergent structures obtained through a non-equilibrium process. Furthermore, recently microtubule/kinesin system has attracted attention in the field of molecular robotics as the smallest self-propelled objects. Molecular robots, relying on a large number of collectively moving self-propelled objects such as gliding microtubules, enables parallel processing in

transporting a large number of small cargos and assembling building blocks into an ordered structure. This work approaches to a concept of programing the self-organization of cytoskeletal filaments through changing their mechanical property which not only provides us with a means to program the active-self organization of self-propelled particles also will be helpful to understand the dynamics of active matters in nature. Therefore, the ideas obtained from the presented research work of gliding microtubules are expected to expand the boundaries in the field of molecular robotics.

Publication List

Papers (related to this dissertation)

Chapter 2

1. *Depletion Force Induced Collective Motion of Microtubules Driven by Kinesin*

D. Inoue, B. Mahmot, A. M. R. Kabir, T. I. Farhana, K. Tokuraku, K. Sada, A. Konagaya, and A. Kakugo.
Nanoscale, 2015, **7**, 18054-18061.

2. *Understanding the emergence of collective motion of microtubules driven by kinesins: role of concentration of microtubules and depletion force*

A. Saito, T. I. Farhana, A. M. R. Kabir, D. Inoue, A. Konagaya, K. Sada, and A. Kakugo.
RSC Adv., 2017, **7**, 13191-13197.

Other publications not including in this dissertation

1. *Catalytic Degradation of an Organic Dye through Electroreduction of Dioxygen in Aqueous Solution*

T. I. Farhana, M. Y. A. Mollah, M. A. B. H. Susan, and M. M. Islam
Electrochimica Acta, 2014, **139**, 244–249.

List of Conference Presentations

Conference (related to this dissertation)

1.Tamanna Ishrat Farhana, Daisuke Inoue, Arif Md. Rashedul Kabir, Kazuki Sada, and Akira Kakugo

Effect of external mechanical stress on active self-organization of microtubules

The 64th SPSJ (society of Polymer Science, Japan) Annual Meeting, May 2015, Sapporo, Japan.

2. Tamanna Ishrat Farhana, Daisuke Inoue, Arif Md. Rashedul Kabir, Kazuki Sada, and Akira Kakugo

Formation of Ultra Large Vortex Pattern by Collectively Moving Microtubules under external Mechanical Perturbation

CSE Summer School, Hokkaido University, August 2015, Otaru, Japan

3. Tamanna Ishrat Farhana, Daisuke Inoue, Arif Md. Rashedul Kabir, Kazuki Sada, and Akira Kakugo

Emergence of ultra-large vortex pattern by collectively moving microtubules on application of external indentation stimuli

The 53rd Annual Meeting of the Biophysical Society of Japan, September 2015, Kanajawa University, Japan.

4. Tamanna Ishrat Farhana, Daisuke Inoue, Arif Md. Rashedul Kabir, Kazuki Sada, and Akira Kakugo

Emergence of ultra large pattern by collectively moving microtubules

50th SPSJ (society of Polymer Science, Japan) Hokkaido Branch Winter Meeting, January 2016, Hokkaido University, Japan.

5. Tamanna Ishrat Farhana, Daisuke Inoue, Arif Md. Rashedul Kabir, Kazuki Sada, and Akira Kakugo

Collective motion of microtubules in presence and absence of external indentation stress

The 4th Frontier Chemistry Center International Symposium, February 2016, Hokkaido University, Japan

6. Tamanna Ishrat Farhana, Arif Md. Rashedul Kabir, Daisuke Inoue, Kazuki Sada, and Akira Kakugo

Ef*fect of external mechanical stress on active self-organization of microtubules*

The 67th Divisional meeting on colloidal and surface chemistry, August 2016, Ashikawa, Japan

7. Tamanna Ishrat Farhana, Daisuke Inoue, Arif Md. Rashedul Kabir, Kazuki Sada, and Akira Kakugo

Collective motion of microtubules with different lengths and rigidity

6th Soft Mater Symposium, October 2016, Hokkaido University, Japan

8. Tamanna Ishrat Farhana, Daisuke Inoue, Arif Md. Rashedul Kabir, Kazuki Sada, and Akira Kakugo

Effect of external mechanical stress on active self-organization of microtubules

The 54th Annual Meeting of the Biophysical Society of Japan, November 2016, Kanajawa University, Japan.

9. Tamanna Ishrat Farhana, Daisuke Inoue, Arif Md. Rashedul Kabir, Kazuki Sada, and Akira Kakugo

Effect of length and rigidity of microtubules on their collective motion

The 17th RIES-Hokudai International Symposium, December 2016, Châteraisé Gateaux Kingdom Sapporo, Japan

10. Tamanna Ishrat Farhana, Ai Saito, Daisuke Inoue, Arif Md. Rashedul Kabir, Kazuki Sada, and Akira Kakugo

Collective motion of microtubules driven by kinesin

11th International Gel Symposium, March 2017, Chiba, Japan.

Conference (others)

1. Tamanna Ishrat Farhana, Md. Yusuf Ali Mollah, Md Abu Bin Hasan Susan, and Md. Mominul Islam

Electrochemical reduction of dioxygen: Reaction of reactive oxygen species generated insitu with methylene blue in acidic solution.

Bangladesh Chemical Congress – 2012, Dhaka, Bangladesh.

2. Tamanna Ishrat Farhana, Md. Yusuf Ali Mollah, Md Abu Bin Hasan Susan, and Md. Mominul Islam

Electrochemical reduction of molecular oxygen: Degradation of methylne blue by in-stu generated reactive oxygen species in aqueous solution

9th Conference of the Islamic World Academy of Science, May 2013, Dhaka, Bangladesh.

3. Tamanna Ishrat Farhana, Md. Yusuf Ali Mollah, Md Abu Bin Hasan Susan, and Md. Mominul Islam

Electrochemical reduction of dioxygen: Reaction of reactive oxygen species generated insitu with methylene blue in acidic solution.

Annual meeting of Bangladesh chemical society, 2013, Dinajpur, Bangladesh.

Acknowledgement

This dissertation is the collection of studies have been carried out under the supervision of Professor Kazuki Sada during October 2014–September 2017 at Hokkaido University, Japan. I would like to express my sincerest gratitude to Professor Kazuki Sada for his kind guidance, invaluable advices, effective discussions and warm encouragement throughout this work. I am highly obliged to Associated Professor Akira Kakugo (Material Chemistry Laboratory, Hokkaido University) for his endless effort to guide this research work and providing me with all the necessary facilities. I also would like to express my sincere appreciation and gratitude to Professor Akira Kakugo for his constant guidance, continuous motivation and fruitful discussion throughout this study.

I gratefully acknowledge the cooperation and suggestions from Assistant Professor Kenta Kokado and Assistant Professor Kenji Hirai of Material Chemistry Laboratory, Hokkaido University. I am indebted to Assistant Professor Arif Md. Rashedul Kabir (Material Chemistry Laboratory, Hokkaido University) for his continuous guidance, helpful discussions, and enthusiastic motivation throughout of this work.

I am also gratefully acknowledge Mr. Yasutaka Sasaki (Hokkaido University) for his cooperation in constructing the ‘indentation chamber.’ I would like to gratefully acknowledge Dr. Daisuke Inoue for his continuous inspiration, kind cooperation, and effective discussions throughout of this work

All the current and former members of the Material Chemistry Laboratory, Hokkaido University are thankfully acknowledged for their cordiality, active cooperation and constant supports. Especially I want to acknowledge Ms. Ai Saito for her help in conducting the experiments. I would like to thank Dr. Sirajul Islam, Dr. Tanjina Afrin, Dr. Jakia Jannat Keya, Ms. Shizuka Anan, Ms. Sayada Rubaiya Nasrin, Mr. Kyohei Uenishi, Mr. Seiji Nishikawa, and Mr. Kentaro Kayano. I am also thankful to all of the staffs in the Graduate School of Chemical Sciences and Engineering and the Department of Chemistry, Hokkaido University for their kind assistance and supports during this study.

I would like to pay tribute to Hokkaido University (Japan) and University of Dhaka (Bangladesh) under Advanced Graduate School of Chemistry and Material

Science (AGS) program and to Professor Md. Abu Bin Hasan Susan to give me the opportunity to study in Japan and enjoy the fascinating and multifaceted cultural life in Japan. I am also grateful to Professor Mohammad Yousuf Ali Mollah (my honorable supervisor in the University of Dhaka, Bangladesh, current Member, University Grants Commission of Bangladesh), Associate Professor Md. Mominul Islam (Department of Chemistry, University of Dhaka) and Associate Professor Mohammad Shah Miran (Department of Chemistry, University of Dhaka) for their encouragement and motivation. I also would like to thank all of the former and present members of the Material Chemistry Research Laboratory (Department of Chemistry, University of Dhaka) for their all sorts of supports.

I gratefully acknowledge my family members especially to my late father Md. Abdul Awal, and my mother Helen Parvin for their endless sacrifices, love and continuous supports during the entire tenure of this study. Finally, I would like to thank my beloved husband Md. Samsuddoha for always supporting me, standing by my side and encouraging me to accomplish the goal.

Tamanna Ishrat Farhana